Modeling Fine-grained Fluxes for Estimating Sediment Yields and Understanding Hydroclimatic and Geomorphic Processes at Lake Peters, Brooks Range, Arctic Alaska

By Lorna Louise Thurston

A Thesis

Submitted in Partial Fulfillment of the Requirements for the

Degree of Master of Science, Majoring in Environment Science and Policy

Northern Arizona University

December 2017

Approved:

Associate Professor Erik Schiefer

Assistant Professor Nicholas McKay

Regents' Professor Darrell Kaufman

Abstract

Hydroclimatic and geomorphic controls of fine-grained sediment transfer and deposition at Lake Peters, Brooks Range, Alaska, were investigated. Fluvial-based and lake-based methods of estimating the suspended component of specific sediment yield (SSYs; sediment yield relative to catchment area) were applied. The fluvial-based method used sediment rating curves, which commonly apply hydrological variables (stream discharges or turbidities) to model suspended sediment concentrations (SSCs), and subsequently calculate yield. To capture maximum variability in SSC, and improve our understanding of the physical processes driving this variability, multivariate sediment rating curves were selected and applied. The rating curves, which incorporate best-fit hydrological, temporal, and climatic predictor variables, were applied to Lake Peters' Carnivore Creek (128 km^2; 9% glacial coverage) and Chamberlin Creek (8 km^2; 26% glacial coverage) sub-catchments for the 2015 and 2016 open-channel seasons. Near-surface sediment cores (9 - 26 cm long) from spatially distributed locations across Lake Peters provided an additional measure of sediment yield at Lake Peters, and fostered our understanding of decadal-scale sediment transfer processes and episodic sedimentation. In this study, surface cores were used to estimate annual average sedimentation over the past *ca*. 42 years, because lack of varves (annual rhythms) made it difficult to measure sediment transfer on an annual basis.

Turbidity-based multivariate models marginally outperformed discharge-based multivariate models of SSC. Data limitations meant multiple models were required to produce continuous sediment transfer records, with annual SSYs estimated to be 53 (44 – 226) Mg km^{-2} yr^{-1} in 2015 and 89 (79 – 234) Mg km^{-2} yr^{-1} in 2016. Although upper confidence band error estimates exceed 200%, annual average lake-based SSYs of 52 Mg km^{-2} yr^{-1} are comparable with fluvial-based results. The last major depositional event at Lake Peters probably occurred early- to mid-1970s, when a thick and relatively coarse marker-bed was deposited across the lake by an event estimated to have a mean daily discharge magnitude of hundreds of cumecs. The majority of annual suspended sediment yield in 2015 and 2016 was transported to Lake Peters from Carnivore Creek (> 96%) during and immediately following rainfall events. Temperature and annual snow-water equivalent were secondary drivers in both sub-catchments. Seasonal exhaustion of the fine sediment fraction was evidenced in the Chamberlin Creek sub-catchment, perhaps because this small, steep sub-catchment has little short-term sediment storage potential within and adjacent to the channel. Sediment from both sub-catchments is transferred to Lake Peters, which acts as an effective sediment trap. Deposition up to 1.5 km down-lake of the primary (Carnivore Creek) inflow is complex, likely because of influx from Chamberlin Creek, and sediment bypassing by interflows and/or overflows carry sediment over 1 km where it is focused into a primary, deep proximal basin. At distances over 1.5 km down-lake sediment deposition declines notably, but thin laminae are distributed throughout the distal basin (over 6 km down-lake) which correlate to proximal basin deposits.

Results from Lake Peters were compared with other suspended sediment yields reported above the Arctic Circle (66° 33' N). Glacial coverage, glacial thermal regime, lithology, and to a lesser extent catchment area, were found to be principal regional-scale drivers of arctic SSYs, which vary by four orders of magnitude (< 1 to > 6000 Mg km^{-2} yr^{-1}). Ultimately, using fluvial- and lake-based approaches proved helpful for understanding sediment transfer processes from source to sink over a range of temporal scales, as well as increasing confidence in yield results. This approach is encouraged for future arctic research on fluvial sediment transfer in catchments with proglacial lakes.

Acknowledgements

Special thanks to the Chair of my Master of Science (MS) Thesis Committee—Associate Professor Erik Schiefer, for never tiring of motivating and supporting my research. Thank you to the National Science Foundation Arctic System Science Program (award # 1418000) for funding the overarching project, and to the field crew and project principal investigators (PIs): Nicholas McKay, Darrell Kaufman, Erik Schiefer, and David Fortin of Northern Arizona University; Anna Liljedahl and Matt Nolan of the University of Alaska, Fairbanks; and Michael Loso of Alaska Pacific University. I am grateful for additional financial support provided by the Environmental Professionals of Arizona (EPAZ). The Northern Arizona University Department of Geography, Planning, and Recreation, School of Earth Sciences and Environmental Sustainability, and Center for International Education are all recognized for their support.

Preface

My thesis is manuscript-style in structure, with Chapters 2 and 3 intended for submission to scientific journals. The journal (or journals) for submission has not been selected at this time, but formatting is consistent with requirements for submission to the journal of *Earth Surface Processes and Landforms* (ESPL), which will likely be a target journal for one of the manuscripts. The theme of my thesis is arctic sediment transfer processes, and the study site pertinent to all chapters is Lake Peters, Brooks Range, Alaska. Chapter 1 introduces the overarching project and theme. In Chapter 2, fluvial-based multivariate models of suspended sediment concentrations are developed. The models are used to estimate suspended sediment yields, and interpret catchment-scale processes. In Chapter 3, a lake-based spatial model of sediment flux is developed, and used to estimate annual average multi-decadal sediment yield to Lake Peters. Additionally, within-lake processes are investigated, and regional variations in specific sediment yields are interpreted. A comparison of the fluvial-based and lake-based methods for estimating sediment yields is incorporated into Chapter 3. Chapter 4 draws overall conclusions from the work in Chapters 2 and 3, and provides recommendations for future work. Finally, the appendices contain additional methods and results that could not be included in the manuscript-style chapters because of publishing length limitations.

1 INTRODUCTION

1.1 Project Outline

A National Science Foundation funded project is underway to develop a model of how weather and climate are filtered through the glacier-hydrology-lake-sedimentation system and recorded in lacustrine deposits. The proposed system model has three components: a spatially-distributed hydrological model, an empirically based sediment flux model, and a process-response basin-filling sedimentation model. The focus sites for the wider project include: Lake Linné, Svalbard (78^{o} N), Lake Peters, Brooks Range, Alaska (69^{o} N), and Eklutna Lake, southern Alaska (61^{o} N), with Lake Peters being the study site for my thesis research. In this thesis, multiple models of suspended sediment concentrations (SSCs) (Chapter 2) and lake-bottom flux (Chapter 3) are developed for Lake Peters, towards the sediment flux model component of the overarching project. The purposes of my research are to estimate suspended sediment yields on seasonal to decadal time-scales, and understand the physical processes driving these yields, considering hydroclimatic and geomorphic processes and change. The main research outcomes are contributions to arctic systems science, and provision of new information on Lake Peters' catchment, which was last researched intensively a half-century ago (Rainwater and Guy, 1961; Hobbie, 1962; Reed, 1968). The following paragraphs provide an introduction to the research site, and some of the key physical characteristics and processes generally contributing to spatial and temporal variability in arctic sediment yields, which will be explored in more detail in Chapters 2 and 3.

1.2 Project Site

1.2.1 Arctic National Wildlife Refuge

The Brooks Range sits between the Arctic Slope and the Kobuk and Yukon Rivers. In the northwest Brooks Range, the Franklin Mountains form one of the east-west trending mountain ranges (Molnia, 2007), and this is where Lake Peters' catchment is situated, inside the Arctic National Wildlife Refuge. The US-wide refuge system was established in 1903—for the benefit of present and future generations of Americans (Docherty, 2001). In 1960, the Secretary of the Interior—Fred Seaton designated 8.9 million acres in northeastern Alaska as the *Arctic National Wildlife Refuge*, known at the time as the *Original Range* (Monaghan, 2009). The approximately 20 million acre Wildlife Refuge, as it exists today, was created by the Alaska National Interest Lands Conservation Act of 1980 (ANILCA). ANILCA cites four main purposes: conservation of fish and wildlife; fulfillment of international treaty obligations; provision of subsistence opportunities for local residents; and ensuring water quality and necessary quantity within the refuge (Docherty, 2001). Most of the 8.9 million acres of land originally designated in 1960, and approximately 40% (8 million acres) of the extension area created under ANILCA, including the Lake Peters' catchment, is classified as *wilderness* (Corn, 2003). *Wilderness* is among the highest levels of protection given to land in the USA, as under the Wilderness Act (1964) all commercial enterprise is prohibited on such lands. W*ilderness* is technically defined as "an area of undeveloped federal land retaining its primeval character and influence without permanent improvements or human habitation, which is protected

and managed so as to preserve its natural conditions…" Wilderness is also recognized as "an area where the earth and its community of life are untrammeled by man, where man himself is a visitor who does not remain" (Wilderness Act, 1964). Only Congress can change the *wilderness* status of land within the Arctic National Wildlife Refuge, including Lake Peters' catchment. Oil and gas interests on the Coastal Plain are currently pressuring Congress to reclassify the land. As such, the *wilderness* status is uncertain into the future. At present, the Wildlife Refuge provides opportunities for scientific research in an arctic environment with minimal human impact, whilst protecting wilderness of outstanding value.

1.2.2 Exploration and Research at Lake Peters

Lakes the size of Peters and the adjoining Lake Schrader are rare in the eastern part of the Arctic Slope, resulting in the catchments historically having been a focal point for indigenous people until the 1930s (Hobbie, 1962). Today, both catchments remain undeveloped owing to the remote location and protection from commercial development provided by their *wilderness* status. The only infrastructure within Lake Peters' catchment comprises one small cabin, two storage/work sheds, and an outhouse constructed by the Arctic Research Laboratory, all situated together on the toe of an alluvial fan, at the base of the southernmost non-glacial catchment on the eastern side of Lake Peters. The area is occasionally used by pack-rafting groups, hikers, and for recreational and subsistence fishing, as well as for scientific research. Staff of the Fish and Wildlife Service occasionally visit the site.

Although explorers first set foot in Lake Peters' catchment in the early 1900s, there has only been one previous period of intensive scientific study—between 1958 and 1962, associated with the International Geophysical Year (Rainwater and Guy, 1961; Hobbie, 1962; Reed, 1968). Rainwater and Guy (1961) published the only known sediment yields for Lake Peters' catchment (before my thesis), and these are compared with contemporary sediment yields in Chapter 2. Detailed descriptions of the Lake Peters' catchment, including geography, geology, climate, glaciers, and fluvial morphology are incorporated into Chapters 2 and 3.

1.3 Arctic Sediment Transfer Processes

1.3.1 Arctic Climate Forcing and Environmental Change

Sustained industrial-era warming of Northern Hemisphere continents, associated with atmospheric greenhouse gases (GHG), developed mid-19th Century (Abram et al., 2016). Tingley and Huybers (2013) estimate that 61% of high northern latitude locations have experienced warm temperatures in the past 20 years, unprecedented in the previous 600 years. The Arctic is warming at an unprecedented rate—glaciers are melting (Molnia, 2007; Kienholz et al., 2015), proglacial lakes expanding (Carrivick and Tweed, 2013), and sea levels rising (Carrivick and Tweed, 2013; Zemp et al., 2015), elevating risks of irreversible change for people and ecosystems (Moore et al., 2009). In addition, rainfall is increasing (Bintanja and Andry O, 2017). Piror to the 20th Century, the Arctic experienced a long-term cooling trend, estimated from reconstructions to be 0.47^{o}C kyr^{-1} (McKay

and Kaufman, 2014). At least since turn of the millennia, the Artic has experienced positive temperature anomalies for all seasons (Serreze et al., 2011). This is a combined result of: a general background warming in response to positive radiative forcing; atmospheric circulation anomalies; changes in characteristics of the surface, especially reduced sea ice and higher sea surface albedo (Serreze et al., 2011); and a positive feedback mechanism associated with precipitable water over the Arctic increasing in response to positive anomalies in air and sea surface temperatures, and negative anomalies in end-of-summer sea ice extent (Serreze et al., 2012). Warming by black carbon aerosols, soot on snow, and changes in cloud cover may also play a role (Serreze et al., 2011).

A phenomenon known as arctic amplification results in larger surface air temperature increases in response to GHG forcing in the Arctic comparative to other parts of the Northern Hemisphere (Serreze et al., 2009). This is principally associated with less sea ice at the end of summer, increasing the sensible heat of the ocean, thus delaying ice formation come autumn and winter. The delay promotes upward heat fluxes, which have been observed as positive surface and lower troposphere anomalies in autumn since the 1990s, relative to the 1979-2007 period. This trend is likely to continue, such that the arctic amplification will eventually be observed in winter and later in spring. By the 2070s, the Arctic is projected to be largely ice-free (Serreze et al., 2009), including Alaska and Canada which comprise ~12% of the global glacierized area outside of ice-sheets (Kienholz et al., 2015).

In Alaska, a general cooling of annual air temperatures has been reported from the 1950s through to 1976, followed by rapid warming (Cassano et al., 2011), driving widespread glacial recession and thinning (Molnia, 2007), and increased winter runoff over pan-Arctic Alaska (Lammers et al., 2001). The temperature shift around 1976 is attributed to a deepening and shifting of the Aleutian Low, and changes unrelated to atmospheric circulation, including: increased nighttime cloudiness, a global warming signal, and/or increased sea surface temperatures (Cassano et al., 2011). Although spatially variable, negative temperature anomalies across Alaska are generally associated with the following synoptic controls: low-pressure systems centered over the Gulf of Alaska; low pressure over the Canadian Archipelago and to the southwest of the Aleutian Islands, with high pressure over eastern Siberia; and low pressure over the Beaufort and Chukchi Seas, with high southerly pressure. Positive temperature anomalies occur when a locality is ahead of a low-pressure system, in the warm southerly flow sector of the cyclone (Cassano et al., 2011).

1.3.2 Sediment and Arctic Environmental Change

Sediment yields provide a useful proxy for arctic environmental change, because they are largely functions of climate-driven glacial, periglacial, and hydrological processes (Irvine-Fynn et al., 2005). In catchments with negligible or minimal human impact, such as Lake Peters' catchment, climate signals are easier to filter from fluvial and lacustrine records, as there are fewer non-climatic parameters that need to be accounted for. In fluvial records this is especially important, because there may be no long-term, pre-development record to indicate how hydroclimatic and geomorphic responses have changed.

The use of sediment yields as proxies for environmental change was initially explored in more accessible temperate Alpine catchments; however, these models are not transferable to arctic catchments. Arctic systems have been found to respond differently to environmental change (Hodson and Ferguson, 1999; Irvine-Fynn et al., 2005), with lower surface temperatures producing lower sediment yields, for example (Syvitski, 2002). This has led to a growing body of literature over the past two decades, but there are with few contemporary sediment yield studies above the Arctic Circle (66^{o} 33') in Alaska (e.g. Tape et al., 2011). Furthermore, research within the same and different areas of the Arctic have returned inconsistent results with regards to sediment yields and interpretation of processes driving these yields, which is likely result of spatial and temporal variability, as well as methodological discrepancies (Orwin et al., 2010). One problem is that sediment yields are often measured over periods of a few weeks to a few years, despite varying significantly on an inter-annual basis (Bogen and Bønses, 2003). Longer periods of record may capture higher magnitude episodic processes, such as supraglacial landslides and ridge-lowering blockfall events, with shorter records underestimating long-term erosion rates (O'Farrell et al., 2009).

Applying a stochastic model with catchment relief and air temperature as positive drivers of sediment yield, and catchment area as a negative driver of sediment yield (because of increased catchment storage), Syvitski (2002) predicted changes in Arctic sediment flux and load. For every 2°C of atmospheric warming, Syvitski (2002) predicted a 22% increase in the flux of sediment carried by arctic rivers, and for every 20% increase in discharge, a 10% increase in sediment load is predicted.

Arctic sediment yields have also been forecast at the catchment-scale. Lewis et al. (2010) applied Intergovernmental Panel on Climate Change (IPCC) emission scenarios for the 20th and 21st Century to model hydrological conditions and sediment yield in West River catchment, Melville Island, Canada. In contrast to Syvitski (2002), precipitation was found to be a more direct driver of sediment yield than surface temperatures. Assuming exponentially increasing atmospheric CO_2 to 800 ppm by 2100, Lewis et al. (2010) predicted: total seasonal runoff will double; daily maximum discharge rates will double; the open-channel season will increase by 30 days mostly in autumn; and sediment yields will increase by 100% to 600%.

1.3.3 Geography and Geology

Small catchments respond faster to forcing (Morehead et al., 2003; Menounos et al., 2006), and in general, perturbations are expected to smooth-out in larger catchments with longer channels. Sediment yields are especially responsive to catchment area because of sediment storage effects (Milliman and Syvitski, 1992; Syvitski, 2002; Lewis et al., 2010), and are often presented as a function of catchment area for comparative purposes, termed specific sediment yield (SSY). Presenting estimates as SSYs may (Schiefer et al., 2001), or may not (Church and Slaymaker, 1989; Hodgkins et al., 2003; Thurston, in prep–Chapter 3), nullify inter-catchment area disparities, depending on the relative significance of sediment storage effects to other processes driving SSYs. The conventional

model is decreasing SSYs with catchment area, but diversions from the conventional model may be related to: an extended paraglacial cycle in larger catchments (Church and Slaymaker, 1989); the thermal regime of glaciers (Hodson and Ferguson, 1999), and/or size of glaciers (Hallet et al., 1996); and catchment physiography (Schiefer et al., 2001). In the Canadian Cordillera, Schiefer et al. (2001) found that the conventional model held true in valleys and plateaus, but increasing SSYs with catchment area were evidenced in the coastal mountains, with absence of any trend in areas of intermediary relief.

Trends in SSYs might depend on the within-catchment monitoring locations. Monitoring of SSCs in the Austre Brøggerbreen Glacier's catchment, Svalbard, has occurred at various locations, and returned variable results (Hodson et al., 1998; Bogen and Bønses, 2003; Irvine-Fynn et al., 2005). Furthermore, Hodgkins et al. (2003) found an inverse trend between catchment denudation and proglacial aggradation for the 44km^2 Finsterwalderbreen Glacier's catchment, Svalbard.

In addition to catchment area, base-level, lithology, vegetation, and anthropogenic land-use change all effect sediment yields. Hamilton (2003) describes periods of alluviation from *ca.* 5-4.8 kyr and at *ca.* 2 kyr in the Atigun River valley, Brooks Range, Alaska (200 km southwest of Lake Peters), unexplained by climate. These alluviation periods are best explained by localized rapid base-level rise resulting from landsliding (Hamilton, 2003). Landsliding may have occurred as the river incised following Pleistocene deglaciation, and could have repeatedly dammed Atigun River (Hamilton, 2003). Bogen and Bønses (2003) compared sediment yields returned in Svalbard with previous research in mainland Norway, the Swiss Alps, Iceland, and Alaska. Glacial sediment production was suggested to depend primarily on the character of bedrock, and secondarily on glaciological parameters, including thermal regime (Bogen and Bønses, 2003). O'Farrell et al. (2009) also found lithology to be important in the Matanuska Glacier's catchment, Alaska. Erosion rates by non-glacial processes were similar to subglacial erosion rates, suggesting that ice-free regions of glaciated catchments contribute significantly to sediment transfer, and that partially glaciated catchments may respond rapidly to change (O'Farrell et al., 2009).

Vegetation is another well-known control on hydrological processes. Arctic vegetation productivity and coverage are currently experiencing change due to climate forcing (Tape et al., 2011; Naito and Cairns, 2015), which might change the hydrology of some arctic environments in the near-future (Tape et al., 2011). It has been suggested that vegetation in river valleys on the North Slope of the Brooks Range, Alaska has recently reached a tipping point, which marks a transition from tundra to shrubland, or towards spatial homogeneity of shrubland (Naito and Cairns, 2015). If current climate trends continue, Naito and Cairns (2015) predict that the vegetation will transition to spatial homogeneity for cover by tall shrubs. Such a transition will likely drive fundamental changes in terrestrial – climate feedback mechanisms, potentially: reducing geomorphic thresholds for change; reducing surface albedo; altering nutrient availability; and promoting increases in atmospheric heating, evapotranspiration, soil active-layer depth, and permafrost degradation (Naito and Cairns, 2015). Feedback mechanisms are sufficiently complex that it is difficult to imply how sediment yields will respond, and there are few comprehensive studies of this. Tape et al. (2011) investigated the

relationship between vegetation productivity and erosion in the in the Chandler River corridor, Brooks Range, Alaska. Erosion was found to be lessening since 1980 due to stabilizing shrub expansion and associated declining peak discharge events; although this negative association could be reversed in coming decades by an increase in permafrost-related erosional events, or an increase in decomposition (Tape et al., 2011).

Anthropogenic land-use activities might also change and expand in coming decades, affecting high latitude sediment transfer. Schiefer (2006) correlated unconformities, turbidities, and cohesive slump failure deposits in varve sequences from Green Lake, British Columbia, with sawmill operations and rail-line construction along the shoreline. Furthermore, Schiefer et al. (2013) investigated 104 catchments in the Canadian Cordillera, finding trends between land-use, including road density and forest clearings, and sediment accumulation. For such trends to be apparent in sediment deposits, the influence of land-use activities on sediment transfer processes must be strong enough that it is not dwarfed by glacial or other forcing signals (Menounos et al., 2006).

1.3.4 Glacial Expansion and Recession

Within the Quaternary, glacial expansion and recession has played a significant role in sediment availability and mobilization, affecting sediment transfer (Menounos et al., 2006; Diedrich and Loso, 2012). In Alaska, Pleistocene glaciers are estimated to have once covered > 1.2 x 10^6 km^2, with the penultimate extent in the Early Wisconsinan (*ca.* 60 – 50 kyr), and coverage of 725,800 km^2 in the Late Wisconsinan (Kaufman et al., 2011). In the Brooks Range, Itkillik I moraines 40 km north of the northern range are associated with the penultimate glaciation, and Itkillik II moraines 25 km north of the northern range are associated with the Late Wisconsinan glacial advance; glaciers retreated from their Late Wisconsinan positions by *ca.* 25 kyr (Kaufman et al., 2011). At Burial Lake, western Brooks Range, Alaska, multi-proxy evidence for climate cooling during the Younger Dryas (*ca.* 13,000 – 12,000 yr BP) was not found, and the Holocence is characterized by landscape stabilization, relatively stable lake levels, and high and variable aquatic productivity (Finkenbinder et al., 2015). In the northeastern Brooks Range, including at Chamberlin Glacier, four major Holocene glacial still-stands are recorded by terminal moraine deposits (Evison et al., 1996). The latter two still-stands are associated with moraine formation during the Little Ice Age (LIA) —*ca.* 1200 – 1850 CE (Evison et al. 1996; Sikorski et al., 2009), which has been associated with prolonged southward shift of the Arctic Front and a drier climate (Sikorski et al., 2009). In southern Alaska, the LIA has been associated with three cool periods, instead of two, and a Medieval warm period (*ca.* 1000 – 1100 CE) is recorded in lacustrine deposits (Loso, 2009). At Kurupa Lake on the northern flank of the Brooks Range, ~400 km southwest of Lake Peters, a lacustrine temperature reconstruction found large century-scale variability, with summer air temperatures increasing by 5-7°C throughout the 20th Century (Boldt et al., 2015). Today, the Brooks Range is estimated to have over 800 cirque and small valley glaciers, most > 1 km long (Sikorski et al., 2009).

Glaciated catchments generally produce higher sediment yields than unglaciated catchments of the same size, with extra-channel sediment worked by the glacier transferred to the proglacial fluvial

system. In glaciated catchments, over centuries to millennia, sedimentation rates reflect changes in ice extent, probably associated with glacial erosion rates, with the highest sedimentation rates associated with transitional periods in the last millennium (Leonard, 1997). Superimposed decadal-scale variability is complexly related to up-valley ice extent, with the highest sedimentation rates associated with glacier maximum stands or periods of advance or recession (Leonard, 1997). Sedimentation associated with advancing ice extent is evident in the Sagavanirktok River valley, Brooks Range, Alaska (150 km west of Lake Peters). Rapid alluviation at approximately 12.8 kyr, with accumulation continuing until 11.4 kyr, is reported, when the Sagavanirktok River was blocked by re-advance of the Atigun piedmont lobe (Hamilton, 2003). Conversely, the processes by which sediment transfer is elevated during deglaciation have been coined 'paraglacial sedimentation' (Church and Ryder, 1972). The temporal 'paraglacial cycle' ceases once fluvial yields reach non-glacial norms (Church and Ryder, 1972). Church and Ryder (1972) and Church and Slaymaker (1989) both contend that fluvial sediment yields do not reflect contemporary primary production of weathered debris associated with geology and climate, but landscape evolution over several tens of thousands of years associated with Quaternary glacial events. However, the ability to define cessation of the paraglacial cycle has been challenged. Orwin and Smart (2004) found that sediment surfaces of increasing maturity (with the oldest surface exposed since 1910) required greater magnitude rainfall events to trigger mobilization, likely because of surface armoring or sediment exhaustion.

Episodic sediment fluxes associated with glacier change may release large volumes of sediment for transport. Moore (2009) describes geomorphic hazards associated with glacial change, including rock avalanches, deep-seated slope sagging (where ice retreat removes debuttress support to glacially undercut slopes), debris avalanches and flows, debris slides, rock fall, moraine dam failures, and glacier outburst floods. Episodic geomorphic sediment release is catchment-specific, and given the high magnitude release of sediment in short time periods, difficult to quantify or predict.

In addition to active or recent deglacierization, the proportion of glacier coverage is important (Church and Ryder, 1972; Guymon, 1974; Lewkowicz and Wolfe, 1994; Hallet et al., 1996; Bogen and Bønses, 2003; Hasholt, 2016), with heavily glaciated catchments in Alaska reportedly producing an order of magnitude more sediment than other Alaskan catchments, for example (Hallet et al., 1996). Faster rates of glacial recession also produce larger sediment yields (Menounos et al., 2006), although sedimentation rates can decline if glaciers decouple from their sediment sinks during recession, forming proglacial lakes (Carrivick and Tweed, 2013).

In the central Brooks Range, Alaska, glacial retreat from the most recent Neoglacial maxima initiated around 1640-1750 CE, with the most rapid retreat from *ca.* 1870 to the mid-1990s. Globally, Neoglacial moraines have been found to be synchronous, suggesting a climatic deterioration of similar magnitude (Ellis and Calkin, 1984). In the northeastern Brooks Range, including at Chamberlin Glacier, four major Holocene glacial still-stands are recorded by terminal moraine deposits, with the most recent at *ca.* 1890 (Evison et al., 1996). Molnia (2007) reported that approximately 98% of Alaska's glaciers are currently thinning or retreating, with only a few, mostly

former tidewater glaciers, advancing. This is consistent with global trends, with the highest recorded global mean annual glacier loss recorded for the most recent 2001-2010 decade, driven by enhanced summer-melt (Zemp et al., 2015). Recession and thinning of McCall Glacier, which is within the same region of Alaska as Lake Peters, has been found to be principally driven by melt-energy supplied by net radiation (Klok et al., 2005). Consequences of contemporary glacial recession include significant increases in global runoff contributions (Zemp et al., 2015), and an increasing number and size of proglacial lakes (Carrivick and Tweed, 2013), which will likely continue until glacial coverage is exhausted. Proglacial lakes are defined as lakes that are, or have been, directly affected by a glacial ice-margin, or subaerial glacial meltwater, including Lake Peters.

The formation and persistence of proglacial lakes, such as Lake Peters, has been closely linked to climate-driven glacial dynamics (Carrivick and Tweed, 2013). During glacial advance, meltwater flows freely onto the sandur. During glacial retreat, an excavated glacial basin is often uncovered between the ice-front and proglacial channels, which is decoupled from the sandur upon further glacial retreat. Meltwater pools in the exposed glacial basin, which acts as a fluvial sediment trap, preventing a large proportion of sediment from flowing into proglacial channels downstream of the newly formed lake, and also trapping sediments transported by eolian and volcanic processes (Carrivick and Tweed, 2013). Calving of ice into ice-contact proglacial lakes can accelerate glacial retreat, and, in turn, lake expansion via a positive feedback mechanism (Carrivick and Tweed, 2013). Proglacial lakes form at the sides of mountain glaciers, at the front and sides of ice-sheet outlet glaciers, and at the edge of nunataks, and may be dammed by ice, moraine, landslide debris, bedrock, or less often glacio-fluvial fans or aprons. Thinner ice-dams result in frequent, low magnitude outburst floods (a type of jökulhlaup), and thicker ice-dams result in less frequent, higher magnitude outburst floods, with ice-dams potentially transitioning to moraine-dams as glaciers retreat (Carrivick and Tweed, 2013). Conversely, if glacial expansion makes a lake ice-contact, such as occurred at Iceberg Lake, southcentral Alaska, during the LIA, sediment can be injected from subglacial and englacial tunnels, depositing sub-aqueous fan-deltas on lake beds (Diedrich and Loso, 2012).

1.3.5 Glacial Thermal Regimes

Patterns of suspended sediment transfer have been found to differ among glacial thermal regimes, which are commonly classified as cold-based, polythermal, or warm-based, with catchments containing warm-based glaciers generally producing larger sediment yields (Hodgkins, 1996; Hallet et al., 1996; Hodson and Ferguson, 1999; Bogen and Bønses, 2003; Irvine-Fynn et al., 2005). Large, fast-moving warm-based valley glaciers in the tectonically active ranges of southeast Alaska have been found to produce higher sediment yields (> 25,000 Mg km^{-2} yr^{-1}) than other glaciated or unglaciated regions in the world (Hallet et al., 1996). In Svalbard, the cold-based Austre Brøggerbreen Glacier on Spitsbergen, Svalbard has been investigated by a number of authors (Hodson et al., 1998; Hodson and Ferguson, 1999; Bogen and Bønses, 2003; Irvine-Fynn et al., 2005), and yields are reportedly low compared with most warm-based and polythermal glaciers (Hodson

et al., 1998). Marginal sediment sources, such as moraines, which store and release sediments through freeze-thaw processes and subaerial erosion, have been reported as major sediment sources in catchments of cold-based glaciers (Hodson and Ferguson, 1999; Bogen and Bønses, 2003; Irvine-Fynn et al., 2005), whereas in catchments of warm-based glaciers sediment supply is often dominated by subglacial reservoirs (Hodson & Ferguson, 1999; Irvine-Fynn et al., 2005). In the case of the former, thermo-erosion and bank destabilization may enhance sediment availability, whereas ground frost may inhibit it (Irvine-Fynn et al., 2005), potentially resulting in a supply-limited environment. For example, short-term sediment availability was found to exert a dominant control on SSCs, above discharge, in the catchment of the cold-based Scott Turnerbreen Glacier, Spitsbergen, Svalbard (Hodgkins, 1999). Catchments of warm-based glaciers can also face sediment supply limitations associated with subglacial network development, but such limitations are less likely to be pronounced early in the season, and more likely to be associated with sediment exhaustion throughout the season (Irvine-Fynn et al., 2005).

Although typical 'cold-based' and 'warm-based' glacial regimes can aid interpretation of geomorphic and glaciofluvial processes, caution should be taken against oversimplifying complex glacial and periglacial processes. Bogen and Bønses (2003) found that considerable englacial and subglacial sediment transfer occurs even in cold-ice, with large floods suggested to have a flushing effect through stable englacial and subglacial cold-ice tunnels, exhausting sediment sources. This contrasts with the interpretation of Hodson et al. (1998) that the relatively low sediment yields and increase in suspended sediment availability to rising discharge for the 1991 and 1992 open-channel seasons in the Austre Brøggerbreen Glacier's catchment resulted from the absence of subglacial delivery processes, with only supraglacial, englacial, and marginal pathways supplying sediment.

McCall Glacier is within the same region of Alaska as Lake Peters, and has been intensively researched since the 1957-1958 International Geophysical Year. McCall Glacier is losing mass exponentially, consistent with regional (Nolan et al., 2005) and global (Zemp et al., 2015) trends. The glacier is thought to be polythermal, with warm-ice deformation and/or basal motion playing a role (Nolan et al., 2005; Pattyn et al., 2009). The basal topography is reportedly complex in the confluence area of different glacial cirques, and downstream from this a confluence of subglacial water has been identified (Pattyn et al., 2009).

1.3.6 Floods and Hysteresis

Elevated SSCs are commonly contemporaneous with elevated discharges, although the relationship between SSCs and discharge can be non-linear and complex. SSCs can vary by an order of magnitude or more for the same discharge, and a number of orders of magnitude through a single season (Morehead et al., 2003). Hysteresis is a circular SSC – discharge relation through a flood event, or diurnally. Clockwise hysteresis loops are associated with higher SSCs on the rising limb of a hydrograph, than for the same discharge on the falling limb. For flood hydrographs, this is commonly attributed to greater in-channel availability of easily erodible sediment from newly tapped sources in the early stages of a flood. Clockwise hysteresis may also be attributed to varying

discharge sources, such as meltwater versus rainfall, or changes in sediment source areas (Morehead et al., 2003). Conversely, counterclockwise hysteresis loops are associated with lower SSCs on the rising limb of a flood hydrograph, than for the same discharge on the falling limb. They are commonly the result of seasonal changes in suspended sediment and water sources, such as late-season glacial-melt discharges carrying higher sediment loads than early season snowmelt (Morehead et al., 2003). Erosion of bed armoring through a flood event can also increase SSCs on the falling limb of a flood hydrograph (Morehead et al., 2003).

At the annual time-scale, the majority of sediment can be transferred during one or more discrete flood events. Rainfall can increase sediment yields by hydrologically connecting otherwise isolated sediment source areas (Lewis et al., 2012), and is an important control of landscape denudation (Rasch et al., 2000). At Bayelva, Svalbard, flooding between 1989-2000 is recorded, especially late in the open-channel season, with peak rainfall and SSC in August 1990. Late-season rainfall-induced flooding has also been recorded at the Zackenbergelven River, Northeast Greenland, following an early-mid-season nival regime (Rasch et al., 2000). Conversely, the highest SSCs and majority of suspended sediment transfer in the Colville River, Alaska, was recorded during early-season snowmelt flooding (Arnborg et al., 1967). At Endalselva, Svalbard, floods caused elevated SSCs between 1994-1997, with SSC reaching 9000 mg/L during the largest flood recorded in 1997 (Bøgen and Bonses, 2003). At Lake Linnévat, Svalbard, inclusion of discharge in the best-fit varve-based sedimentation model for 1991-2009, in addition to summer temperature and rainfall, indicated the importance of flooding (Schiefer et al., 2017).

Variable hydrographic conditions are reported between open-channel seasons at both Lake Linnévat, Svalbard (Schiefer et al.,2017) and Cape Bounty, Melville Island, Canada (Lewis et al., 2012). At Lake Linnévat, rainfall induced flooding was recorded in 2004, but not in 2005 or 2006 (Schiefer et al.,2017). At Cape Bounty, rainfall induced flooding, associated with peak SSCs and elevated sediment yields, was recorded in 2007-2009, but not in 2006 when discharge followed a nival regime (Lewis et al., 2012). On an inter-annual scale, extreme flood events that carry unusually high sediment loads can cause morphological changes that affect long-term sediment sources and delivery processes within a catchment or region (Menounos et al., 2006). For example, a rare summer rainstorm delivered more suspended sediment to Green Lake, British Columbia, Canada, than recorded in the past 3000 years (Menounos et al., 2006).

1.3.7 Sediment Exhaustion

Sediment depletion may occur after the first major flood of the season (Bogen and Bønses, 2003; Morehead et al., 2003), or alternatively sediment may remain persistently high following flood events of various scales (Menounos et al., 2006). Within a season, sediment exhaustion may be associated with the flushing effect of flood events (Bogen and Bønses, 2003; Morehead et al., 2003), exhaustion of the snowpack (Forbes and Lamoureux, 2005), or exhaustion of subglacial reservoirs (Bogen and Bønses, 2003; Hodgkins et al., 2003; Irvine-Fynn et al., 2005).

Forbes and Lamoureux (2005) found that snowpack exhaustion throughout the open-channel season exerted a significant control on SSC in a large deglaciated mid-Arctic catchment on Boothia Peninsula, Nunavut, Canada. Approximately half the annual sediment yield was transferred during maximum snowmelt periods, resulting in a sediment yield four times higher in 2001 with greater snow-water equivalent (SWE), compared with 2002 (Forbes and Lamoureux, 2005).

Subglacial sediment exhaustion has been found to vary in space (Irvine-Fynn et al., 2005) and time (Hodgkins et al., 2003). Irvine-Fynn et al. (2005) show seasonal exhaustion of the subglacial reservoir at the polythermal Midre Lovénbreen in Spitsbergen, Svalbard, but no seasonal exhaustion of the polythermal Stagnation (B28) Glacier on Bylot Island, Nunavut. Potential explanations for absence of exhaustion at the latter include: scouring of the subglacial source area via a hydraulically efficient route, or a less extensive subglacial network resulting in ice-marginal and icing sources outweighing the subglacial signal (Irvine-Fynn et al., 2005). Hodgkins et al. (2003) inferred exhaustion of sediment sources from the polythermal Finsterwalderbreen Glacier in 1999, but not in 2000. This was related to an episodic runoff regime in 1999 associated with proglacial aggradation, and a sustained runoff regime in 2000 associated with proglacial denudation (Hodgkins et al., 2003).

1.4 Conclusion

The Arctic is experiencing disproportionate climate warming, predicted to significantly increase sediment yields over the coming century (Syvitski, 2002; Lewis and Lamoureux, 2010), and this will have consequences for people and ecosystems (Moore et al., 2009). Processes driving arctic sediment transfer are complex, and relatively little hydroclimatic systems science has been undertaken for catchments above the Arctic Circle. A number of forces influence sediment yields, including: climate, geography, geology, glacial coverage, glacial thermal regimes and processes, and sediment storage, availability, and exhaustion. Untangling dominant processes driving arctic sediment transfer at regional- and catchment-scales will help our understanding of how the Arctic will change in coming decades, as well as informing reconstructions of past environments.

1.5 References

Abram NJ, McGregor HV, Tierney JE, Evans MN, McKay NP, Kaufman DS, PAGES 2k Consortium. 2016. Early onset of industrial-era warming across the oceans and continents. *Nature* **536**: 411-432. DOI: 10.1038/nature19082.

Alaska National Interest Lands Conservation Act. 1980. Retrieved December 2016 from: https://fs.usda.gov/Internet/FSE_DOCUMENTS/fsbdev2_037581.pdf.

Arnborg L, Walker HJ, Peippo J. 1967. Suspended Load in the Colville River, Alaska. *Geografiska Annaler* **49 A** (2-4): 131-144.

Bintanja R, Andry O. 2017. Towards a rain-dominated Arctic. *Nature Climate Change* **7**: 263-268. DOI: 10.1038/NCLIMATE3240**.**

Bogen J, Bønsnes TE. 2003. Erosion and sediment transport in High Arctic rivers, Svalbard. *Polar Research* **22**(2): 175-189.

Boldt BR, Kaufman DS, McKay NP, Briner JP. 2015. Holocene summer temperature reconstruction from sedimentary chlorophyll content, with treatment of age uncertainties, Kurupa Lake, Arctic Alaska. *The Holocene* **25**(4): 641-650. DOI: 10.1177/0959683614565929.

Carrivick JL, Tweed FS. 2013. Proglacial lakes: character, behavior and geological importance. *Quaternary Science Reviews* **78**: 34-52. DOI: 10.1016/j.quascirev.2013.07.028.

Cassano EN, Cassano JJ, Nolan M. 2011. Synoptic weather pattern controls on temperature in Alaska. *Journal of Geophysical Research* **116**: 1-19. DOI: 10.1029/2010JD015341.

Church M, Ryder M. 1972. Paraglacial Sedimentation: A Consideration of Fluvial Processes Conditioned by Glaciation. *Geological Society of America Bulletin* **83**: 3059-3072.

Church M, Slaymaker O. 1989. Disequilibrium of Holocene sediment yield in glaciated British Columbia. *Nature* **337**: 452-454.

Corn ML. 2003. Arctic National Wildlife Refuge: Background and Issues. Report for Congress. The Library of Congress: USA.

Diedrich KE, Loso MG. 2012. Transient impacts of Little Ice Age glacier expansion on sedimentation processes at glacier-dammed Iceberg Lake, southcentral Alaska. *Journal of Paleoclimatology* **48**: 115-132. DOI 10.1007/s10933-012-9614-5.

Docherty B. 2001. Challenging Boundaries: The Arctic National Wildlife Refuge and International Environment Law Protection. *New York University Environmental Law Journal* **10**: 70-116.

Ellis JM, Calkin PE. 1984. Chronology of Holocence glaciation, central Brooks Range, Alaska. *Geological Society of America Bulletin* **95**: 897-912.

Evison LH, Parker EC, Ellis JM. 1996. Late-Holocene glaciation and twentieth-century retreat, northeastern Brooks Range, Alaska. *The Holocene* **6**(1): 17-24.

Finkenbinder MS, Abott MB, Finney BP, Stoner JS, Dorfman JM. 2015. A multi-proxy reconstruction of environmental change spanning the last 37,000 years from Burial Lake, Arctic Alaska. *Quaternary Science Reviews* **126**: 227-241. DOI: 10.1016/jquascirev.2015.08.031.

Forbes AC, Lamoureux SF. 2005. Climatic Controls on Streamflow and Suspended Sediment Transport in Three Large Middle Arctic Catchments, Boothia Peninsula, Nunavut, Canada. *Arctic, Antarctic, and Alpine Research* **37**(3): 304-315.

Guymon GL. 1974. Regional Sediment Yield Analyses of Alaska Streams. *Journal of the Hydraulics Division—ASCE* **100**: 41-50.

Hallet B, Hunter L, Bogen J. 1996. Rates of erosion and sediment evacuation by glaciers: A review of field data and their implications. *Global and Planetary Change* **12**: 213-235.

Hamilton TD. 2003. Surficial Geology of the Dalton Highway (Itkillik-Sagavanirktok Rivers) Area, Southern Arctic Foothills, Alaska. Professional Report 121. State of Alaska Department of Natural Resources / Division of Geological and Geophysical Surveys: Fairbanks, Alaska.

Hasholt B. 2016. Sediment and solute transport from Greenland. In Source-to-Sink Fluxes in Undisturbed Cold Environments, Beylich A, Dixon J, Zwoliński Z (eds). Cambridge University Press: Cambridge; 79-95. DOI:10.1017/CBO9781107705791.010.

Hobbie JE. 1962. Limnological Cycles and Primary Productivity of Two Lakes in the Alaskan Arctic, PhD Thesis. Indiana University, IN; 131 pp.

Hodgkins R. 1996. Seasonal trend in suspended-sediment transport from an Arctic glacier, and implications for drainage-system structure. *Annals of Glaciology* **22**: 147-151.

Hodgkins R, Cooper R, Wadham J, Tranter M. 2003. Suspended sediment fluxes in a high-Arctic glacierised catchment: implications for fluvial sediment storage. *Sedimentary Geology* **162**: 105-117. DOI: 10.1016/S0037-0738(03)00218-5.

Hodson AJ, Ferguson RI. 1999. Fluvial Suspended Sediment Transport from Cold and Warm-Based Glaciers in Svalbard. *Earth Surfaces Processes and Landforms* **24**: 957-974.

Hodson A, Gurnell A, Tranter M, Bogen J, Hagen JO, Clark M. 1998. Suspended sediment yield and transfer processes in a small High-Arctic glacier basin, Svalbard. *Hydrological Processes* **12**: 73-86.

Irvine-Fynn TDL, Moorman BJ, Willis IC, Sjogren DB, Hodson AJ, Mumford PN, Walter FSA, Williams JLM. 2005. Geocryological processes linked to High Arctic proglacial stream suspended sediment dynamics: examples from Bylot Island, Nunavut, and Spitsbergen, Svalbard. *Hydrological Processes* **19**: 115-135. DOI: 10.1002/hyp.5759.

Kaufman DS, Young NE, Briner JP, Manley WF. 2011. Alaska Palaeo-Glacier Atlas (Version 2). In Developments in Quaternary Science **15**, Ehlers J, Gibbard PL, Hughes PD (eds). Elsevier: Amsterdam, The Netherlands; 427-445. DOI: 10.1016/B978-0-444-53447-7.00033-7.

Kienholz C, Herreid S, Rich JL, Arendt AA, Hock R, Burgess EW. 2015. Derivation and analysis of a complete modern-date glacier inventory for Alaska and northwest Canada. *Journal of Glaciology* **61**(227). DOI: 10.3189/2015/JoG14J230.

Klok EJ, Nolan M, Van Den Broeke MR. 2005. Analysis of meteorological data and the surface energy balance of McCall Glacier, Alaska, USA. *Journal of Glaciology* **51**(174): 451-461. DOI: 10.3189/172756505781829241.

Lammers RB, Shiklomanov AI, Vörösmarty CJ, Fekete BM, Peterson BJ. 2001. Assessment of contemporary Arctic river runoff based on observational discharge records. *Journal of Geophysical Research* **106**(D4): 3321-3334.

Leonard EM. 1997. The relationship between glacial activity and sediment production: evidence from a 4450-year varve record of neoglacial sedimentation in Hector Lake, Alberta, Canada. *Journal of Paleolimnology* **17**: 319-330.

Lewis T, Lafrenière MJ, Lamoureux SF. 2012. Hydrochemical and sedimentary responses of paired High Arctic watersheds to unusual climate and permafrost disturbance, Cape Bounty, Melville Island, Canada. *Hydrological Processes* **26**. DOI: 10.1002/hyp.8335.

Lewkowicz AG, Wolfe PM. 1994. Sediment Transport in Hot Weather Creek, Ellesmere Island, N.W.T., Canada, 1990-1991. *Arctic and Alpine Research* **26**(3): 213-226.

Loso MG. 2009. Summer temperatures during the Medieval Warm Period and Little Ice Age inferred from varved proglacial lake sediments in southern Alaska. *Journal of Paleolimnology* **41**: 117-128. DOI 10.1007/s10933-008-9264-9.

McKay NP, Kaufman DS. 2014. An extended Arctic proxy temperature database for the past 2,000 years. *Scientific Data* **1**: 140026. DOI: 10.1038/sdata.2014.26.

Menounos B, Schiefer E, Slaymaker O. 2006. Nested temporal suspended sediment yields, Green Lake Basin, British Columbia, Canada. *Geomorphology* **79**: 114-129. DOI: 10.1016/j.geomorph.2005.09.020.

Milliman JD, Syvitski JPM. 1992. Geomorphic/Tectonic Control of Sediment Discharge to the Ocean: The Importance of Small Mountainous Rivers. *The Journal of Geology* **100**: 525-544.

Molnia BF. 2007. Late nineteenth to early twenty-first century behavior of Alaskan glaciers as indicators of changing regional climate. *Global and Planetary Change* **56**: 23-56. DOI: 10.1016/j.gloplacha.2006.07.011.

Monaghan NJ. 2009. Symposium on the Environment: "Note: Drill, Baby, Drill!": The Arctic National Wildlife Refuge and America's Energy Reckoning. *Notre Dame Journal of Law, Ethics & Public Policy* **23**: 649-672.

Morehead MD, Syvitski JP, Hutton EWH, Peckham SD. 2003. Modeling the temporal variability in the flux of sediment from ungauged river basins. *Global and Planetary Change* **39**: 95-110. DOI: 10.1016/S0921-8181(03)00019-5.

Moore RD, Fleming SW, Menounos B, Wheate R, Fountain A, Stahl K, Holm K, and Jakob M. 2009. Glacier change in western North America: influences on hydrology, geomorphic hazards and water quality. *Hydrological Processes* **23**: 42-61. DOI: 10.1002/hyp.7162.

Naito AT, Cairns DM. 2015. Patterns of shrub expansion in Alaskan arctic river corridors suggest phase transition. *Ecology and Evolution* **5**(1): 87-101. DOI: 10.1002/ece3.1341.

Nolan M, Arendt A, Rabus B, Hinzman L. 2005. Volume change of McCall Glacier, Arctic Alaska, USA, 1956-2003. *Annals of Glaciology* **42**: 409-416.

O'Farrell CR, Heimsath AM, Lawson DE, Jorgensen LM, Evenson EB, Larson G, Denner J. 2009. Quantifying periglacial erosion: insights on a glacial sediment budget, Matanuska Glacier, Alaska. *Earth Surface Processes and Landforms* **34**: 2008-2022. DOI: 10.1002/esp.1885.

Orwin JF, Lamoureux SF, Warburton J, Beylich A. 2010. A Framework for Characterizing Fluvial Sediment Fluxes from Source to Sink in Cold Environments. *Geografiska Annaler* **92 A**(2): 155-176.

Orwin JF, Smart CC. 2004. The evidence for paraglacial sedimentation and its temporal scale in the deglacierizing basin of Small River Glacier, Canada. *Geomorphology* **58**: 175-202. DOI: 10.1016/j.geomorph.2003.07.005.

Pattyn F, Delcourt C, Samyn D, De Smedt B, Nolan M. 2009. Bed properties and hydrological conditions underneath McCall Glacier, Alaska, USA. *Annals of Glaciology* **50**(51): 80-84.

Rainwater FH, Guy HP. 1961. Some Observations on the Hydrochemistry and Sedimentation of the Chamberlin Glacier Area Alaska. In *Shorter Contributions to General Geology*, United States Geological Survey (eds), USGS Professional Paper 414-C. United States Government: Washington; C1-C14.

Rasch M, Elberling B, Jakobsen BH, Hasolt B. 2000. High-Resolution Measurements of Water Discharge, Sediment, and Solute Transport in the River Zackenbergelven, Northeast Greenland. *Arctic, Antarctic, and Alpine Research* **32**(3): 336-345.

Reed BL. 1968. Geology of the Lake Peters Area Northeastern Brooks Range, Alaska. *Geological Survey Bulletin.* **1236**: 1-132.

Schiefer E. 2006. Contemporary sedimentation rates and depositional structures in a montane lake basin, southern Coast Mountains, British Columbia, Canada. *Earth Surface Processes and Landforms* **31**: 1311-1324. DOI: 10.1002/esp.1332.

Schiefer, E, Kaufman D, McKay N, Retelle M, Werner A, Roof S. 2017. Fluvial suspended sediment yields over hours to millennia in the High Arctic at proglacial lake Linnévatnet, Svalbard. *Earth Surface Processes and Landforms*. DOI: 10.1002/esp.4264.

Schiefer E, Slaymaker O, Klinkenberg B. 2001. Physiographically Controlled Allometry of Specific Sediment Yield in the Canadian Cordillera: a Lake Sediment-Based Approach. *Geografiska Annaler* **83 A**(1-2): 55-65.

Schiefer E, Petticrew EL, Immell R, Hassan MA, Sonderegger DL. 2013. Land use and climate change impacts on lake sedimentation rates in western Canada. *Anthropocene* **3**: 61-71. DOI:10.1016/j.ancene.2014.02.006.

Serreze MC, Barrett AP, Stroeve JC, Kindig DN, Holland MM. 2009. The emergence of surface-based Arctic amplification. *The Cryosphere* **3**: 11-19.

Serreze MC, Barrett P, Cassano JJ. 2011. Circulation and surface controls on the lower tropospheric air temperature field of the Arctic. *Journal of Geophysical Research* **116**: 1-20. DOI: 10.1029/2010JD015127.

Serreze MC, Barrett AP, Stroeve J. 2012. Recent changes in tropospheric water vapor over the Arctic as assessed from radiosondes and atmospheric reanalyses. *Journal of Geophysical Research* **117**: 1-21. DOI: 10.1029/2011JD017421.

Syvitski JPM. 2002. Sediment discharge variability in Arctic rivers: implications for a warmer future. *Polar Research* **21**(2): 323-330.

Tape KD, Verbyla D, Welker JM. 2011. Twentieth century erosion in Arctic Alaska foothills: The influence of shrubs, runoff, and permafrost. *Journal of Geophysical Research* **116**: 1-11, DOI: 10.1029/2011JG001795.

Tingley MP, Huybers P. 2013. Recent temperature extremes at high northern latitudes unprecedented in the past 600 years. *Nature* **496**: 201-208. DOI:10.1038/nature11969.

Thurston (in prep). Modeling Fine-grained Fluxes for Estimating Sediment Yields and Understanding Hydroclimatic and Geomorphic Processes at Lake Peters, Brooks Range, Arctic Alaska, Unpublished MS Thesis. Northern Arizona University, Flagstaff; 89 pp.

Wilderness Act. 1964. Retrieved December 2016 from: http://www.wilderness.net/NWPS/documents //publiclaws/PDF/16_USC_1131-1136.pdf.

Zemp M, Holger F, Gärtner-Roer I, Nussbaumer SU, Hoelzle M, Paul F, Haeberli W, Denzinger F, Ahlstrøm AP, Anderson B, Bajracharya S, Baroni C, Braun LN, Cáceres BE, Casassa G, Cobos G, Dávila LR, Degado Grandadoes H, Demuth MN, Espizua L, Fischer A, Fujita K, Gadek B, Ghazanfar A, Hagen JO, Holmlund P, Karimim N, Zhongqin L, Pelto M, Pitte P, Popovnin VV, Portocarrero CA, Prinz R, Sangewar CV, Severskiy I, Sigurdsson O, Soruco A, Usubaliev R, Vincent C. 2015. Historically unprecedented global glacier decline in the early 21st century. *Journal of Glaciology* **61**(228): 745-760. DOI: 10.3189/2015JoG15J017.

2 MULTIVARIATE MODELING OF SUSPENDED SEDIMENT DISCHARGE TO LAKE PETERS, NORTHEAST BROOKS RANGE, ALASKA

2.1 Abstract

Multivariate statistical models of suspended sediment concentrations, incorporating hydrological, climatic, and temporal explanatory variables, are used to reconstruct sediment yields for the 2015 and 2016 open-channel seasons in the Carnivore Creek and Chamberlin Creek sub-catchments of Lake Peters, Brooks Range, Alaska. For both sub-catchments, incorporating explanatory variables additional to discharge or turbidity statistically improved model performance. Turbidity-based models outperformed discharge-based models, but data limitations required models to be bridged to estimate annual specific sediment yields of: 53 (40-230) Mg km^{-2} yr^{-1} in 2015, and 90 (80-230) Mg km^{-2} yr^{-1} in 2016. Rainfall was found to be the dominant driver of sediment transfer in both sub-catchments, with temperature and snow-water equivalent found to be secondary. Albeit comparable drivers, sediment transfer processes differed between the sub-catchments. Carnivore Creek sub-catchment (128 km^2) captured comparatively high magnitude discharges from rainfall and rain-on-snow events, driving high suspended sediment concentrations during these events. Evidence for seasonal sediment exhaustion was only observed for the small, steep Chamberlin Creek sub-catchment.

2.2 Introduction

Quantitative estimates of annual fluvial suspended sediment yields (sediment yields) are sought after by physical scientists as signals of hydroclimatic and geomorphic dynamics, by ecologists for their associations with water quality and habitat, and by engineers for development applications. Estimating sediment yields presents a challenge, because suspended sediment concentrations (SSCs) are inherently variable in space and time (Orwin et al., 2010). SSCs, and associated sediment yields, typically reflect catchment-scale processes (Hodgkins et al., 2003), including climate forcing (Syvitski, 2002; Lewis and Lamoureux, 2010), and geomorphic processes, especially sediment supply and exhaustion (Bogen and Bønses, 2003; Morehead et al., 2003; Hodgkins et al., 2003; Forbes and Lamoureux, 2005; Irvine-Fynn et al., 2005). The majority of a catchment's sediment yield can be transported during one or a few discrete events (Arnborg et al., 1967; Bøgen and Bonses, 2003; Menounos et al., 2006; Lewis et al., 2012; Schiefer et al., 2017). Sediment yields also vary significantly on inter-annual and decadal bases (Bogen and Bønses, 2003; Lewkowicz and Wolfe, 1994; Menounos et al., 2006; Tape et al., 2011; Lewis et al., 2012), and may reflect landscape evolution over several tens of thousands of years associated with Quaternary glacial events (Church and Ryder, 1972; Church and Slaymaker, 1989). Instrumentation and sampling programs to directly measure SSCs at less than daily, or preferably less than hourly sampling intervals (Orwin et al., 2010), over periods greater than one year are very limited, especially in the Arctic (Guymon, 1974; Fenn et al., 1985). Consequently, statistical models are relied upon to reconstruct sediment yields from discontinuous samples of SSC.

Statistical models traditionally comprise simple sediment rating curves, using either discharge or turbidity as a single predictor of SSC, but failure to adequately account for quasi-autocorrelation has been identified as a pitfall associated with their use (Hodgkins, 1999; Hodson and Ferguson, 1999). Quasi-autocorrelation arises from shortfalls in formulation of the regression model, including: applying an incorrect fit; failing to identify the presence of lags, and/or changes in response between the dependent and independent variables; and omissions of relevant independent variables (Fenn et al., 1985; Hodson and Ferguson, 1999). Under-prediction of high SSCs and over-prediction of low SSCs is common, meaning errors are reduced over longer monitoring periods (Horowitz, 2003), but these are rare in remote arctic environments (Guymon, 1974; Bogen and Bønses, 2003). Statistical methods can be applied to address quasi-autocorrelation, improving the predictive ability of sediment rating curves. For example, separating rating curves according to discrete temporal periods, or stage, have both proven popular, with varied success (Walling, 1977; Asselman, 2000; Horowitz, 2003; Irvine-Fynn et al., 2005; Harrington and Harrington, 2013).

Multivariate regression models are often preferable over rating curve separation, because they are part of an inverse chain of forward–system models, required to understand multifaceted, dynamic processes driving glacier-hydrology-lake-sedimentation (Walling, 1977; Hodson and Ferguson, 1999; Irvine-Fynn et al., 2005). Changes in sediment transfer response to system forcing can be addressed by the inclusion of multiple explanatory variables, and optimal lag times selected for

modeling. Temporal variables can account for sediment supply unrelated to discharge, including: seasonal variations, hysteresis effects, transient flushes of sediment from glacial or proglacial sources, and rainfall-induced sediment dynamics (Fenn et al., 1985). Climate variables can also capture temporal variability in SSCs, including diurnal and longer cycles of solar radiation and temperature, and rainfall-induced events. Additionally, understanding climate forcing on sediment transfer helps assess the sensitivity of the Arctic to climate change, and supports interpretation of past climates from paleo-sedimentary records, as well as hydroclimatic system forecasting (Syvitski, 2002; Forbes and Lamoureux, 2005; Lewis and Lamoureux, 2010).

Despite potential advantages, multivariate sediment models are uncommon in catchments above the Arctic Circle (Hodgkins, 1999; Hodson and Ferguson, 1999; Irvine-Fynn et al., 2005; Schiefer et al., 2017). In Arctic Alaska (defined here as Alaskan land above the Arctic Circle—66.33°N), even simple sediment rating curves have rarely been constructed (Rainwater and Guy, 1961; Arnborg et al., 1967). The objective of this paper is to use multivariate regression models to estimate sediment yields, and interpret physical processes driving these yields, over two open-channel seasons at Lake Peters, Brooks Range, Alaska.

2.3 Study Area

2.3.1 Geography and Geology

Lake Peters (69.32°N 145.05°W) is situated in the Arctic National Wildlife Refuge, north-eastern Brooks Range, approximately 300 km north of the Arctic Circle, and 70 km from the Arctic Ocean (**Figure 2.1**). Lake Peters' catchment (169 km^2) is ringed by steep mountains, and as of August 2016 was 8% glaciated with some of the largest valley glaciers in Arctic Alaska. Bedrock comprises low-grade metasedimentary and sedimentary rocks, primarily southward-dipping sandstone, semischist, and phyllite, with minor chert and quartzite (Reed, 1968). In the north-eastern Brooks Range, including at Chamberlin Glacier, four major Holocene glacier still-stands are recorded by terminal moraine deposits (Evison et al., 1996). Terminal cirque and lateral moraines attributed to the latter two still-stands during the Little Ice Age (LIA)—*ca.* 1200-1850 CE are conspicuous below and adjacent to glaciers. Since the LIA, medium sized glaciers (~1 km^2) within Lake Peters' catchment have reduced in length by approximately 20%, and the largest valley glaciers (1.9-3.6 km^2) have reduced in length by at least 30%. Soils are sparse, and vegetation largely consists of arctic grasses, herbs, and shrubs. Channel-side vegetation is sparse above 1300 m, but vegetation persists on some higher slopes less affected by debris movement.

2.3.2 Fluvial Geomorphology

At present-day Lake Peters (6.8 km^2; 52 m deep; 854 m asl), lake ice persists for most of the year. Lake Peters drains into Lake Schrader, and Lake Schrader drains into the Kekiktuk River, a tributary of the Sadlerochit River, which discharges into the Arctic Ocean. Carnivore Creek (128 km^2 catchment area; 9% glacial coverage), and Chamberlin Creek (8 km^2 catchment area; 26% glacial

coverage), contribute the two largest discharges to Lake Peters, respectively, although several minor non-glacial catchments also flow into Lake Peters over and through alluvial fans (**Figure 2.1**).

The Carnivore Creek sub-catchment covers 76% of the total area of Lake Peters' catchment. The eastern side of the valley is glacierized, channels are more deeply incised, and distances from alluvial fan apexes to toes are shorter, compared to the western side of the valley. Lower Carnivore Creek has a shallow slope and plane bed morphology. The surrounding floodplain has hummocky terrain, with periglacial surface features. Chamberlin Creek's catchment is comparatively steep, with the summit of Mount Chamberlin (2750 m asl) only 4.7 km from Lake Peters. Chamberlin Glacier (1.9 km²) is the third largest glacier in Lake Peters' catchment, behind the two glaciers at the head of Carnivore Creek. In the upper-catchment, Chamberlin Creek flows over and through moraines; in the mid-catchment the channel has incised into a confined bedrock-controlled valley, with steep step-pools; and downstream of the alluvial fan apex, the creek flows over lower-grade step-pools.

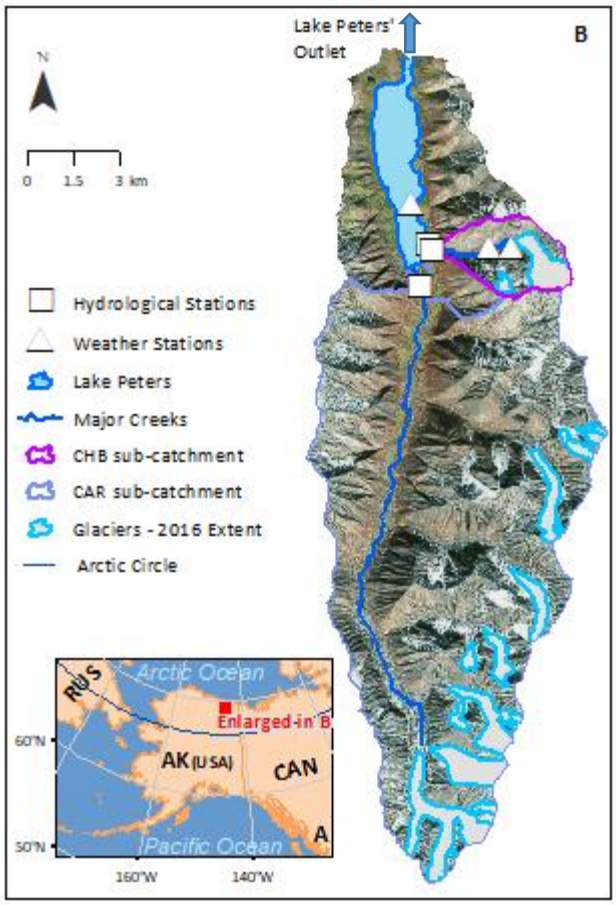

Figure 2.1: Map of the study area. A) Location of Lake Peters' catchment in Alaska (AK), and adjacent Canada (CAN) and Russia (RUS) B) Lake Peters' catchment, showing geographical features, hydrological stations, and weather stations, all described in-text. Base-map imagery sourced from ESRI DigitalGlobe.

2.3.3 Climate

From the 11th to the 19th Century, the Arctic experienced a long-term cooling trend, estimated from reconstructions to be 0.47°C kyr^{-1}, followed by rapid 20th Century warming (McKay and Kaufman, 2014). In Alaska, a general cooling of annual air temperatures has been reported from the 1950s through to 1976, followed by rapid warming (Cassano et al., 2011), driving widespread glacial recession and thinning (Molnia, 2007), and increased winter runoff over pan-Arctic Alaska (Lammers et al., 2001). The temperature shift around 1976 is attributed to a deepening and shifting of the Aleutian Low, and changes unrelated to atmospheric circulation, including: increased nighttime cloudiness, a global warming signal, and/or increased sea surface temperatures (Cassano et al., 2011). The mean temperature increase in Alaska since the mid-20th century is ~2°C (Molnia, 2007). Interpolated climate data for Lake Peters (1980 - 2009) shows mean annual precipitation of 360 mm, and mean January and July monthly temperatures of -22.0°C and 10.5°C, respectively (Stavros and Hill, 2013).

2.4 Methods

SSCs near the outlets of Carnivore and Chamberlin Creeks to Lake Peters were modeled using a combination of hydrologic, climatic, and temporal variables. The modeling periods are the 2015 and 2016 open-channel seasons (18 May - 18 September each year; expected to capture the majority of annual sediment transfer). The collection and reconstruction of candidate variables input to the modeling process is described below, with supplementary information provided in **Appendix I**, followed by a description of the regression technique.

2.4.1 Continuous Monitoring

Hydrological and meteorological stations were setup for continuous monitoring at 30 or 60 minute intervals (**Figure 2.1**). At the hydrological stations, we used In-Situ TROLL 9500 ("TROLL") instruments to measure water-pressure and turbidity, and Hobo Onset U20 ("Hobo") instruments to measure water-pressure. During the 2015 and 2016 open-channel seasons in Carnivore Creek, and 2015 open-channel season in Chamberlin Creek, the TROLL and Hobo instruments were attached to a cage constructed from aluminum pipes and chicken-wire, then loaded with boulders to prevent movement. We situated the cages in thalwegs of relatively stable reaches close to Lake Peters, upstream from where the main channel anabranches. During the 2016 open-channel season in Chamberlin Creek, the TROLL and Hobo instruments were attached to a PVC pipe secured to channel-side bedrock at the apex of the alluvial fan. Time-lapse cameras were setup to photograph the hydrological stations every half-hour throughout the open-channel seasons.

At meteorological stations, we recorded air temperature, ground temperature (2 and 30 cm depth), and precipitation, all at elevations of 854 m, 1425 m, and 1750 m. The meteorological station at 854 m elevation also recorded solar radiation and barometric pressure (**Figure 2.1**). Hobo Onset instruments were used, including: a RG3-M rain gauge with 0.2 mm pendant; a U23-001 Pro v2 air temperature and relative humidity sensor; S-TMB-M002 air temperature and relative humidity

sensor, housed within a protective RS1 solar radiation shield; U-23-003 ground temperature sensors; a S-LIB-M003 barometric pressure sensor; and a Silicon Pyranometer Sensor and Light Sensor Bracket to measure incoming solar radiation.

2.4.2 Field Sampling

SSCs in Carnivore and Chamberlin Creeks were sampled manually at the gauge stations using a depth-integrated handheld device (US DH-48). The liquid volume of each sample was recorded prior to filtering with GN-4 Metricel membrane disc filters (0.8 µm). Filters were later dried in a laboratory oven and weighed (± 0.01 mg).

We used a Hach FH950 portable velocity meter to measure current velocities and cross-sections near the gauge stations, and compute discharge. In the 2016 field-season the velocity meter was inoperable, so only cross-sections were measured. Discharge or cross-sections were sampled concurrently with SSC, at a range of times throughout day and night. Two (2016) or four (2015) field stints of up to three weeks occurred each open-channel season, with hydrological sampling balanced among other field priorities.

2.4.3 Continuous Record Processing

Turbidity data was used as logged, with erroneous data due to fouling or instrument dislodgement removed upon visual inspection of the data, resulting in discontinuous time-series. Conversely, missing and erroneous stage and meteorological data could be reconstructed to give uninterrupted time-series for each open-channel season (refer to **Appendix I** for raw meteorological data and **Appendix II** for regressions used to fill data gaps).

For stage, water-pressure sensors (TROLL or Hobo) and/or timelapse cameras were operative at almost all times throughout both open-channel seasons, enabling data from different sampling methods to be bridged. Where multiple data sources were available, the water-pressure sensor with the greatest data availability for each creek was preferred, resulting in the TROLL primarily being used for Carnivore Creek, and the Hobo primarily being used for Chamberlin Creek. For Chamberlin Creek in 2015, Hobo data was recorded in two different vertical positions, and Hobo Position 1 was adjusted upward to be consistent with Hobo Position 2 using the difference between the average TROLL and Hobo data for each period. We used a consistent method to convert all water-pressure data to stage: barometric pressures were converted from units of mb to m^3 (assuming a water temperature of 4°C); barometric pressures were subtracted from water-pressures; and the heights of the water-pressure sensors above the stream-beds were added.

For precipitation, ground temperature, and air temperature, simple linear regressions between the same, or similar (ground temperature – air temperature), variables at different elevations were used to fill data gaps (section 5.3.2 of **Appendix II**). Additionally, two gaps in barometric pressure (totaling 9.4 days) were filled using a linear regression with data from the nearby McCall catchment

(D. Fortin, personal communication, November 10, 2015), allowing the complete water-pressure records to be adjusted to stage.

2.4.4 Stage – Discharge Rating Curves

For each discharge computed by the velocity meter, a corresponding stage was interpolated to match the sampling time. Subsequently, we used discharge–stage regressions to construct continuous half-hourly discharge for the 2015 open-channel season. For the 2016 open-channel season, alternative methods were applied due to lack of velocity data required to compute discharge. We assumed consistent discharge-stage relations between open-channel seasons.

To reconstruct Carnivore Creek discharge throughout the 2016 open-channel season, we first regressed stage against cross-sectional area for both open-channel seasons separately. Subsequently, we adjusted the 2016 stage record upward to be consistent with the 2015 stage record, thereby accounting for the shift in instrument positioning between years. The 2015 stage-discharge regression relation could then be used to reconstruct 2016 discharge.

The same method could not be applied for Chamberlin Creek, because the TROLL and Hobo instruments were secured in different reaches between 2015 (shallow pool on the alluvial fan) and 2016 (deep pool near the fan apex). Instead, we regressed 2015 discharge against cross-sectional area, and applied this relation to construct "sampled" 2016 discharges from available 2016 cross-sectional areas. Following interpolation, new 2016 stage—discharge relations were used to reconstruct continuous half-hourly discharge through to 06/20/16.

Options for reconstructing a discharge record were explored for Chamberlin Creek following the pipe holding the sensors becoming loose on 06/20/16 and subsequently breaking away, and an ad-hoc approach selected. Methods included: photographic records from time-lapse cameras (46 days of discharge were reconstructed using this method; described in-text below); a regression of discharge in Chamberlin Creek against discharge in Carnivore Creek using all available data and a 2-hour lag (3.6 days); a 3-point stage-discharge rating curve, sampled downstream of the rating curve applied prior to 06/20/16 (8.8 days); and where none of the aforementioned alternatives were possible five 2–19-hour gaps were interpolated.

2.4.5 Photographic Reconstructions

Water levels measured on photographs using image viewing and analysis software (as vertical (y) differences) can either be applied to reconstruct stage, or to directly reconstruct discharge. Stage is the more similar independent variable; therefore, may be expected to provide a stronger relation. However, if stage is reconstructed from photographs, more processing steps are required to ultimately find discharge, which increases room for error.

For Carnivore Creek, photographs were used to reconstruct 2.6 days of stage in 2015. The photographic reconstruction was necessary because the cage rolled during a flood on 08/03/15, resulting in missing data. The water level (photographed) – stage (measured using a water pressure

sensor) regression used nine photographs, selected to capture maximal water level variability. The reconstruction of stage was undertaken using a point-to-point method, to capture temporal variability.

For Chamberlin Creek, photographs were used to reconstruct discharge from 06/20/16 when the pipe holding the sensors became loose, to 08/05/16. The photographic reconstruction was necessary because data was too noisy to be used, or filtered for use. A range of water levels visible on 13 photographs were measured using two different reference points. We regressed the results from each reference point separately against discharge. The first reference point was suitable for the majority of flows, but was not accurate after 7/16/16, when water levels dropped low enough to expose a small bar. The second reference point was suitable for low flows, but overtopped during high flows.

2.4.6 Multivariate Regression Modeling of SSCs

We modified the approaches of Hodgkins (1999) and Schiefer et al. (2017) to develop multivariate models for Carnivore and Chamberlin Creeks separately, involving a total of 60 hydrologic, climatic, and time-related explanatory variables, all interpolated to match times of SSC sampling. Hydrologic variables included: turbidity (NTU), discharge ($m^3\ s^{-1}$), cumulative discharge throughout the season ($m^3\ s^{-1}$), change in discharge (since the last measurement; $m^3\ s^{-1}$), and time since discharge was last exceeded (hours), for each creek separately. Turbidity and discharge were both log-transformed to address heteroscedasticity in the data, and meet the assumption that model residuals are (approximately) normally distributed. Climate variables included: summed precipitation (mm), averaged air temperature (^oC), averaged ground temperature (^oC), and averaged solar radiation ($W\ m^{-2}$) at available elevations, all for 2, 6, 12, and 24-hour periods prior to each SSC sample. Temporal variables included: time since sampling was initiated (for each season; hours), and two 24-hour cycle diurnal hysteresis variables, emphasizing noon versus midnight, and early morning (6:00) versus early evening (18:00; dimensionless).

Correlations among predictor variables were calculated in R software, accounting for autocorrelation between predictor variables, within an if-else loop (**Appendix I**). Correlated variables (significance: $p > 0.05$), which could introduce spurious relations if applied as input covariates together, were grouped to ensure that they would not be selected in the same multivariate model. A for-loop was constructed to cycle through the correlated groups, applying the 'glmulti' function for exhaustive candidate testing for each sub-catchment separately (Calcagno and de Mazancourt, 2010). Akaike's information criterion (AIC) was used to assess the relative goodness of fit for each candidate model, while avoiding overfitting (Burnham and Anderson, 2002). Turbidity was removed from the Boolean for-loop and the same method reapplied, to find the best-fit discharge-based model, in addition to the best turbidity-based model.

2.4.7 Sediment Yields

Turbidity-based and discharge-based modeled SSCs (mg m^{-3}) were multiplied by discharge (m^3 s^{-1}) separately to give sediment yield (mg s^{-1}), and units were converted to integrate mass over longer time intervals (g hr^{-1} to Mg yr-1). Prediction intervals for each modeled SSC were calculated in R, and converted to lower and upper sediment yields using the same method. Turbidity-based and discharge-based models were bridged to give continuous records of sediment yield for both Carnivore and Chamberlin Creeks for the majority of the 2015 and 2016 open-channel seasons. For times modeled SSCs could not be reconstructed due to lack of data (early and late open-channel seasons), average sediment yield below the corresponding estimated base-discharge was used. Subsequently, annual sediment yields for the entire open-channel seasons in both creeks could be estimated. Uncertainty in modeled sediment yields was estimated using 95% confidence intervals, but uncertainty was plotted as 95% prediction intervals on the timeseries to capture error associated with random variables and samples of variables.

2.5 Results

2.5.1 Hydrology

Classic discharge – stage power regression relations enabled continuous discharge to be reconstructed in both Carnivore and Chamberlin Creeks for the majority of the 2015 open-channel season (**Figure 2.2 – A and B**). In Carnivore Creek, we used photographs to reconstruct the peak discharge of August 3 2015 (**Figure 2.2 – C**), and estimated the margin of error for the flood peak from photographs. In Chamberlin Creek, linear relations between stage from the Hobo and TROLL instruments permitted compilation of a seamless Hobo record (**Figure 2.2 – D**), prior to conversion to discharge (**Figure 2.2 – B**). For the 2016 open-channel season, we found cross-sectional areas to be a suitable substitute for missing discharge (velocity) data (**Figure 2.2 – E and F**). Adjustments to cross-sectional areas enabled use of the 2015 discharge – stage rating curve in Carnivore Creek (**Figure 2.2 – A**). Salvaged discharge data enabled construction of additional discharge – stage rating curves for May-June 2016 in Chamberlin Creek (**Figure 2.2 – G**).

On the 06/20/16 the PVC pipe holding the Hobo and TROLL instruments in Chamberlin Creek came loose, and an ad-hoc method was used to construct stage and discharge thereafter (**Figure 2.2 – H, I, and J**). We reconstructed the majority of the 2016 stage record from photographs (**Figure 2.2 – I**), with error conservatively 10 to 20 pixels (y differences), except for the flood peak on 7/8/16 at 2:00, for which error is estimated to be 100 pixels because water level and control points were obscured. We favored the photographic method over a regression with Carnivore Creek discharge data for all times photographs were available, to keep the discharge record of each creek independent. Considerable scatter is observed in the latter, even with lags applied, which is attributed to hydrological differences between the catchments (**Figure 2.2 – J**). A Chamberlin Creek hydrological station was re-established in a new location, resulting in a fourth method–a new rating curve being used to construct discharge from 8/8/16 at 18:00 to 8/17/16 at 13:00, recognizing the wider error bands associated with only three discharge measurements being available (**Figure 2.2 – H**).

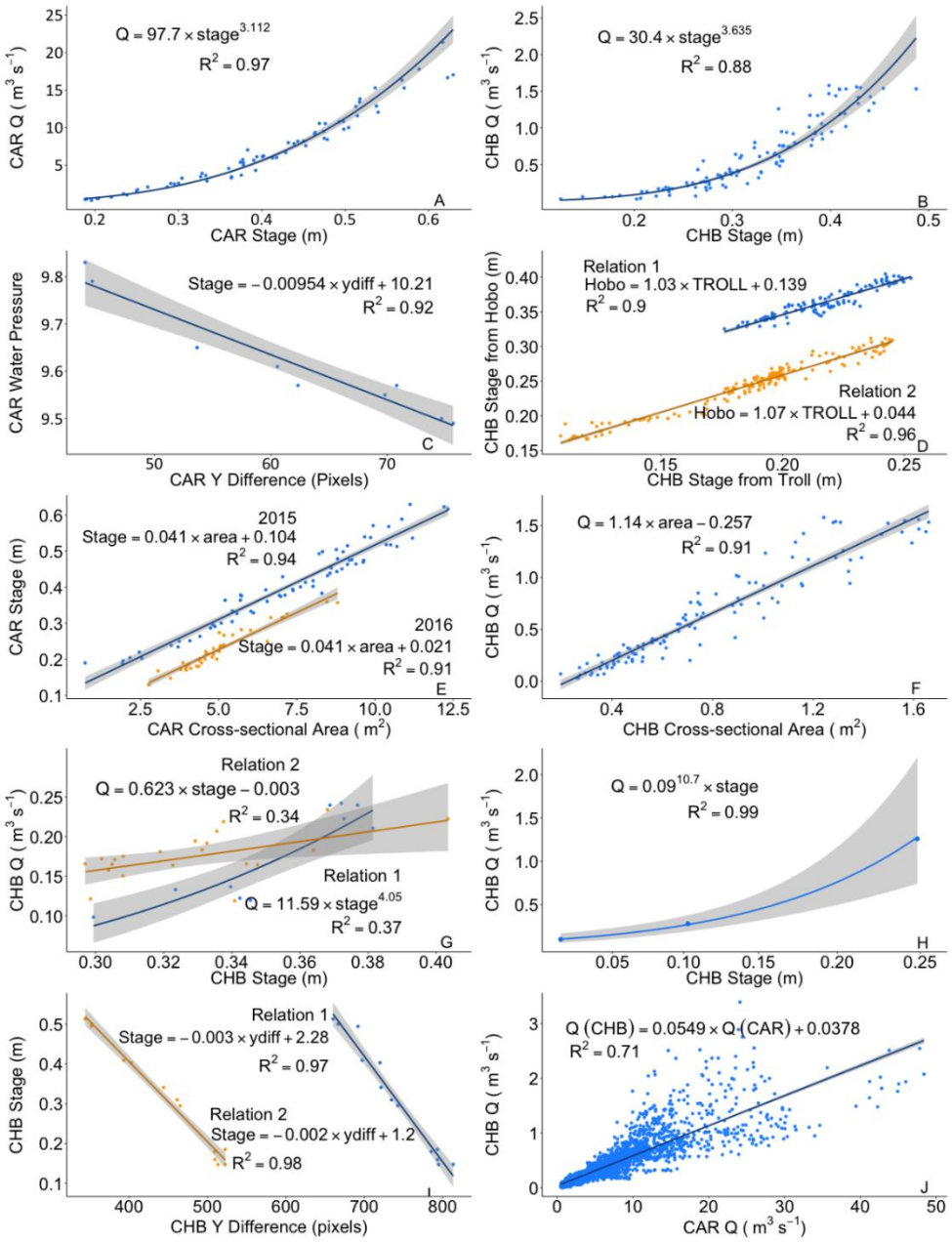

Figure 2.2: Regression relations and associated prediction bands used to create continuous discharge timeseries throughout the 2015 and 2016 open-channel seasons in Carnivore (CAR) and Chamberlin (CHB) Creeks, Brooks Range, Alaska. A) Discharge (Q) – stage relation for CAR (2015); B) Q – stage relation for CHB (2015); C) Water-pressure (from TROLL) – y difference (y-diff; shown on photographs) relation for CAR (2015); D) Relations of stage calculated from Hobo U20 water-pressure against stage calculated from Troll 9500 water-pressure for CHB (both 2015); E) Stage – cross-sectional area linear relation for CAR (2015 and 2016); F) Q – cross-sectional area linear relation for CHB (2015); G) Q – stage (from Hobo) power relation for CHB (2016); H) Q – stage exponential relation for CHB (2016); I) Stage – y difference (y-diff; shown on photographs) linear relations for CHB (both 2016); and J) Relation of Q in CHB against Q in CAR with a 2 hr lag (2015 and 2016). Please refer to section 5.3.1 of **Appendix II** for additional information.

Throughout both creeks and both seasons discharge follows diurnal cycles, peaking around midnight; but between-seasons hydrographs are substantially different (**Figure 2.3**). In 2015, discharge charts five distinct peaks (> 20 $m^3 s^{-1}$ in Carnivore Creek; > 1 $m^3 s^{-1}$ in Chamberlin Creek). In 2016, discharge is elevated for an extended period between mid-June and mid-July in both creeks, with distinct peaks observed in elevated and shoulder periods. Total water discharged from Carnivore Creek during the period of record in 2016 was 28% greater than in 2015, and total water discharged from Chamberlin Creek during the period of record in 2016 was 1% greater than in 2015. Carnivore Creek discharged approximately 95% of the total water volume to Lake Peters in 2015 and 2016. The largest flood peak in both creeks occurred on 07/07/16. Maximum 2016 discharge in Carnivore Creek during this flood (98 $m^3 s^{-1}$) was more than double the maximum 2015 discharge (48 $m^3 s^{-1}$) (**Table 2.1**). Maximum 2016 discharge during this flood in Chamberlin Creek has a wider error margin because it was largely constructed from photographs (**Figure 2.3**), but is estimated to be 21 $m^3 s^{-1}$—seven times larger than the maximum discharge of 3 $m^3 s^{-1}$ in 2015 (**Table 2.1**). Photographic evidence supports quantitative conclusions that the flood of 07/07/16 was more peaked and substantial in Chamberlin Creek, compared with Carnivore Creek.

Table 2.1: Hydrologic and climate statistics for Lake Peters for the period 5/24 – 8/5 (capturing the central open-channel season; 60% of the total open-channel season) in both 2015 and 2016 separately. Variables include: manually sampled (discontinuous) suspended sediment concentration (SSC) in mg L^{-1}; turbidity in NTU; discharge (Q) in $m^3 s^{-1}$; precipitation (Precip.) in mm; air temperature (AT.) in ^oC; and ground temperature (GT.) in ^oC at 2 cm depth, all recorded at elevations of 854 m, 1425 m, and 1750 m. Statistics include the mean (where relevant), minimum (Min) and maximum (Max) for each variable.

	2015			2016		
	Mean	**Min**	**Max**	**Mean**	**Min**	**Max**
CAR SSC	74	2	1434	18	3	99
CHB SSC	53	8	655	32	6	78
[1]CAR NTU	44	6	2617	62	11	2520
[2]CHB NTU	89	3	1201	96	22	539
CAR Q	9	0	48	12	0	98
CHB Q	0.5	0	3	0.5	0	21
[3]Precip. 854 m		0	4		0	3
[4]Precip. 1425 m		0	5		0	8
[5]Precip. 1750 m		0	5		0	7
AT. 854 m	7	-6	20	6	-5	23
[6]AT. 1425 m	6	-10	27	5	-9	19
AT. 1750 m	5	-9	17	3	-11	17
[7]GT. 854 m	6	0	13	5	0	14
GT. 1425 m	7	0	12	5	0	11
[8]GT. 1750 m	8	-1	23	7	-1	21

[1] In 2015 3% of the record is missing, and in 2016 35% of the record is missing.

[2] In 2015 35% of the record is missing, and is 2016 63% of the record is missing.

[3] The record is complete, and precipitation totaled 91.4 mm in 2015 and 155 mm in 2016.
[4] In 2016 31% of the record is missing.
[5] In 2015 12% of the record is missing.
[6] In 2015 4% of the record is missing.
[7] In 2015 9% of the record is missing.
[8] In 2015 12% of the record is missing.
Other records are complete, noting that SSC is discontinuous data, with no high flows sampled in 2016.

Turbidity maxima over 2500 NTU were recorded in Carnivore Creek in both 2015 and 2016. The maximum manually sampled SSC (1400 mg L^{-1}) corresponds with the maximum 2015 NTU, but SSC was not sampled during the 2016 flood. Neither turbidity measurements nor SSC records are available for Chamberlin Creek during the 2016 flood. Available turbidity and manually sampled SSC records for Chamberlin Creek peaked on 6/22/15, reaching 1200 NTU and 650 mg L^{-1}, respectively, corresponding with a period of elevated discharge. Two high, spurious SSC samples, which do not correspond with high NTU or discharge, were taken in Chamberlin Creek on 7/24/15.

2.5.2 Climate

Climate variables were highly correlated between elevations, and ground temperature correlated well with air temperature. Simple linear regressions were used to fill gaps in the continuous data records (**Table 2.2**). Climate data filled using regressions was applied to calculate sediment yields, but was not used for SSC modeling.

Table 2.2: Climate regressions used to fill gaps in precipitation (Precip.) at 1425 m elevation, air temperature (AT) at 1425 m elevation, and ground temperature (GT) at 1750 m elevation. The table shows the percentage of the data series filled using the regression (%), the model intercept, model coefficient (Coeff.), and Adjusted R^2 (Adj. R^2).

Model	%	Intercept	Coeff.	Adj. R^2
Precip. 1425 m – Precip. 854 m (summed over 24-hours)	8	0.267	1.22	0.868
Precip. 1425 – Precip. 1750 m (summed over 24-hours)	23	0.055	0.919	0.954
AT 1425 m – AT 854 m (averaged over 24-hours)	2	-2.22	1.49	0.987
GT 1750 m – AT 854 m (averaged 2-hourly)	3	2.62	0.918	0.883
GT 1750 m – GT 1425 m (averaged 2-hourly)	11	-1.09	1.025	0.960

Precipitation fell at higher intensities in 2016 than in 2015 (**Figure 2.3; Table 2.1**). In 2016, maximum hourly precipitation was 7.6 mm on 6/22 (1425 m); whereas in 2015, maximum hourly precipitation was 5.2 mm on 6/30 (1750 m). Conversely, the highest precipitation recorded over a 24-hour period was in 2015, when 42 mm was measured from 7/17 – 7/18. For comparison, during the July 2016 flood maximum 24-hour precipitation was 33 mm.

Air temperature, ground temperature, and solar radiation all followed diurnal cycles, and were found to be significantly correlated. Throughout the study periods, 1425 m elevation air temperature ranged from a minimum of -10°C on 6/3/15 to a maximum of 27°C on 5/24/15, averaging 5-6°C throughout the central study period (**Table 2.1**). Ground temperature at 2 cm depth increased with elevation, averaging 7 °C throughout the study period. Ground temperature at 2 cm depth rarely dropped below 0 °C, peaking at 21-23 °C in early July both seasons (**Table 2.1**; **Figure 2.3**).

2.5.3 Regression Models Predicting SSC

We used the AIC to select best-fit multivariate regression models of SSC for both Carnivore and Chamberlin Creeks separately, using either turbidity or discharge as the "base" predictor (i.e. the independent variable explaining the most variability in the dependent variable). Turbidity-based models show slightly higher R^2 for both creeks, compared with discharge-based models (**Table 2.3**). In all cases, inclusion of additional predictor variables improved the models compared with simple sediment rating curves; however, best-fit combinations varied between creeks, and with the base predictor. Precipitation (1425 m; 24-hours) was selected as an additional predictor in both the Carnivore Creek discharge-based model and Chamberlin Creek turbidity-based model, statistically out-performing precipitation at 854 m and 1750 m. Temperature variables were significant additional predictors in both the turbidity-based models. Climate variables did not significantly improve the Chamberlin discharge-based model, but we found time since the beginning of the season to be a significant additional predictor in this model (**Table 2.3**). The Akaike Information Criterion (AIC) value for the Chamberlin discharge-based model with time incorporated (AIC = 260) was an improvement over the same model without time (AIC = 281). SSCs output by the turbidity-based models reached maximums of 1400 mg L^{-1} and 1500 mg L^{-1} in Carnivore Creek, and 310 and 180 mg L^{-1} in Chamberlin Creek, in 2015 and 2016, respectively.

Table 2.3: Optimal multivariate regression models predicting SSC in Carnivore Creek (CAR) and Chamberlin Creek (CHB). Overall model values include residual standard error (Res. SE), adjusted R^2 (Adj. R^2), F-statistic (F-stat), degrees of freedom (DF), and p-value significance (Signif.), respectively. Variables include log-transformed discharge (Log Q.), log transformed turbidity (Log NTU.), precipitation at 1425 m elevation summed over 24-hours (Precip. 1425), ground temperature at 1750 m and 2 cm depth averaged over 2-hours (GT. 1750), air temperature at 1425 m averaged over 24-hours (AT. 1425), and cumulative half-hourly time since the beginning of the season (Cumu. Time). Individual variable values include coefficients, standard error (SE) of the coefficients, and p-value significance of the coefficients (Signif.), respectively. Significance codes are `***´ (p < 0.001), `**´ (p = 0.001 to 0.01), `*´ (p = 0.01 to 0.05), `.´ (p = 0.05 to 0.1), and ` ´ (p > 0.1).

	CAR Q-based	**CHB Q-based**	**CAR NTU-based**	**CHB NTU-based**
Res. SE	0.787	0.577	0.601	0.559
Adj. R^2	0.690	0.377	0.709	0.476
F-stat	58.8	45.2	86.3	28.8
DF	50	144	68	89
Sig.	***	***	***	***
Intercept	0.711	4.57	-1.25	1.10
SE	0.262	0.131	0.307	0.345
Sig.	**	***	***	**
Predictor 1.	**Log Q.**	**Log Q.**	**Log NTU.**	**Log NTU.**
Coeff.	0.959	0.602	1.03	0.497
SE	0.141	0.064	0.083	0.091
Sig.	***	***	***	***
Predictor 2.	**Precip. 1425**	**Cumu. Time**	**GT. 1750**	**Precip. 1425**
Coeff.	0.160	-0.000570	0.061	0.045
SE	0.036	0.0001104	0.013	0.018
Sig.	***	***	***	*
Predictor 3.				**AT. 1425**
Coeff.				0.053
SE				0.015
Sig.				*

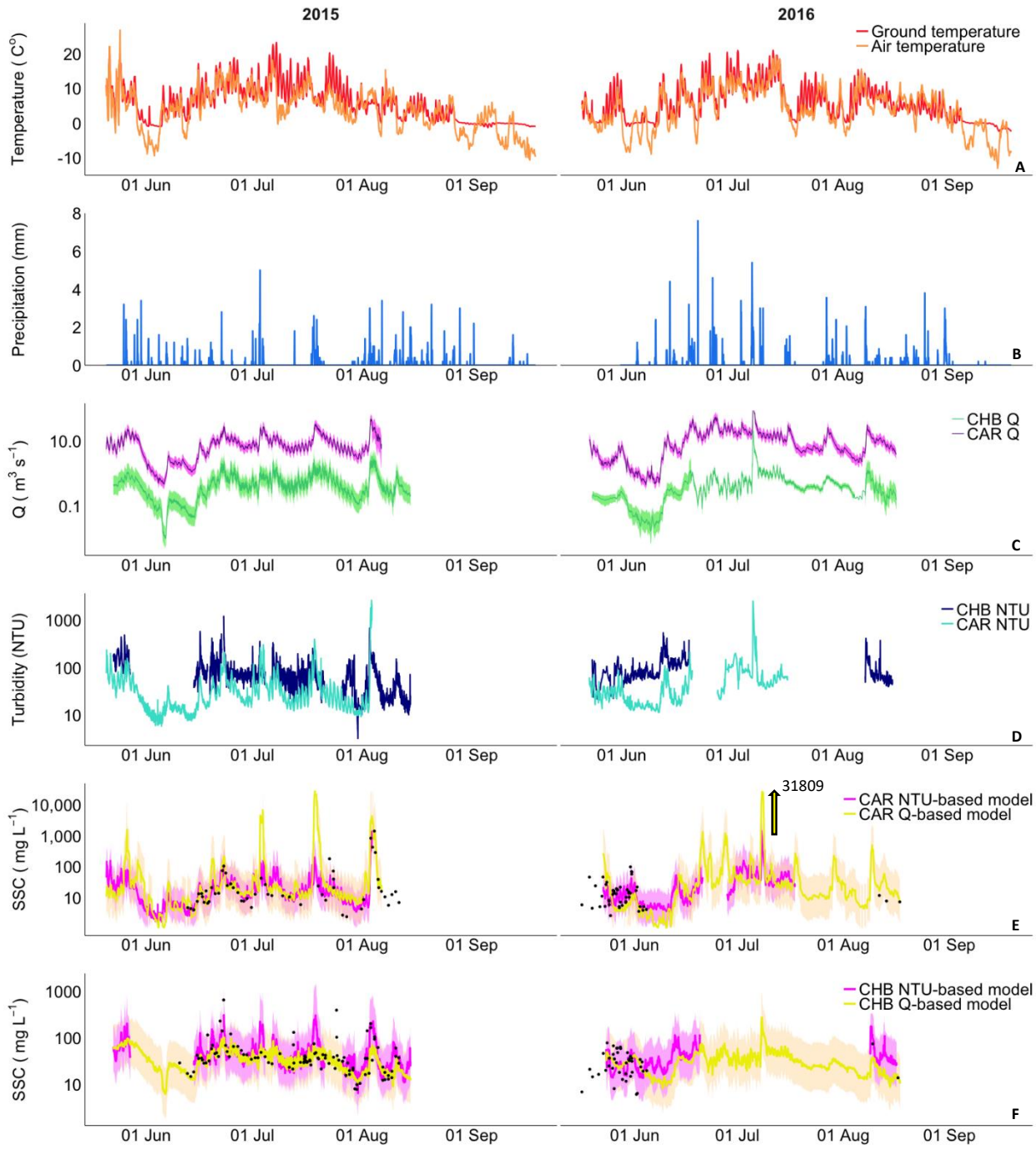

Figure 2.3: Time-series of selected hydrological and meteorological data for the periods 5/20/15 to 9/18/15 and 5/20/16 to 9/18/16 at Lake Peters, Brooks Range, Alaska: A) air temperature at 1425 m and ground temperature at 1750 m; B) precipitation at 1425 m; C) discharge reconstructed from water-pressure measured at the Carnivore Creek and Chamberlin Creek hydrological stations (Figures 2.1 and 2.2); D) turbidity measured at the Carnivore Creek and Chamberlin Creek hydrological stations (see Figure 2.1); E) and F) SSC in Carnivore (CAR) and Chamberlin (CHB) Creeks respectively, reconstructed using turbidity-based and discharge-based multivariate models, with manual SSC samples (dependent variable) overlaid.

2.5.4 Sediment Yields

At both Carnivore Creek and Chamberlin Creek, turbidity-based multivariate regression models explain more variability in SSCs than discharge-based models (**Table 2.3**), making them our first choice for reconstructing annual (open-channel season) sediment yields. However, fouling of the turbidity sensor and dislodgement of the TROLL, together with there being no alternative options for reconstructing turbidity, meant that turbidity-based models could not be used alone. Discharge-based models could be applied with fewer gaps, but data were still lacking for shoulder periods. Photographic evidence of base-flow discharge throughout all ungauged shoulder periods led us to use average SSCs at base-flow to fill early- and late-season gaps. Bridging the three aforementioned methods in preferential order allowed annual sediment yields to be estimated (**Table 2.4**). Given there is minimal sediment transfer at base-flow, using our coarse method of approximation for shoulder periods makes little difference to the estimated sediment yields; the bridged models contribute < 3% in Carnivore Creek and < 11% in Chamberlin Creek of total annual yields.

Sediment yields discharging into Lake Peters from Carnivore Creek are one or two orders of magnitude higher than sediment yields from Chamberlin Creek, with Carnivore Creek contributing over 96% of the total yield from these two major tributaries (**Table 2.4**). Sediment yield for Carnivore Creek in 2016 is 42% greater than the yield for 2015. Sediment yield for Chamberlin Creek in 2016 is also higher than 2015. SSYs in Carnivore and Chamberlin Creeks are similar for 2015, but disparate in 2016. In 2016, SSY is over three times that of 2015 in Carnivore Creek, but only marginally higher than that of 2015 in Chamberlin Creek.

Table 2.4: Comparison of suspended sediment yields and specific sediment yields (SSYs) between Carnivore Creek (CAR) and Chamberlin Creek (CHB), and between the 2015 and 2016 open-channel seasons. Confidence bands (95%) are shown in parentheses.

Yield Type	[1]CAR	[2]CHB	CAR and CHB
2015 sediment yield Mg yr^{-1}	7000 (3000-22000)	280 (170-460)	7000 (3000-22000)
2016 sediment yield Mg yr^{-1}	12000 (6400-23000)	320 (230-460)	12000 (7000-23000)
2015 SSY Mg km^{-2} yr^{-1}	55 (23-170)	35 (21-57)	53 (40-230)
2016 SSY Mg km^{-2} yr^{-1}	92 (50-178)	40 (29-57)	89 (80-230)

[1] Carnivore – models used to estimate sediment yield: 62% turbidity-based model, 2% discharge-based model, 20% average sediment yield at < 10 $m^3 s^{-1}$, 16% average sediment yield below 5 $m^3 s^{-1}$ (2015); 40% turbidity-based model, 31% discharge-based model, 13% average sediment yield below 10 $m^3 s^{-1}$, 16% average sediment yield at < 5 $m^3 s^{-1}$ (2016).

[2] Chamberlin – models used to estimate sediment yield: 47% turbidity-based model, 21% discharge-based model, and 32% average sediment yield at < 0.25 $m^3 s^{-1}$ (2015); 29% turbidity-based model, 41% discharge-based model, 30% average sediment yield at < 0.25 $m^3 s^{-1}$ (2016).

The majority of sediments in both creeks are transported during discrete events (**Figure 2.4**). In Carnivore Creek, over 70% of the 2015 annual yield is modeled to have discharged in just two days (August 3-4), and 30% of the 2016 yield is modeled to have discharged in two days (July 7-8). In Chamberlin Creek, 18% of the 2015 annual yield is modeled to have discharged in just two days (August 3-4), and 50% of the 2016 yield is modeled to have discharged in two days (July 7-8).

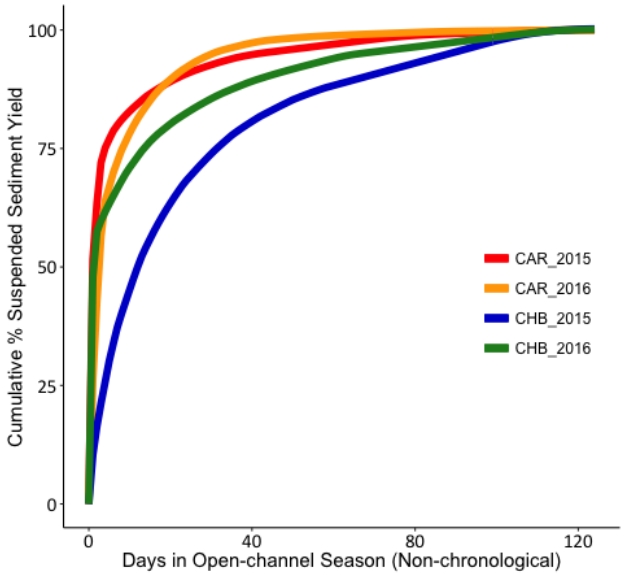

Figure 2.4: Cumulative rank plot of the percentage of suspended sediment yield transferred to Lake Peters, Brooks Range, Alaska, from the Carnivore Creek (CAR) and Chamberlin Creek (CHB) sub-catchments over 24 hour periods, ending at 12 noon. Suspended sediment yields were calculated using fluvial-based multivariate sediment modeling.

2.6 Discussion

2.6.1 Discharge and Turbidity

Turbidity and discharge are traditional explanatory variables used for modeling SSCs, and when applied as the base-predictor, both returned significant models, with turbidity-based models outperforming discharge-based models for both sub-catchments. The discharge-based models appear to under-predict high SSCs and over-predict low SSCs, especially for the Carnivore Creek sub-catchment, as often observed for simple sediment rating curves (Horowitz, 2003). This is probably because the discharge-based models are overly sensitive to discharge, and do not adequately account for lack of suspended sediment entrainment during low flows, or sediment mobilization of extra-channel and hillslope sources during elevated flows.

Differences between discharge and turbidity in Carnivore Creek and Chamberlin Creek makes for interesting comparison. Chamberlin Creek has greater ability to transport sediment in suspension during base-flows, resulting in persistently turbid water (**Table 2.1**; **Figure 2.3**). This is attributed to the steeper slope increasing stream power, coupled with little transient storage potential. The higher glacial coverage, with potential to produce relatively more rock flour, may also contribute to

the turbidity. Lower Carnivore Creek has a comparatively low slope, with short-term sediment storage potential in pools, and low, vegetated floodplain segments, lending to high water clarity during base-flow conditions, and more turbid waters (> 1000 NTU) during periods of elevated discharge. Furthermore, the Carnivore Creek sub-catchment is much larger (128 km^2) than the Chamberlin Creek sub-catchment (8 km^2), and a lesser relative proportion of the Carnivore Creek sub-catchment is at high elevations, favoring rainfall over snowfall. Consequently, Carnivore Creek receives greater volumes of discharge from rainfall and rain-on-snow events, which drive high SSCs and associated turbidity (**Figure 2.3**).

2.6.2 Rainfall and Temperature

Rainfall is a fundamental control of landscape denudation (Rasch et al., 2000), and dominance of rainfall as a driver of sediment transfer has similarly been inferred for other arctic and sub-arctic catchments (Bogen and Bønses, 2003; Lewis and Lamoureux, 2010; Lewis et al., 2012). Precipitation summed over 24-hours is a highly significant predictor in the discharge-based model for Carnivore Creek, and improves the turbidity-based model for Chamberlin Creek (**Table 2.3**), which is related to the majority of sediment being transported during and immediately following rainfall events. Up to 70% of the annual sediment yield in Carnivore Creek, and up to 50% of the annual sediment yield in Chamberlin Creek, was transported in just two days over the study period (**Figure 2.3**). Rainfall response was probably enhanced by shallow soils and relatively low shrub-coverage, associated with Lake Peters' high-latitude location.

Temperature is also a significant driver of sediment transfer at Lake Peters (**Table 2.3**), but because the majority of sediment is transported during rainfall-induced flood events, we interpret temperature forcing as secondary to rainfall. This contrasts results from Ellesmere Island, Arctic Canada where temperature has been reported as the dominant driver of sediment yields in the Lake C2 catchment (21 km^2; Hardy, 1996), and results from Cape Bounty, Arctic Canada where antecedent soil moisture dampens rainfall response for some events (Favaro and Lamoureux, 2014). Despite the comparably lesser significance of temperature variables, the selection of medium-elevation air temperature over low- or high-elevations in our turbidity-based model for Chamberlin Creek is akin with Lake C2 (Hardy, 1996).

The inferred secondary importance of temperature at Lake Peters is also at odds with modeling by Syvitski (2002), predicting that surface temperature is the dominant driver of pan-Arctic sediment yields. For the Colville River, Alaska, Syvitski (2002) forecasted that sediment flux will increase 22% for every 2^oC of warming. Our results are more comparable with Lewis and Lamoureux's (2010) finding that SSC models are better expressed with precipitation (over temperature) as the direct predictor for a small (8 km^2) catchment on Melville Island, Canada. A key difference between sediment modeling by Syvitski (2002), and modeling by Lewis and Lamoureux (2010), is the size and elevation of catchments, with Lake Peters' catchment, especially the Chamberlin Creek sub-catchment, being more comparable with the catchment modeled by Lewis and Lamoureux (2010).

We accordingly consider that relatively small, mountainous arctic catchments might have greater response to rainfall comparative to larger coastal arctic catchments.

Turbidity might be expected to serve as a surrogate for SSCs, without additional explanatory variables being needed, but this was not the case for Chamberlin Creek nor Carnivore Creek. The significance of precipitation in the turbidity-based model for Chamberlin Creek, might represent the coarser fraction of suspended sediment, perhaps not captured by the turbidity sensor. The significance of ground temperature in the turbidity-based model for Carnivore Creek suggests mobilization of suspended load sediment from different source areas, depending on temperature, is not captured by the turbidity sensor. We note that supplementing turbidity-based models for Carnivore Creek with ground temperature or air temperature both produce highly significant models ($p < 2.2E-16$), but supplementing with ground temperature ($R^2 = 0.65$) explains slightly more variability in SSCs than supplementing with air temperature ($R^2 = 0.70$). Ground temperature is smoothed and delayed compared to air temperature (**Figure 2.3**), which may explain why it performs better in the model. Although ground conditions have been related to SSCs (Irvine-Fynn et al., 2005; Syvitski, 2002; Favaro and Lamoureux, 2014), our turbidity-based Carnivore Creek model is the first to incorporate ground temperature as a supplementary predictor variable.

2.6.3 Snow-water Equivalent

Neither rainfall nor air temperature fully explain the disparities between the 2015 versus 2016 hydrographs (**Figure 2.3**), which affects total sediment yields (**Table 2.4**). In 2016, discharge was elevated for an extended period between mid-June and mid-July in both creeks, but there were no noteworthy differences in precipitation, nor any notable increase in mean temperature in 2016. By order of elimination, the difference in the hydrographs may be explained by snow-water equivalent (SWE) available for melt being greater in 2016 compared to 2015. Together with the significance of temperature variables in our models, this suggests that both SWE and melt-energy are important drivers of sediment transfer at Lake Peters. Our results are comparable with Forbes and Lamoureux (2005) who found that sediment yield is a function of SWE, rather than melt-energy, in three high-latitude catchments below the Arctic Circle (Forbes and Lamoureux, 2005), and Cockburn and Lamoureux (2008) who found early-season SWE to be the primary driver of sediment transfer in two nonglacial catchments in the Canadian High Arctic. Varying snow-melt conditions can affect the stability of drainages and exposure of sediment to erosion, producing year-to-year differences in sediment yields (Bogen and Bønses, 2003), but our monitoring period is not long enough to assess inter-annual variability in this study (see Thurston, in prep—Chapter 3).

2.6.4 Sediment Supply and Exhaustion

Temporal variables were incorporated into the multivariate models to represent variations in sediment supply, including: hysteresis variables to capture diurnal variability; the rate of change of discharge (over half-hourly or hourly periods) to represent other hysteresis effects; time since discharge was last exceeded to represent sediment supply variability within a season; and

cumulative time and discharge as indicators of seasonal sediment upsurges or exhaustion. There is no evidence from our multivariate models of any significant diurnal or within-season sediment exhaustion or upsurges in either Carnivore Creek or Chamberlin Creek. Lack of coherent diurnal hysteresis patterns, related to complex SSC response, is not uncommon in arctic catchments, especially those with polythermal and cold-based glaciers (Hodgkins, 1996; Hodgkins, 1999; Irvine-Fynn et al., 2005).

Seasonal exhaustion of the fine sediment fraction is evidenced by inclusion of the negative time coefficient in the discharge-based model for the Chamberlin Creek sub-catchment (**Table 2.3**), much lower (improved) AIC compared to the same model without time, and downward SSC trend in 2015 (**Figure 2.3**). It is probable that Chamberlin Creek's characteristics boost sensitivity to mechanisms of seasonal exhaustion; and/or that paraglacial sediment is nearing exhaustion in Chamberlin Creek, but not in Carnivore Creek. Despite moderate glacial coverage (26%), Chamberlin Creek sub-catchment only contains one large valley glacier (Chamberlin Glacier) and one small glacier (Peters Glacier) available to produce sediment, and is small and steep compared to the Carnivore Creek sub-catchment, with less room for extra-channel sediment storage. Carnivore Creek sub-catchment contains two valley glaciers larger than Chamberlin Glacier, and five medium-sized glaciers, which have all retreated since the LIA, likely leaving behind a larger total quantity of erodible proglacial sediment. The gently-sloping lower valley of the Carnivore Creek sub-catchment has ample room for sediment storage. Catchment characteristics lend towards seasonal exhaustion mechanisms in Chamberlin Creek, which may include: 1) stream power dwarfing weathering and erosion (Østrem, 1975; Rasch et al., 2000); 2) exhaustion of the snowpack (Forbes and Lamoureux, 2005); or 3) exhaustion of subglacial sediment sources (Hodson and Ferguson, 1999; Bogen and Bønses, 2003; Irvine-Fynn et al., 2005). Under the first explanation, wintertime glacial weathering might not keep pace with glaciofluvial entrainment and transport throughout the open-channel season (Østrem, 1975; Hodgkins, 1999). Early-season washout of extra-channel sediment could occur, with supply thereafter dependent on material being delivered to the channel from exterior sources (Rasch et al., 2000). Under the second explanation, snow would be exhausted by melt-energy consequently reducing discharge and sediment transfer (Forbes and Lamoureux, 2005), but this is less likely given there are not conspicuous downward trends in discharge (**Figure 2.3**). Chamberlin Glacier may have a different thermal regime to glaciers in the Carnivore Creek sub-catchment; therefore, the third explanation is plausible. Subglacial sediment sources and subglacial network development would give rise to pronounced fine sediment exhaustion (Hodson and Ferguson, 1999; Bogen and Bønses, 2003). The nearby polythermal McCall Glacier (~50 km west of Lake Peters) was found to have a zone of basal sliding, and moulins—likely transferring surface meltwater to the glacier's base, but a complex subglacial drainage network was probably not active (Pattyn et al., 2009). Without a focused glacial study, it is unknown whether there is an active subglacial network beneath Chamberlin Glacier, and how this compares to nearby valley glaciers.

Although there is good evidence for seasonal-scale mechanisms of sediment exhaustion in the Chamberlin Creek sub-catchment, paraglacial sediment exhaustion associated with landscape

denudation following glacial events throughout the Quaternary may also give rise to a seasonal exhaustion signal. Church and Ryder (1972) hypothesized that maximum paraglacial sediment transfer occurs soon after deglaciation, followed by an asymptotic decline towards an unglaciated norm, and Church and Slaymaker (1989) contended that this process takes several tens of thousands of years. The ability to define cessation of the paraglacial cycle has been challenged because mature surfaces have been found to require higher magnitude rainfall events for mobilization, likely because of sediment armoring or exhaustion effects (Orwin and Smart, 2004). Nevertheless, the fine sediment fraction produced by Quaternary glaciations could be nearing exhaustion in the small, steep Chamberlin Creek sub-catchment.

2.6.5 Suspended Sediment Yields

Prior to this paper, sediment yields had only been sampled and reported 0.24 km downstream of Chamberlin Glacier's terminus for 1958 (Rainwater and Guy, 1961), and had not been reported for the Carnivore Creek sub-catchment. Rainwater and Guy (1961) report a total of 990 Mg (700 – 1300 Mg using the reported 30% error margin) of suspended sediment for a mean daily discharge of 0.648 $m^3\ s^{-1}$ between 07/01/1958 and 08/13/1958. These are much higher estimates than 165 Mg (45 – 600 using prediction band error margins) for a mean daily discharge of 0.618 $m^3\ s^{-1}$ (2015) and 240 Mg (30 – 800 Mg using prediction band error margins) for a mean daily discharge of 0.767 $m^3\ s^{-1}$ (2016) calculated near the mouth of Chamberlin Creek for the same days of the year in this study. Daily peaks at 4 pm for SSC and 6 pm for discharge reported by Rainwater and Guy (1961) preceded our recorded peaks around midnight. There are several possible explanations for disparities in sediment yields, including: 1) limitations associated with methods, such as daily averaging in the Rainwater and Guy (1961) study versus half-hourly or hourly measurements in our study; 2) higher sediment yields near Chamberlin Glacier compared to the alluvial fan, because of sediment storage effects; 3) inter-annual variability in processes driving sediment transfer (evidenced by Thurston, in prep–Chapter 3) and suspended sediment supply, especially because the glacier was larger in 1958; and 4) and/or longer-term alterations in physical processes driving suspended sediment between 1958 and the 2015 and 2016 open-channel seasons. The second and fourth explanations are less likely because: lack of observed storage reservoirs, and evidence of sediment exhaustion (**Table 2.3**) does not indicate significant sediment storage; and the Alaskan climate shift reported in the 1970s (Cassano et al., 2011) is more likely to have driven higher sediment yields than lower (Syvitski, 2002; Lewis and Lamoureux, 2010).

SSYs estimated for Lake Peters' catchment can be compared with other, albeit limited, SSYs reported in Alaska to assess the spatial uniformity of sediment transfer patterns. Arnborg et al. (1967) reports a total SSY of 116 Mg $km^{-2}\ yr^{-1}$ transiting the Colville River Delta towards the Arctic Ocean in 1962 (50,000 km^2 catchment area), which is comparable with the 2016 SSY estimated for Lake Peters' catchment (169 km^2 catchment area; **Table 2.4**). SSYs typically decline with increasing catchment area owing to sediment storage effects (Schiefer et al., 2001), but the considerable

paraglacial sediment sources and remobilization of Quaternary sediments in major lowland reaches (Church and Slaymaker, 1989), likely explain the relatively high SSY for the Colville catchment.

In a more recent lake-based study, three out of four SSYs (0.25 – 52 Mg km^{-2} yr^{-1}) reported by Tape et al. (2011) for the Chandler River corridor are lower than SSYs for Lake Peters' catchment and sub-catchments. The lower SSYs can be explained by absence of glacial coverage, presence of shrub cover, and associated declines in discharge since around 1980 (Tape et al., 2011). One considerly larger SSY (52 Mg km^{-2} yr^{-1}) reported by Tape et al. (2011) is associated with episodic, extreme-regime sedimentation, and is comparable with Lake Peters' catchment. All of the SSYs reported for Arctic Alaska are lower than SSYs reported for southeastern Alaska, where erodible bedrock, and warm-based glacial processes in some catchments (Loso et al., 2004), drive SSYs up to the order of 25,000 Mg km^{-2} yr^{-1} (Hallet et al., 1996).

2.7 Conclusion

Multivariate models of SSCs have been used to estimate sediment yields and infer physical processes driving sediment transfer. In remote and mountainous settings like Lake Peters, where gauging data is not generally available for entire open-channel seasons, and turbidity sensors are prone to fouling, bridging multiple models and estimating sediment yields for shoulder periods provides scope to reconstruct annual sediment yields. Although errors associated with multivariate models can still be large (**Table 2.5**), model performance is improved over simple sediment rating curves, and models can capture signals from complex catchment- and sub-catchment-scale system processes.

Sediment yields at Lake Peters are not simply a function of rain, snow, temperature, or sediment supply, but a complex response to all of these forcing variables. The majority of sediment transfer in both Carnivore Creek and Chamberlin Creek was associated with rainfall events, and we therefore conclude that rainfall is a dominant driver of catchment-scale sediment transfer at Lake Peters. Temperature variables and winter SWE are secondary drivers of sediment transfer. There is evidence of seasonal sediment exhaustion in the Chamberlin Creek sub-catchment, perhaps because this small, steep sub-catchment has little short-term sediment storage potential within and adjacent to the channel, and/or plausibly lesser quantities of fine proglacial and paraglacial sediment available for erosion. Furthermore, models indicate that turbidity does not act as a direct surrogate for SSC, because incorporation of climatic variables increases the SSC variability explained. This is probably because sediment source areas and sediment character change with rainfall and temperature conditions.

Given significant increases in both arctic temperatures and rainfall (Bintanja and Andry, 2017) are forecast to drive larger Arctic sediment yields over the coming century (Syvitski, 2002; Lewis and Lamoureux, 2010), our results indicate that Lake Peters' catchment will likely be no exception to these trends. Negative feedback mechanisms, such as exhaustion of proglacial sediment sources (Church and Slaymaker, 1989) and shrub expansion stabilizing soils (Tape et al., 2011), might buffer

such increases, but feedback mechanisms are uncertain without further systems research of arctic hydrology and geomorphology.

2.8 Acknowledgements

The authors are grateful for support from the National Science Foundation, Arctic System Science Program, which provided collaborative grant funding (award # 1418000) for the umbrella project "*Developing a system model of arctic glacial-lacustrine sedimentation for investigating past and future climate change*". The authors also acknowledge additional support from the Environmental Professionals of Arizona (EPAZ) Environmental Scholarship Program (2016-2017), awarded to Lorna Louise Thurston. Permits to undertake this research in the Arctic National Wildlife Refuge were granted by the United States Department of the Interior - Fish and Wildlife Service, and we are thankful for the opportunity to access this remote part of Alaska. Last, but not least, thank you to all field and laboratory assistants who have assisted with this project.

2.9 References

Arnborg L, Walker HJ, Peippo J. 1967. Suspended Load in the Colville River, Alaska. *Geografiska Annaler* **49 A** (2-4): 131-144.

Asselman NEM. 2000. Fitting and interpretation of sediment rating curves. *Journal of Hydrology* **234**: 228-248. DOI: 10.1016/S0022-1694(00)00253-5.

Bintanja R, Andry O. 2017. Towards a rain-dominated Arctic. *Nature Climate Change* **7**: 263-268. DOI: 10.1038/NCLIMATE3240**.**

Bogen J, Bønsnes TE. 2003. Erosion and sediment transport in High Arctic rivers, Svalbard. *Polar Research* **22**(2): 175-189.

Burnham KP, Anderson DR. 2002. Model Selection and Multi-Model Inference. Springer-Verlag: New York.

Calcagno V, de Mazancourt C. 2010. glmulti: An R Package for Easy Automated Model Selection with (Generalized) Linear Models. *Journal of Statistical Software* **34**(12): 1-28.

Cassano EN, Cassano JJ, Nolan M. 2011. Synoptic weather pattern controls on temperature in Alaska. *Journal of Geophysical Research* **116**: 1-19. DOI: 10.1029/2010JD015341.

Church M, Ryder M. 1972. Paraglacial Sedimentation: A Consideration of Fluvial Processes Conditioned by Glaciation. *Geological Society of America Bulletin* **83**: 3059-3072.

Church M, Slaymaker O. 1989. Disequilibrium of Holocene sediment yield in glaciated British Columbia. *Nature* **337**: 452-454.

Cockburn JMH, Lamoureux SF. 2008. Hydroclimate controls over seasonal sediment in two adjacent High Arctic watersheds. *Hydrological Processes* **22**: 2013-2027. DOI: 10.1002/hyp.6798.

Evison LH, Parker EC, Ellis JM. 1996. Late-Holocene glaciation and twentieth-century retreat, northeastern Brooks Range, Alaska. *The Holocene* **6**(1): 17-24.

Favaro EA, Lamoureux SF. 2014. Antecedent controls on rainfall runoff response and sediment transport in a High Arctic catchment. *Geografiska Annaler* **96 A**(4): 433-446. DOI: 10.1111/geoa.12063.

Fenn CR, Gurnell AM, Beecroft IR. 1985. An Evaluation of the Use of Suspended Sediment Rating Curves for the Prediction of Suspended Sediment Concentration in a Proglacial Stream. *Geografiska Annaler* **67 A**(1-2): 71-82.

Forbes AC, Lamoureux SF. 2005. Climatic Controls on Streamflow and Suspended Sediment Transport in Three Large Middle Arctic Catchments, Boothia Peninsula, Nunavut, Canada. *Arctic, Antarctic, and Alpine Research* **37**(3): 304-315.

Gao P. 2008. Understanding watershed suspended sediment transport. *Progress in Physical Geography* **32**(3): 243-263. DOI: 10.1177/0309133308094849.

Guymon GL. 1974. Regional Sediment Yield Analyses of Alaska Streams. *Journal of the Hydraulics Division—ASCE* **100**: 41-50.

Hallet B, Hunter L, Bogen J. 1996. Rates of erosion and sediment evacuation by glaciers: A review of field data and their implications. *Global and Planetary Change* **12**: 213-235.

Hardy DR. 1996. Climatic influences on streamflow and sediment flux into Lake C2, northern Ellesmere Island, Canada. *Journal of Paleolimnology* **16**: 133-149.

Harrington ST, Harrington JR. 2013. An assessment of the suspended sediment rating curve approach for load estimation on the Rivers Bandon and Owenabue, Ireland. *Geomorphology* **185**: 27-38. DOI: 10.1016/j.geomorph.2012.12.002.

Hodgkins R. 1996. Seasonal trend in suspended-sediment transport from an Arctic glacier, and implications for drainage-system structure. *Annals of Glaciology* **22**: 147-151.

Hodgkins R. 1999. Controls on Suspended-Sediment Transfer at a High-Arctic Glacier, Determined from Statistical Modelling. *Earth Surface Processes and Landforms* **24**: 1-21.

Hodgkins R, Cooper R, Wadham J, Tranter M. 2003. Suspended sediment fluxes in a high-Arctic glacierised catchment: implications for fluvial sediment storage. *Sedimentary Geology* **162**: 105-117. DOI: 10.1016/S0037-0738(03)00218-5.

Hodson AJ, Ferguson RI. 1999. Fluvial Suspended Sediment Transport from Cold and Warm-Based Glaciers in Svalbard. *Earth Surfaces Processes and Landforms* **24**: 957-974.

Horowitz AJ. 2003. An evaluation of sediment rating curves for estimating suspended sediment concentrations for subsequent flux calculations. *Hydrological Processes* **17**: 3387-3409. DOI: 10.1002/hyp.1299.

Irvine-Fynn TDL, Moorman BJ, Willis IC, Sjogren DB, Hodson AJ, Mumford PN, Walter FSA, Williams JLM. 2005. Geocryological processes linked to High Arctic proglacial stream suspended sediment dynamics: examples from Bylot Island, Nunavut, and Spitsbergen, Svalbard. *Hydrological Processes* **19**: 115-135. DOI: 10.1002/hyp.5759.

Lammers RB, Shiklomanov AI, Vörösmarty CJ, Fekete BM, Peterson BJ. 2001. Assessment of contemporary Arctic river runoff based on observational discharge records. *Journal of Geophysical Research* **106**(D4): 3321-3334.

Lewis T, Lafrenière MJ, Lamoureux SF. 2012. Hydrochemical and sedimentary responses of paired High Arctic watersheds to unusual climate and permafrost disturbance, Cape Bounty, Melville Island, Canada. *Hydrological Processes* **26**. DOI: 10.1002/hyp.8335.

Lewis T, Lamoureux SF. 2010. Twenty-first century discharge and sediment yield predictions in a small high Arctic watershed. *Global and Planetary Change* **71**: 27-41. DOI: 10.1016/j.gloplacha.2009.12.006.

Lewkowicz AG, Wolfe PM. 1994. Sediment Transport in Hot Weather Creek, Ellesmere Island, N.W.T., Canada, 1990-1991. *Arctic and Alpine Research* **26**(3): 213-226.

Loso MG, Anderson RS, Anderson SP. 2004. Post-Little Ice Age record of coarse and fine clastic sedimentation in an Alaskan proglacial lake. *Geological Society of America* **32**(12): 1065-1068. DOI: 10.1130/G20839.1.

McKay NP, Kaufman DS. 2014. An extended Arctic proxy temperature database for the past 2,000 years. *Scientific Data* **1**: 140026. DOI: 10.1038/sdata.2014.26.

Menounos B, Schiefer E, Slaymaker O. 2006. Nested temporal suspended sediment yields, Green Lake Basin, British Columbia, Canada. *Geomorphology* **79**: 114-129. DOI: 10.1016/j.geomorph.2005.09.020.

Molnia BF. 2007. Late nineteenth to early twenty-first century behavior of Alaskan glaciers as indicators of changing regional climate. *Global and Planetary Change* **56**: 23-56. DOI: 10.1016/j.gloplacha.2006.07.011.

Morehead MD, Syvitski JP, Hutton EWH, Peckham SD. 2003. Modeling the temporal variability in the flux of sediment from ungauged river basins. *Global and Planetary Change* **39**: 95-110. DOI: 10.1016/S0921-8181(03)00019-5.

Orwin JF, Lamoureux SF, Warburton J, Beylich A. 2010. A Framework for Characterizing Fluvial Sediment Fluxes from Source to Sink in Cold Environments. *Geografiska Annaler* **92 A**(2): 155-176.

Orwin JF, Smart CC. 2004. The evidence for paraglacial sedimentation and its temporal scale in the deglacierizing basin of Small River Glacier, Canada. *Geomorphology* **58**: 175-202. DOI: 10.1016/j.geomorph.2003.07.005.

Østrem G. 1975. Sediment Transport in Glacial Meltwater Streams. In Glaciofluvial and Glaciolacustrine Sedimentation, Special Publication 23, Jopling AV, McDonald BC (eds). Society of Economic Paleontologists and Mineralogists: USA; 101-122.

Pattyn F, Delcourt C, Samyn D, De Smedt B, Nolan M. 2009. Bed properties and hydrological conditions underneath McCall Glacier, Alaska, USA. *Annals of Glaciology* **50**(51): 80-84.

Rainwater FH, Guy HP. 1961. Some Observations on the Hydrochemistry and Sedimentation of the Chamberlin Glacier Area Alaska. In *Shorter Contributions to General Geology*, United States Geological Survey (eds), USGS Professional Paper 414-C. United States Government: Washington; C1-C14.

Rasch M, Elberling B, Jakobsen BH, Hasolt B. 2000. High-Resolution Measurements of Water Discharge, Sediment, and Solute Transport in the River Zackenbergelven, Northeast Greenland. *Arctic, Antarctic, and Alpine Research* **32**(3): 336-345.

Reed BL. 1968. Geology of the Lake Peters Area Northeastern Brooks Range, Alaska. *Geological Survey Bulletin.* **1236**: 1-132.

Schiefer, E, Kaufman D, McKay N, Retelle M, Werner A, Roof S. 2017. Fluvial suspended sediment yields over hours to millennia in the High Arctic at proglacial lake Linnévatnet, Svalbard. *Earth Surface Processes and Landforms*. DOI: 10.1002/esp.4264.

Schiefer E, Slaymaker O, Klinkenberg B. 2001. Physiographically Controlled Allometry of Specific Sediment Yield in the Canadian Cordillera: a Lake Sediment-Based Approach. *Geografiska Annaler* **83 A**(1-2): 55-65.

Stavros C, Hill DF. 2013. National Centers for Environmental Information: National Oceanic and Atmospheric Administration. Retrieved May 2017 from: ftp://ftp.ncdc.noaa.gov/pub/data/gridded-nw-pac/.

Syvitski JPM. 2002. Sediment discharge variability in Arctic rivers: implications for a warmer future. *Polar Research* **21**(2): 323-330.

Tape KD, Verbyla D, Welker JM. 2011. Twentieth century erosion in Arctic Alaska foothills: The influence of shrubs, runoff, and permafrost. *Journal of Geophysical Research* **116**: 1-11. DOI: 10.1029/2011JG001795.

Thurston (in prep). Modeling Fine-grained Fluxes for Estimating Sediment Yields and Understanding Hydroclimatic and Geomorphic Processes at Lake Peters, Brooks Range, Arctic Alaska. Unpublished Master of Science Thesis. Northern Arizona University, Flagstaff AZ; 89 pp.

Walling DE. 1977. Limitations of the rating curve technique for estimating suspended sediment loads, with particular reference to British rivers. In *Erosion and solid matter transport in inland waters : symposium,* International Association of Hydrological Sciences (eds), IAHS Publication **122**. IAHS Press: Wallingford; 34-48.

3 SUSPENDED SEDIMENT YIELDS AT LAKE PETERS, NORTHEAST BROOKS RANGE, ALASKA: FLUVIAL-BASED AND LAKE SEDIMENT-BASED APPROACHES

3.1 Abstract

Lacustrine sedimentation was used as a paleo-record of mean inter-decadal suspended sediment yield to Lake Peters, Brooks Range, Alaska. Geochronology from $^{240}Pu/^{239}Pu$ and ^{137}CS dating of two surface cores in a spatially correlated marker bed, together with dry bulk density (DBD) patterns, in 40 short sediment cores were used to calculate mass sediment accumulation rates (g cm^{-2} yr^{-1}). Subsequently, lake area was used to estimate mean inter-decadal sediment yield (Mg yr^{-1}). Results were compared with fluvial-based sediment delivery for the 2015 and 2016 open-channel seasons (Thurston, 2017—Chapter 2), as well as SSYs reported for other arctic catchments. Using the lake-based method, mean SSY to Lake Peters between *ca.* 1973 and 2015 was calculated to be 52 ± 12 Mg km^{-2} yr^{-1}, which is comparable with fluvial-based modeling: 50 Mg km^{-2} yr^{-1} in 2015, and 90 Mg km^{-2} yr^{-1} in 2016 (Thurston, in prep—Chapter 2). Although 2016 was a year of above average sedimentation (for the past *ca.* 42 years), the last extreme depositional event at Lake Peters probably occurred between 1970 and 1976 when a basal lens of fine sand was deposited in a spatially distributed, relatively thick and coarse lacustrine sediment structure. Sediment deposition within Lake Peters over the past *ca.* 42 years was spatially modeled using distance from the primary inflow and lake water depth. Deposition within 1.5 km from the primary inflow is complex, likely because Carnivore Creek (the primary inflow) and Chamberlin Creek (secondary inflow 0.7 km down-lake) both provide significant influx, and sediment bypassing probably carries sediment over 1 km into the lake where it is focused into a deep lake basin. SSYs deposited in Lake Peters are comparable with regional arctic trends, which vary by four orders of magnitude (< 1 to > 6000 Mg km^{-2} yr^{-1}). Only glaciated arctic catchments produce SSYs exceeding 500 Mg km^{-2} yr^{-1}. Anomalously high SSYs are reported for three arctic catchments, which can be explained by their erodible lithology, or thermal subglacial processes. One arctic catchment showed anomalously low SSY, which is attributed to lack of inflows and stabilizing vegetation. Using a fluvial- and lake-based dual-method approach proves helpful for understanding sediment transfer processes from source to sink, and is encouraged for future arctic research.

3.2 Introduction

Suspended sediment transfer patterns and yields for fluvial systems are dominantly supply-controlled and climate responsive, making useful proxies for catchment-scale environmental change (Hodgkins et al., 2003). Records of suspended sediment transfer are commonly used for hydroclimatic and geomorphic reconstruction, but can also inform environmental system forecasting (e.g. Syvitski, 2002; Lewis and Lamoureux, 2010). Geomorphic and climate signals are easier to filter in many arctic catchments[1] absent of significant land-use impacts, and if glaciers are present this makes for sensitive response to climate forcing.

At high latitudes, low air temperatures reduce sediment production, erosion, and transport comparative to sub-Arctic and Alpine environments, by less frequent and expansive freeze-thaw transitions, greater snowfall, and lower intensity rainfall, resulting in dampened flooding (Syvitski, 2002). This makes arctic sediment transfer processes susceptible to change with disproportionate contemporary high-latitude warming (Syvitski, 2002), associated with increasing air temperatures, precipitation (Lewis and Lamoureux, 2010), and winter runoff in Alaska (Lammers et al., 2001). Enhanced melt and widespread glacial recession (Zemp et al., 2015) are driving elevated arctic sediment yields (Hallet et al., 1996; Syvitski, 2002; Lewis and Lamoureux, 2010), with few exceptions (Loso et al., 2004; Tape et al., 2011), contrasting dominant global trends of stable or decreasing sediment transfer (Walling and Fang, 2003). Negative feedback mechanisms, such as shrub expansion stabilizing soils and reducing peak runoff, might buffer such increasing sediment yields to a degree (Tape et al., 2011); however, this is uncertain given minimal hydrological systems research in the Arctic.

Despite evidence for complex and accelerated arctic change, monitoring of arctic rivers declined significantly around the turn of the millennia (Guymon, 1974; Syvitski, 2002; Lewis and Lamoureux, 2010); there are relatively few studies and limited temporal data (Orwin et al., 2010) for estimating arctic sediment yields compared to other environments; and few sediment yields have been published for Arctic Alaska (Rainwater and Guy, 1961; Arnborg et al., 1967; Tape et al., 2011; Thurston, in prep—Chapter 2). Furthermore, most sediment yields are estimated using fluvial rating curve methods (described in Thurston, in prep—Chapter 2), meaning they are temporally limited by the length of fluvial monitoring, which has only once spanned more than a decade above the Arctic Circle (Bogen and Bønsnes, 2003). Lake sediment studies can provide longer yield records to improve our understanding of sediment transfer processes (Desloges and Gilbert, 1994; Lamoureux, 2000; Tape et al., 2011; Schiefer et al., 2017), but this method has been under-utilized in the Arctic to date. There are constraints associated with estimating sediment yields without spatially distributed core data (Lamoureux, 2000; Schiefer et al., 2017), and resources and logistics limit spatially distributed sampling (Evans and Church, 2000). For these reasons, arctic coring projects have focused on relating hydroclimate forcing to records of bottom flux from a single core

[1] In this paper "arctic catchments" and "the Arctic" are defined as being situated above the Arctic Circle—(i.e. north of 66.56° N).

(or a few cores), which has returned fruitful information (Moore et al., 2001; Smith et al., 2004; Lamoureux and Gilbert, 2004; Hambley and Lamoureux, 2006; Bird et al., 2009; Thomas and Briner, 2009; Striberger et al., 2011; Ólafsdóttir et al., 2013), but results insufficient for determining sediment yields.

Ideally, lake-based sediment yield records should supplement more direct, albeit shorter, fluvial-based estimates of sediment yield (e.g. Menounos et al., 2006), unifying our fluvial-based achievements with an understanding of decadal- to millennial-scale landscape evolution (Evans and Church, 2000; Hodder et al., 2007); however, this approach is rare in the arctic (Taconite Inlet Lakes Project, Canada—Hardy, 1996; Lake Linnévatnet, Svalbard—Schiefer et al., 2017). Objectives of this paper are to: 1) apply a lake-based approach to estimate longer-term sediment yield to Lake Peters, Brooks Range, Alaska; 2) compare lake-based results with fluvial-based estimates by Thurston (in prep—Chapter 2); and 3) consider regional uniformity by comparing SSYs for Lake Peters to other arctic SSYs reported in literature.

3.3 Study Area

Lake Peters' catchment (69.32°N 145.05°W) is situated in the Arctic National Wildlife Refuge, north-eastern Brooks Range, approximately 300 km inside the Arctic Circle, and 70 km south of the Arctic Ocean (**Figure 3.1**). The catchment is 169 km^2, ringed by steep mountains, and as of August 2016 was 8% glaciated with some of the largest valley glaciers in Arctic Alaska. Present-day Lake Peters (6.8 km^2, 52 m deep, and 854 m asl) has weak stratification (Hobbie, 1962; D. Fortin, personal communication, June 10, 2016). The catchment remains undeveloped owing to the remote location and protection provided by the Arctic National Wildlife Refuge.

Carnivore Creek (128 km^2 catchment; 9% glacial coverage) is the primary tributary draining into Lake Peters. Several minor glacial and non-glacial catchments also drain into Lake Peters, including the second largest tributary–Chamberlin Creek (8 km^2 catchment; 26% glacial coverage) (**Figure 3.1**). Channel morphologies are described by Thurston (in prep—Chapter 2). Lake Peters is separated into two basins by a comma-shaped sill, with the deeper primary basin fed by the major tributaries at the south end of the lake, and the distal basin adjacent to the northward draining outflow. The surface of Lake Peters is frozen for most of the year, but sub-surface drainage occurs year-round. Lake Peters drains into Lake Schrader, and Lake Schrader drains into the Kekiktuk River, a tributary of the Sadlerochit River, which discharges into the Arctic Ocean.

From the 11th to the 19th Century, the Arctic experienced a long-term cooling trend, estimated from reconstructions to be 0.47^{o}C kyr^{-1}, followed by rapid 20th Century warming (McKay and Kaufman, 2014). At least since turn of the millennia, the Artic has experienced positive temperature anomalies for all seasons (Serreze et al., 2011). In Alaska, a general cooling of annual air temperatures has been reported from the 1950s through to 1976, followed by rapid warming (Cassano et al., 2011), driving widespread glacial recession and thinning (Molnia, 2007), and increased winter runoff over pan-Arctic Alaska (Lammers et al., 2001). The mean temperature increase in Alaska since the mid-

20th Century is ~2°C (Molnia, 2007). At Lake Peters (1980 - 2009) mean annual precipitation was 360 mm, and mean January and July monthly temperatures were -22.0°C and 10.5°C, respectively (Stavros and Hill, 2013).

Within Lake Peters' catchment, glaciers approximately 1 km^2 have reduced in length by 20% since the Little Ice Age (LIA)—*ca.* 1200-1850 CE, and the largest valley glaciers (2 - 4 km^2) have reduced in length by at least 30% since the LIA. Bedrock is the upper Neruokpuk section of the northeastern Brooks Range, comprising low-grade metasedimentary and sedimentary rocks, primarily southward-dipping sandstone, semischist, and phyllite, with minor chert and quartzite (Reed, 1968). Soils are sparse, and vegetation primarily consists of arctic grasses, herbs, and shrubs. Channel-side vegetation is sparse above 1300 m, but vegetation persists on some valley walls at higher elevations. Increases in vegetation productivity associated with longer, warmer summers is causing a phase transition from tundra to shrubland on the North Slope of the Brooks Range (Naito and Cairns, 2015; Tape et al ., 2011), but the rate of shrub expansion at Lake Peters is unknown.

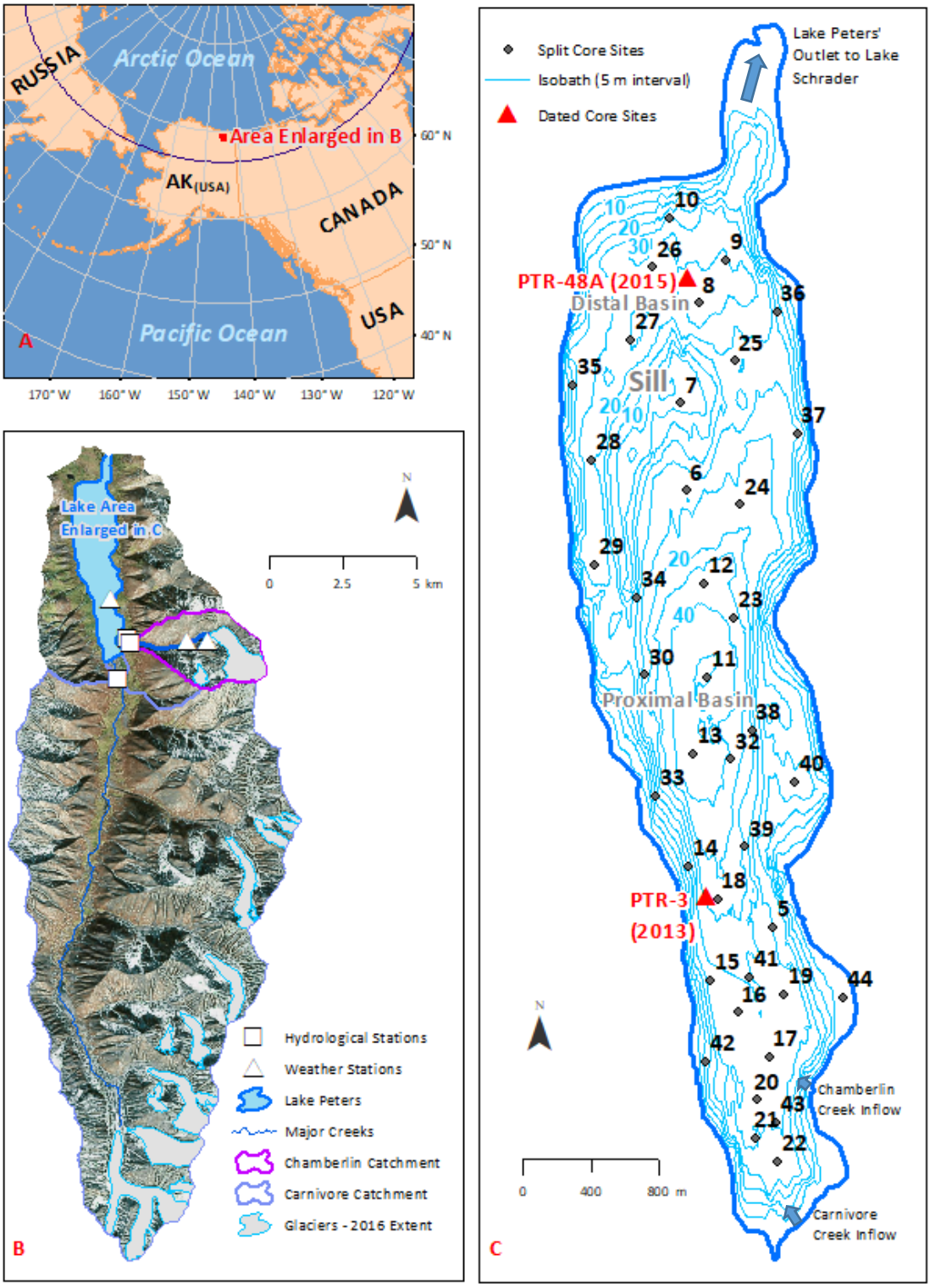

Figure 3.1: Map of the study area. A) Location of Lake Peters' catchment in the Brooks Range, Alaska (AK). B) Lake Peters' catchment, showing geographical features, hydrological stations, and weather stations. C) Lake Peters, showing isobaths, primary inflows and outflows, locations of sedimentary surface cores, and locations of dated cores. Base-map imagery sourced from ESRI DigitalGlobe.

3.4 Methods

3.4.1 Lake Coring and Bulk Physical Properties

An Aquatic Research Instruments Universal Percussion Corer with 6.7 cm diameter tubes was used to obtain 40 spatially distributed short sediment cores (9 – 26 cm long) from Lake Peters during late June and early July, 2015 (**Figure 3.1**). A distributed sampling program is important for obtaining unbiased accumulation chronologies over the depositional area (Evans and Church, 2000; Schiefer, 2006b). Cores were split lengthwise and the exposed surface was lightly scraped parallel to lamina at the lake-side research station, revealing fine sediment structures. Surfaces of cores were photographed while wet, and again after air-drying to near maximum visual contrast of laminae, using a digital camera on a fixed stand (refer to **Appendix I** for instrument details). When wet, 30 cores were volumetrically subsampled (1 cm^3) for dry bulk density (DBD; g cm^{-3}) using a 5 mL syringe at 0 – 1 cm and 2.5 – 3.5 cm down-core depths. An additional 15 DBD subsamples were obtained at a sediment depth of 5 – 6 cm, and occasional subsamples were obtained at 10 – 11 cm, 15 – 16 cm, and 20 – 21 cm down-core depth using the same method. Organic content was also estimated for all the subsamples using standard loss on ignition (LOI) methods (Håkanson and Jansson, 2002).

3.4.2 Marker Bed Correlations and Sediment Fluxes to Marker Bed A

The depth of a distinct lens of sand within Marker Bed A (denoted as the reference depth; **Figure 3.2**) was measured on both wet and dry core photographs using image viewing and analysis software. Measurements were made from the center of each core, unless there was asymmetric coning deformation of laminae, in which case measurements were made from the cone apex. Four cores proximal to the primary inflows were not long enough to capture Marker Bed A (Cores 17, 19, 21, and 22). For these cores, depths to shallower laminae were measured and adjusted proportionally to the reference depth by visually correlating them with nearby Core 20, which has similar sediment character and structure.

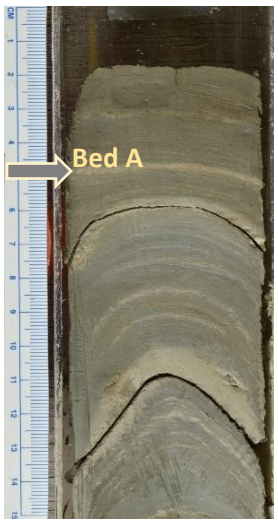

Figure 3.2: Core 8 (distal basin), showing Marker Bed A, Lake Peters, Brooks Range, Alaska.

Dry core reference depths adjusted for shortening were used for analysis (section 5.2.2 of **Appendix I**), to improve accuracy by measuring at maximal laminae contrast. The average relative difference between reference depths from corresponding wet and dry cores was used to make the adjustment. Sediment flux (g cm^{-2}) from core surfaces to the reference depth for each core site was calculated by the product of DBD (g cm^{-3}) and reference depth (cm), including spatial extrapolation to cores not sampled for DBD. Spatial trends in DBD down-core, down-lake, and with water depth were considered in calculating sediment flux, and for spatial extrapolation. Where necessary, regression models were developed in R software to model DBD based on spatial parameters.

3.4.3 Spatial Extrapolation of Sediment Fluxes

A multivariate spatial model was developed using R software to estimate sediment flux (g cm^{-2}) above the reference depth for any point within Lake Peters. Log-transformed distance from the primary inflow and water depth were used as predictors in the model, consistent with Schiefer (2006a). A 100 m by 100 m grid was overlaid on the suspended sediment depositional area of Lake Peters using GIS software, and the model was applied to the gridded points (refer to section 5.2.2 of **Appendix I** for model output data). Lake suspended sediment depositional area was defined as the total area of Lake Peters excluding areas shallower than 5 m water depth, where suspended load sedimentation is assumed negligible because of wind and wave mixing, and excluding the delta foreset slope areas of the primary Carnivore and Chamberlin Creek inflows, where sedimentation is assumed to be dominated by bedload.

3.4.4 Radiometric Dating and Sediment Flux

$^{240}Pu/^{239}Pu$ (2013 core (PTR-2); near Core 18, proximal basin) and ^{137}Cs (2016 core (PTR-48A); near Core 8, distal basin) isotope fallout testing was used to date Marker Bed A and estimate the temporal component of sediment fluxes (**Figure 3.1**). The maximum fallout in each core represents the peak of atmospheric weapons testing in 1963. PTR-2 was sampled at 0.5 cm intervals using Quadrupole Inductively Coupled Plasma Mass Spectrometry (ICPMS) at the Metropolitan State University of Denver (the ICPMS method is described in Ketterer et al., 2002). The top 7 cm of PTR-48A was sampled at 0.5 cm intervals and gamma counted at the University of Southern California. Gamma counting to determine ^{137}Cs (661 keV) activity was undertaken on an Ortec well-type intrinsic Ge detector (100 cc active volume). Minimum and maximum ages of the reference depth were estimated by scaling the Core 8 reference depth to the interval range of the ^{137}Cs maximum depths measured in PTR-48A. Sediment flux to the reference depth (g cm^{-2}) was divided by the scaled age estimates, to give the range of annual average fluxes (g cm^{-2} yr^{-1}) at each grid point. To test the consistency of this methodology in the proximal basin, minimum and maximum ages of the reference depth at the Core 18 site were estimated by applying the same method using PTR-2; results were compared with the range of annual average sediment flux found for Core 18 by spatially extrapolating the original method.

Spatial patterns of sediment flux within the suspended sediment depositional area of Lake Peters, calculated by averaging minimum and maximum sediment fluxes, were mapped for visual interpretation. Averaged sediment fluxes were multiplied by depositional area, to give sediment yield, and subsequently by lake catchment area to give SSY (Mg km^{-2} yr^{-1}). Confidence bands were used to find the lower and upper yield estimates.

3.4.5 Comparing Lake- and Fluvial-based Sediment Yields

In addition to the lake-based method, sediment yields to Lake Peters were calculated using a fluvial-based method by Thurston (in prep—Chapter 2). Multivariate regression models of suspended sediment concentrations (SSCs) were developed for Carnivore and Chamberlin Creeks separately,

using an optimized subset of 60 hydrological, climate, and time-related explanatory variables, all interpolated to match the times of suspended sediment sampling. Correlated variables were grouped together to ensure that they would not be selected in the same multivariate model. To find the best multivariate models for predicting SSCs, a Boolean for-loop was constructed in R software to cycle through the correlated groups, applying the 'glmulti' function and associated Akaike Information Criterion (AIC) (Calcagno and de Mazancourt, 2010).

Sediment yields and SSYs calculated using the lake-based method (long-term average), and fluvial-based method (2015-2016) (Thurston, in prep—Chapter 2) were compared. SSYs discharging to Lake Peters were also compared with those reported in literature for other locations above the Arctic Circle, with a minimum length of two open-channel seasons. All SSYs were plotted based on catchment area and glacial coverage for assessment of spatial trends and regional sediment transfer patterns.

3.5 Results

3.5.1 Sediment Character and Reference Depths

Sediments observed in surface cores (9-26 cm long) are light golden brown, inconsistently laminated, highly clastic, and dominantly fine grained (clays and silts) (**Figure 3.2**). No major slump deformation or massive deposits indicative of mass movements were observed in the lake sediments. Organic content (LOI) steadily increases down-lake from 2 to 3.5%. The lamina denoted Marker Bed A is the most readily identified sedimentary structure that is spatially distributed throughout the lake. The thickness of Marker Bed A ranges from 1.25 cm to 0.25 cm from proximal to distal lake settings. Comprising a distinct basal sand lens with yellow-hue, Marker Bed A is coarser than more recently deposited laminae. There are six laminae of equivalent or greater thickness than Marker Bed A in distal Core 8 (11.5 cm long), all deposited below Marker Bed A, but many cores were not long enough to capture these deeper beds. The reference depth in Marker Bed A ranged from a maximum of 28.2 cm in Core 22 near the primary inflows, to 2.4 cm in distal Core 25 (**Figure 3.1**). A parting surface formed in 70% of cores at the reference depth upon drying, allowing for relatively easy identification and correlation. Of the 40 short-cores sampled, Core 7 was disregarded because of bioturbation, and Core 31 was disregarded because it is in the same location as the longer and less disturbed Core 32.

3.5.2 Dry Bulk Density (DBD) and Measured Sediment Flux

Systematic trends in sediment DBD (g cm^{-3}) were observed both down-lake and down-core. Sediment becomes less dense with increasing distance from the primary Carnivore Creek inflow. Within 1.5 km of the primary inflow, DBD showed no significant down-core trend, and was approximately constant down-lake (**Figure 3.3**). Beyond 1.5 km from the primary inflow, near-core-surface DBD (0 - 1 cm) declines more rapidly with distance from the primary inflow, than for deeper sediments (≥ 2.5 cm down-core). Some additional variability in near-surface DBD is related to lake

water depth, with less dense sediment in shallower settings farther from the inflows; whereas deeper sediment densities are unrelated to water depth.

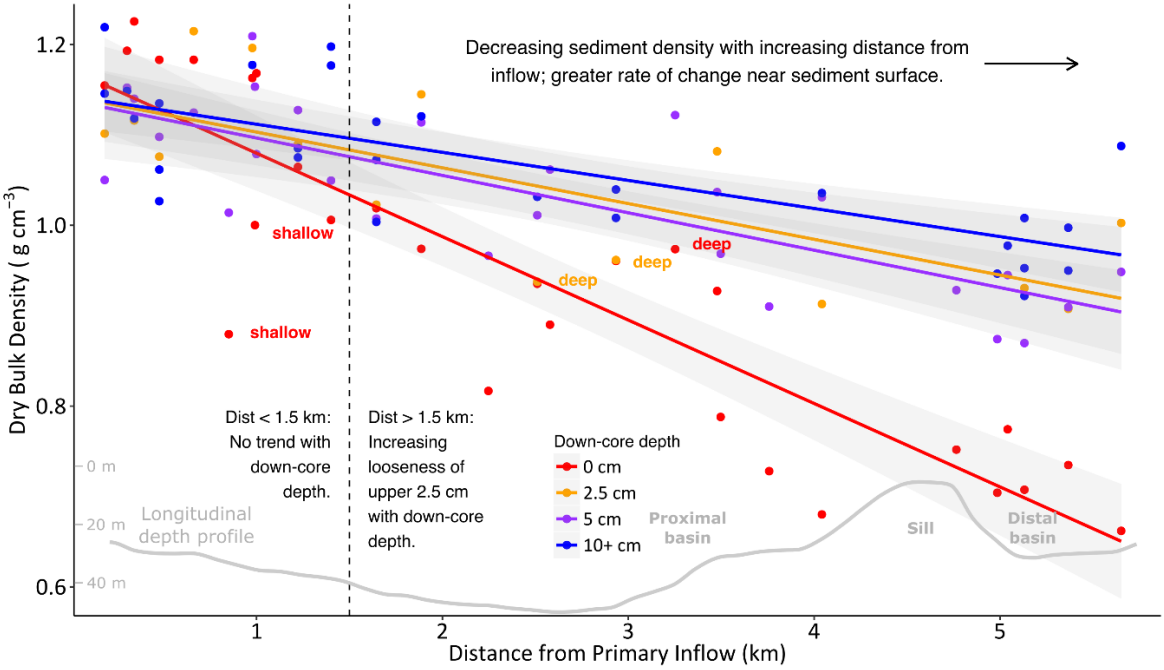

Figure 3.3: Down-lake trends in dry bulk density (DBD) for sampled down-core depths at Lake Peters, Brooks Range, Alaska. Additional spatial variability in near-surface DBDs is related to lake water depth (**Table 3.1**). Labels "shallow" and "deep" denote DBD samples from shallowest water depths (< 20 m) to deepest water depths (> 42 m), respectivley.

For cores within 1.5 km of the Carnivore Creek inflow, multiplying the mean DBD of 1.12 g cm^{-3} by the reference depth measured from wet sediment core imagery gave sediment fluxes. For cores beyond 1.5 km of the primary inflow, two separate regression models were built to account for systematic differences in spatial patterns of DBD sampled at 0-1 cm and at ≥ 2.5 cm down-core sediment depths, respectively (**Table 3.1**). The more negative coefficient for the distance model variable at near-surface sediment depths (0-1 cm) reflects the more rapid down-lake DBD decline, compared with deeper sediment (≥ 2.5 cm). The positive lake water depth variable in the same model captures the influence of water depth, with denser near-surface sediment in deeper water. The regression models were used to spatially interpolate DBD to all core sites beyond 1.5 km of the primary inflow. We assumed a linear decline in DBD from the near-surface sampled depth of 0-1 cm down to 2.5 cm, and constant DBD at ≥ 2.5 cm down-core depth.

3.5.3 Spatially Modeled Sediment Flux and Surface Core Dating

Distance from the primary inflow and water depth were both found to be significant predictors of calculated sediment fluxes (g cm^{-2}) at coring sites within Lake Peters (**Table 3.2**). This spatial

modeling was used to extrapolate sediment fluxes to points on a 100 m by 100 m grid across Lake Peters, prior to assigning a temporal dimension to the sediment fluxes.

Table 3.1: Regression models for dry bulk density (DBD) in Lake Peters beyond 1.5 km from the primary inflow. Overall model values include residual standard error (Res. SE), adjusted R^2 (Adj. R^2), F-statistic (F-stat), degrees of freedom (DF), and p-value significance (Signif.), respectively. Individual variable values include coefficients, standard error (SE) of the coefficients, and p-value significance of the coefficients (Signif.), respectively. Significance codes are `***´ (p < 0.001), `**´ (p = 0.001 to 0.01), `*´ (p = 0.01 to 0.05), `.´ (p = 0.05 to 0.1), and ` ´ (p > 0.1).

Statistic	**Model for > 1.5 km from primary inflow at 0-1 cm core depth**	**Model for > 1.5 km from primary inflow at ≥ 2.5 cm core depths**
Res. SE	0.075	0.060
Adj. R^2	0.829	0.561
F-stat	66.34	88.32
DF	25	68
Signif.	***	***
Intercept	1.079	1.140
SE	0.052	0.012
Signif.	***	***
Distance from Primary Inflow (km)	-0.096	-0.036
SE	0.008	0.004
Signif.	***	***
Lake Water Depth (m)	0.003	
SE	0.002	
Signif.	*	

Table 3.2 Spatial model of sediment flux (g cm^{-2}) to the Marker Bed A reference depth. Overall model values include residual standard error (SE), adjusted R^2 (Adj. R^2), F-statistic (F-stat), degrees of freedom (DF), and p-value significance (Signif.), respectively. Individual variable values include coefficients, standard error (SE) of the coefficients, and p-value significance of the coefficients (Signif.), respectively. Significance codes are `***´ (p < 0.001), `**´ (p =0.001 to 0.01), `*´ (p = 0.01 to 0.05), `.´ (p = 0.05 to 0.1), and ` ´ (p > 0.1).

Statistic	**Model Output**
Res. SE	0.218
Adj. R^2	0.917
F-stat	206.2
DF	35
Signif.	***
Intercept	9.376
SE	0.394
Signif.	***
Logged[1] Distance from Primary Inflows (m)	-1.039
SE	0.051
Signif.	***
Lake Water Depth (m)	0.021
SE	0.004
Signif.	***

[1]Natural logarithm

$^{240}Pu/^{239}Pu$ (2013 core (PTR-2); near Core 18, proximal basin) and ^{137}Cs (2016 core (PTR-48A); near Core 8, distal basin) isotope dating allowed us to estimate the temporal dimension to sediment deposition, from core surfaces down to measured reference depths. Maximum ^{137}Cs activity (1963) was recorded between 3.75 and 4.25 cm sediment depths in PTR-48A (the dated 2016 core; distal basin). Scaling 1963 to each end of the ^{137}Cs maximum range, and linearly adjusting for the shallower 3.33 cm reference depth in nearby Core 8, Marker Bed A is estimated to have been deposited 39 to 45 years prior to short core collection—between 1970 and 1976. Core 18 is situated near the PTR-3 (2013 dated core; proximal basin), and was used for testing replicability of our dating control. At Core 18, sediment flux to the reference depth (8.56 cm) was calculated to be 0.18 g cm^{-2} yr^{-1} by stratigraphically correlating dating results from PTR-48A, consistent with the sediment flux of 0.17 – 0.22 g cm^{-2} yr^{-1} calculated by similarly applying dating results from PTR-3 (8 - 10 cm maximum $^{240}Pu/^{239}Pu$ activity). Sediment fluxes (g cm^{-2}) to reference depths were divided by 39 and 45 years, respectively, to give an upper and lower mean annual sediment flux (g cm^{-2} yr^{-1}) for each grid point (**Figure 3.4**).

A systematic non-linear down-lake trend in sediment flux was shown, decreasing from 0.94 g cm^{-2} yr^{-1} to 0.04 g cm^{-2} yr^{-1} within the primary basin (**Figure 3.4**). Spatially modeled sediment flux is greatest within 800 m of primary inflows (0.44 – 0.94 g cm^{-2} yr^{-1}), but some large negative residuals suggest the model performs poorly here, with overestimated sediment fluxes. Between 800 m and 1.5 km from the primary inflow modeled sediment flux is dominantly within the range of 0.27 – 0.44 g cm^{-2} yr^{-1}, but here the model consistently underestimates sediment flux. Sediment fluxes decrease beyond this distance, and greater sediment deposition is observed centrally in deeper waters (0.17 to 0.27 g cm^{-2} yr^{-1}), than at lake peripheries (0.10 – 0.17 g cm^{-2} yr^{-1}) through most of the proximal basin. At the distal end of the proximal basin and in the distal basin, sediment flux does not exceed 0.10 g cm^{-2} yr^{-1}.

3.5.4 Suspended Sediment Yields and Discharge

Lower and upper means of the gridded sediment fluxes were calculated, and converted to a sediment yield range by multiplying by lake depositional area. Using this method, average sediment yield transferred to Lake Peters is estimated to be 8700 Mg yr^{-1}. Dividing by catchment area, this equates to an estimated average SSY of 52 Mg km^{-2} yr^{-1}. Annual average sediment yields calculated using the lake-based method are comparable with fluvial-based sediment yield estimates by Thurston (in prep—Chapter 2) (**Table 3.3**). Considering the average sediment yield to Lake Peters of 8700 Mg yr^{-1}, sediment yield in 2015 was about 40% below average, and sediment yield in 2016 was about 30% above average.

Rearrangement of fluvially modeled SSC to extrapolate discharge, assuming deposition over two to five days by a flood in Carnivore Creek, suggests mean daily discharges an order of magnitude greater than the discharges observed during the 2016 peak flood would have deposited Marker Bed A. Mean daily discharges are estimated to have been hundreds of cumecs during the 1970s event, rather than tens of cumecs as for the 2016 event.

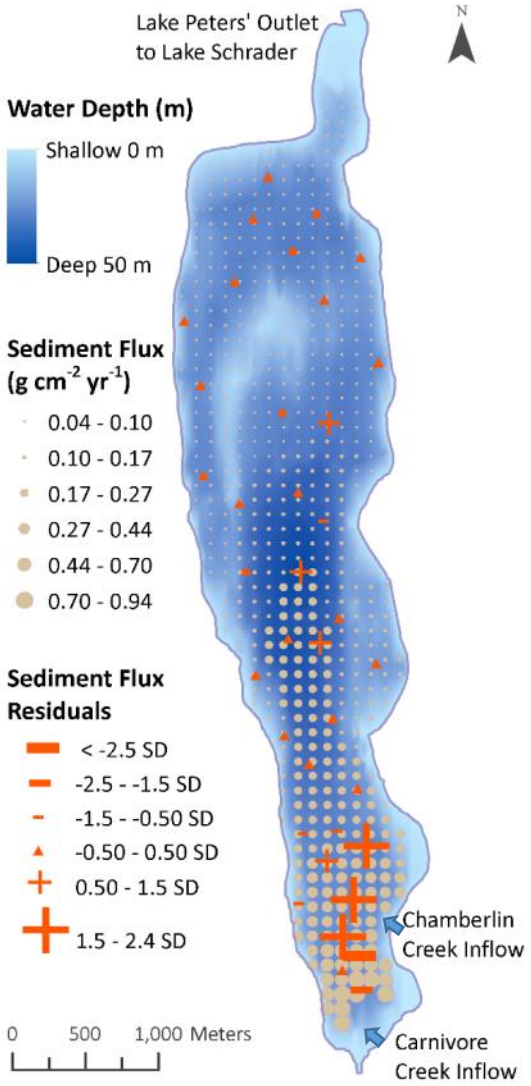

Figure 3.4: Spatial extrapolation of sediment fluxes sampled at core sites in 2015 to points on a 100 m grid across Lake Peters, Brooks Range, Alaska. Sediment flux was measured using a reference depth deposited in *ca.* 1973 and DBD. Sediment flux residuals represent the difference between measured sediment flux, and spatially modeled sediment flux, using standard deviations (SD). Modeled sediment flux was calculated by applying the regression model shown in Table 3.2 (g cm^{-2}), and subsequently extrapolating ^{137}CS dating results to gridded points (g cm^{-2} yr^{-1}). Positive residuals indicate that the regression model is under-predicting sediment flux, and negative residuals indicate that the regression model is over-predicting sediment flux.

Table 3.3: Comparison of sediment yields (Mg yr^{-1}) and SSYs (Mg km^{-2} yr^{-1}) using lake-based and fluvial-based methods. Error bands are shown in parentheses. Error bands for average sediment yields (1973-2015) calculated using the lake-based method incorporate 95% confidence band error for the sediment flux model and estimated error in the dating method (estimated deposition over 39 years or 45 years). Error bands for sediment yields calculated using the fluvial-based method are 95% confidence bands for the suspended sediment concentration (SSC) models.

Yield Type	CAR[1]	CHB[2]	CAR and CHB[3]
1973-2015 average sediment yield			8700 (7000-11000)
2015 fluvial model sediment yield	7000 (3000-22000)	280 (170-460)	7000 (3000-22000)
2016 fluvial model sediment yield	12000 (6400-23000)	320 (230-460)	12000 (7000-23000)
1963-2015 average SSY			52 (42-64)
2015 fluvial model SSY	55 (23-170)	35 (21-57)	53 (44-230)
2016 fluvial model SSY	92 (50-180)	40 (29-57)	89 (79-230)

[1] Annual SY for Carnivore Creek (CAR) calculated using the fluvial-based method. Fluvial models used to estimate SY (Chapter 2) include: 62% NTU-base model, 2% Q-base model, 20% average SY at < 10 $m^3 s^{-1}$, 16% average SY below 5 $m^3 s^{-1}$ (2015); 40% NTU-base model, 31% Q-base model, 13% average SY below 10 $m^3 s^{-1}$, 16% average SY at < 5 $m^3 s^{-1}$ (2016).

[2] Annual SY for Chamberlin Creek (CHB) calculated using the fluvial-based method. Fluvial models used to estimate SY (Chapter 2) include:39% NTU-base model, 29% Q-base model, and 32% average SY at < 0.25 $m^3 s^{-1}$ (2015);29% NTU-base model, 41% Q-base model, 30% average SY at < 0.25 $m^3 s^{-1}$ (2016).

[3] Annual average SY calculated using the lake-based method. This also includes contributions from minor tributaries, additional to Carnivore and Chamberlin Creeks.

Arctic SSYs span about four orders of magnitude, and SSYs estimated for Lake Peters' catchment are comparable to other lightly glacierized catchments (**Figure 3.5**). Continuous sediment yields spanning at least two open-channel seasons in Arctic Alaska are sparse (Tape et al., 2011, Thurston, in prep—Chapter 2). SSYs for heavily glaciated catchments are significantly higher than SSYs for catchments with little or no glacial coverage. For dominantly non-glacial catchments, SSYs show a weak declining trend with catchment area, which is statistically significant when the highest and lowest outliers are removed; whereas SSYs from heavily glaciated catchments show no trend with catchment area (**Figure 3.5**).

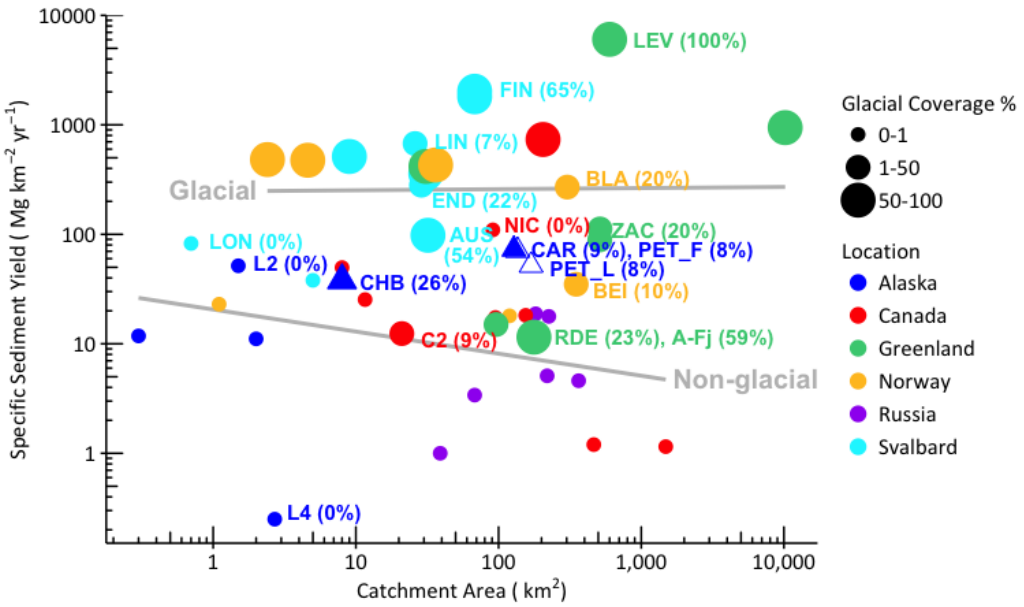

Figure 3.5: Comparison of SSYs estimated for catchments above the Arctic Circle, considering catchment area and glacial coverage (tabled in section 5.3.3 of **Appendix II**). Criteria for selecting SSYs included that they must be based on at least two seasons of records that extend over most of the season (e.g. 3-4 months). Locations discussed in-text are denoted with abbreviated labels and glacial coverage in parentheses. Abbreviations and data sources are: Carnivore fluvial-based SSY (**CAR**); Chamberlin fluvial-based SSY (**CHB**); combined Carnivore and Chamberlin fluvial-based SSY (**PET_F**); and lake-based SSY for Lake Peters (**PET_L**), Brooks Range, Alaska (this study; Thurston, in prep); Beiarelva at Klipa (**BEI**), and Blakkaga (**BLA**), Norway (Bogen, 1996); Lake C2 (**C2**), Canada (Hardy et al., 1996); Austre Broggerbreen (**AUS**), and Finsterwalderbreen (**FIN**), Svalbard (Hodson et al., 1997); Nicolay Lake (**NIC**), Canada (Lamoureux, 2000); Endalselva (**END**), and Londonelva (**LON**), Svalbard (Bogen and Bønsnes, 2003); Finsterwalderbreen (**FIN**), Svalbard (Hodgkins et al., 2003); Lake 2 (**L2**), and Lake 4 (**L4**), Brooks Range, Alaska (Tape et al., 2011); A-Fjord, Marmorilik (**A-Fj**), Røde Elv, Disko Island (**RDE**), Leverett Glacier, Watson River (**LEV**) and Zackenbergelven River, below Linderman Rive (**ZAC**), Greenland (Hasholt, 2016; and for L18 Cowton et al., 2012); Lake Linnévatnet (**LIN**), Svalbard (Schiefer et al., 2017). Additional data sources: Church and Ryder, 1972; Cogley, 1975; Barsch et al., 1994; Lewkowicz and Wolfe, 1994; Rasch et al., 2000; Sollid et al., 1994; Forbes and Lamoureux, 2005; Gordeev, 2006; Lewis et al., 2012. SSY **–** catchment area relation for non-glacial catchments: SSY = 20.6 × Area$^{\wedge -0.2}$; Res. SE = 1.6 on 19 DF; Adj. R^2 = 0.05; F-stat = 2.06; p-value = 0.17, and with the highest (**NIC**) and lowest (**L4**) SSYs removed: SSY = 32.6 x Area$^{\wedge -0.31}$; Res. SE = 1.08 on 17 DF; Adj. R^2 = 0.33; F-stat = 9.71; p-value = 0.006. Equivalent relation for glacial catchments: SSY = 247 × Area$^{\wedge 0.01}$; Res. SE = 1.736 on 19 DF; Adj. R^2 = -0.05; F-stat = 0.002; p-value = 0.96.

3.6 Discussion

Although sediment yield is the primary output of our analyses, spatial patterns of sediment character and sedimentation rates (requisite to find sediment yield by the lake-based approach) provide important complementary information towards understanding sediment transfer processes from source to sink. Sediment character and sedimentation rates are primarily related to

within-lake processes, whilst sediment yields are helpful for understanding processes driving catchment- and regional-scale patterns of sediment delivery.

3.6.1 Laminations and Major Sedimentation Events

Sedimentation processes at Lake Peters fail to produce varves, which are often sought after in proglacial lakes for their high-resolution chronological record of deposition. The lack of varves is attributed to the relatively low ratio of catchment area to lake area (ratio of 25), together with relatively low glacial coverage (8%) (Desloges and Gilbert, 1994), producing sediment yields too low for distinct annual laminations. Discernable laminae are of varying thickness, suggesting high intra- or inter-annual variability.

The last extreme depositional event in Lake Peters probably occurred between 1970 and 1976 (39 to 45 years ago) when Marker Bed A was deposited. The younger age estimate for Marker Bed A (1976) corresponds with the significant upward temperature shift reported in Alaska (Cassano et al., 2011). An extreme event around the same time is observed in sedimentary records extracted from 'Lake 2', Chandler River corridor (Tape et al., 2011), although the same event is not recorded in three other cored water bodies in the same corridor. The Kuparuk River record, measured near Deadhorse, Alaska (165 km northwest of Lake Peters), peaks at almost one and a half times the envelope of visually non-outlying discharges in 1978, but regional events in Alaska are estimated to peak two times above visually non-outlying discharges (J. Curran, personal communication, July 19, 2017). A search of fluvial and lacustrine discharge records available for the 1970s in Alaska did not return any other comparable events (Curran et al., 2016); however, Alaskan discharge records are infrequent and sparse, making it difficult to determine whether Marker Bed A was deposited by a local event, or by a regional rainfall event. The lens of sand near the bottom of Marker Bed A (the reference depth) is spatially distributed, indicating that sediment eroded from the shoreline, or littoral sources transported by overland flow, may have contributed to deposition of the bed. The non-contact glacial-fed nature of Lake Peters, coupled with weak thermal stratification, affords possibility that high density interflows carried sediment to lake peripheries and the distal basin, over (< 5 m deep) or around (> 20 m deep) the sill; however, this is less likely given the lake is 6.2 km long. There is only one notably thick and coarse lamina above Marker Bed A, but it is not spatially distributed throughout the distal basin, and is thinner (0.6 cm – 0 cm thickness down-lake) than Marker Bed A (1.25 cm – 0.25 cm thickness down-lake). Coarse-grained deposits at Lake Peters, which may be associated with large pulses of sediment transfer, such as flood events, appear less frequent than reported for late 20th Century periods in the sub-Arctic Canadian cordillera, Canadian High Arctic, southern Alaska, and Svalbard (Desloges and Gilbert, 1994, and Menounos et al., 2006; Lamoureux, 2000; Loso, 2009; Schiefer et al., 2017, respectively).

3.6.2 Within-Lake Processes

DBD is a measure of sediment character, relatable to particle size, sediment composition, and other depositional processes. In Lake Peters, the low-density sediment in the uppermost 1 cm of surface

cores may reflect a combination of increasing down-core compaction, with higher porosity in sediments near the surface, and a decreasing up-core trend related to trends in sediment input to the lake, such as a decreasing abundance of glacial rock flour. The down-lake trend of decreasing DBD has similarly been observed in Green Lake, Canada, which was primarily associated with the grading pattern of particle size (Schiefer, 2006c). At Lake Peters, the down-lake trend may also be associated with particle size, and/or biogenic processes. High-energy deposition near the inflows, especially where sediment is focused in the proximal basin (0.6 to 1.5 km down-lake), may deposit coarser particles. Coarser particles may result in greater sediment density, compared with deposition of finer material down-lake. Near-surface organic content in Lake Peters is relatively low (2-3.5%), compared to Burial Lake, western Brooks Range, Alaska (11.6%) (Finkenbinder et al., 2015), for example, and significant bioturbation was only observed in one core situated on the sill between the proximal and distal basins (Core 7; **Figure 3.1**). However, autochthonous organic content inferred by LOI decreased down-lake, and this small percentage of organic content could affect DBD.

Spatial patterns in bottom sediment flux are valuable for understanding within-lake transport and deposition. Distance from the primary inflows and water depth together explained 90% of the spatial variability in sediment fluxes at Lake Peters, with distance from the primary inflow exerting dominant control (**Table 3.2**). Systematic non-linear down-lake trends in sediment flux are typical of proglacial lacustrine sedimentation (Evans and Church, 2000; Schiefer, 2006a), and relatable to changing and weakening currents and circulation processes down-lake. Observed evidence of silt on snow in Spring suggests eolian processes may also carry sediment into Lake Peters (D. Fortin, personal communication, July 10, 2017), as has been observed in the Canadian Arctic (Lewis et al., 2002; Lamoureux and Gilbert, 2004), and Svalsbard (Schiefer et al., 2017). Relatively strong underflows and interflows are interpreted to be active up to 3 km down-lake (D. Fortin, personal communication, July 10, 2017), where average fluxes of 0.36 g cm^{-2} yr^{-1} are deposited in deeper mid-lake waters (**Figure 3.4**). Beyond this distance sediment fluxes drop considerably, and weaker lake currents result in less than 0.10 g cm^{-2} yr^{-1} on average at the distal end of the proximal basin. Fluxes towards the distal end of the proximal basin are similar to fluxes in the distal basin, indicating that currents exert a greater control on sediment deposition than topographical basin separation.

Water depth explains additional spatial variability in sediment flux at near-surface sediment depths (0-1 cm down-core), and has been related to sediment settling from a still water column under ice, and to the effectiveness of sediment focusing processes (Evans and Church, 2000), including density flow currents, peripheral wave action, and intermittent water column mixing (Schiefer, 2006a). By substituting maximum lake water depth and half of the maximum lake water depth into multivariate regression equations estimating sediment flux, while leaving distance down-lake constant, we found that sediment flux in Lake Peters is less sensitive to water depth than Green Lake, southern Coast Mountains, British Columbia, Canada (44 m maximum depth; Schiefer, 2006a), but much more sensitive than shallow lakes in Cathedral Provincial Park, Cascade Mountains, southern British Columbia (< 10 maximum depth; Evans and Church, 2000). This comparison

supports sediment focusing, which is probably more significant in deeper, steep-sided lakes, as an explanation of the water depth variable. Sediment focusing is evidenced by cross-lake trends in sediment flux in the proximal basin of Lake Peters (52 m maximum depth; **Figure 3.4**), where interflows and underflows are interpreted to actively deposit sediment mid-lake. The potentially lesser significance of sediment focusing in Lake Peters compared to Green Lake could be explained by the fewer number of sub-basins, weaker turbidity currents, and less in-lake slope failure activity.

Residuals are used to assess patterns in biases of the spatial sediment flux model. Deviations between measured and modeled fluxes are smaller and less complex than those reported in a similar study (Schiefer, 2006a), probably because of the concentration of inflows at one end of Lake Peters and elongate shape, with simple bathymetry. Sediment flux models for alpine lakes in British Columbia, with elongate shapes and simple morphometry, have been found to outperform models for lakes with complex shapes and morphometry (Evans and Church, 2000). Sediment flux residuals reveal that deposition within 1.5 km of the Carnivore Creek inflow is more irregular than deposition farther down-lake (**Figure 3.4**). The spatial model overestimates sediment fluxes (highly negative residuals) within 0.60 km of the inflow, likely because strong, sediment-rich currents originating from the Carnivore Creek inflow bypass this distance prior to sediment deposition. A sharp transition to underestimation of sediment flux (highly positive residuals) between 0.60 km and 1.5 km down-lake (**Figure 3.4**) might be an expected outcome of the secondary Chamberlin Creek inflow not being accounted for in the model, similar to multiple-inflow Green Lake (Schiefer, 2006a). However, if the fluvially estimated range of 2015-2016 sediment yields for Chamberlin Creek are representative of sediment delivery over recent decades, only a small fraction of the highly positive residuals can be attributed to sediment originating from Chamberlin Creek. The highly positive residuals are, therefore, most likely explained by focused deposition of sediment between 0.60 km and 1.5 km down-lake that has bypassed the 0.60 km length of Lake Peters near the Carnivore Creek inflow. Farther down-lake, underestimation of sediment flux (moderate positive residuals) occurs in deeper mid-lake waters, suggestive of sediment focusing not captured by the model in the most steep-sided part of the lake. Smaller residuals in both directions are difficult to interpret (**Figure 3.4**), but broadly reflect complex near-inflow and near-shore sediment transport and depositional processes.

3.6.3 Catchment and Regional Scale Processes

Modeling spatially distributed sediment flux allowed us to make an inter-decadal, lake-based estimate of SSY (**Table 3.3**). The average SSY for Lake Peters' catchment calculated using the lake-based method returned results similar to the 2015 fluvial-based modeling, but less than 2016 fluvial-based modeling (**Table 3.3**). Although disparity in methods appears minimal, consistent with Menounos et al. (2006), the lake-based method is more likely to return larger sediment yields than the fluvial-based method because: it incorporates sources additional to the Carnivore and Chamberlin Creek inflows, including littoral sources, minor side gullies and catchments, and autochthonous sources; it includes deposition for entire years, rather than only the open-channel

seasons; and is more likely to include inter-annual extreme events. This supports reasoning that sediment yield in 2016 was above the average regime for the period *ca.* 1973 to 2015, as a result of high snow-water equivalent (SWE) and a rainfall event in July (Thurston, in prep—Chapter 2). However, sediment coring in 2017 revealed that the 2016 event did not deposit a distinct thick, coarse bed, which may have required an order of magnitude more discharge per day of flooding.

Catchment area (Milliman and Syvitski, 1992; Syvitski, 2002; Lewis and Lamoureux, 2010) and glacial coverage (Church and Ryder, 1972; Guymon, 1974; Lewkowicz and Wolfe, 1994; Hallet et al., 1996; Hasholt, 2016) are two well-known controls of sediment yield. Arctic-wide SSYs are one to three orders of magnitude greater in heavily glaciated catchments, which show no trend with catchment area (**Figure 3.5**). Lack of trend is probably related to glacier thermal regimes, glacier size, and underlying lithology (Hallet et al., 1996; Hodson and Ferguson, 1999), and potentially also to the extended length of the paraglacial cycle in larger catchments (Church and Ryder, 1972; Church and Slaymaker, 1989). Large, fast-moving glaciers often have higher effective erosion rates comparative to small cirque glaciers (Hallet et al., 1996), counteracting sediment storage in larger catchments. Conversely, SSYs in non-glaciated arctic catchments show a weak, albeit declining, trend with catchment area (**Figure 3.5**), consistent with the conventional model of increasing potential for lowland sediment storage within larger catchments (Schiefer et al., 2001). Other factors exerting control on arctic SSYs explain the variability around these trends.

Four arctic catchments show anonymously high SSYs (**Figure 3.5**). The high SSYs for the glaciated Finsterwalderbreen, Svalbard (65% glaciated; Hodson et al., 1997; Hodgkins et al., 2003), and Leverett (Location 18), Greenland (100% glaciated; Cowton et al., 2012; Hasolt, 2016), catchments are both attributed to glacial processes. Finsterwalderbreen Glacier is warm-based, with a significant subglacial drainage system providing the primary source of sediment, in contrast to the nearby cold-based Austre Brøggerbreen Glacier, which has a significantly lower estimated SSY (Hodson et al., 1997; Hodgkins et al., 2003). Similarly, Leverett Glacier's high SSY is attributed to a zone of rapid erosion at the ice-sheet margin, driven by efficient subglacial drainage of surface meltwaters (Cowton et al., 2012). The two non-glaciated catchments showing relatively high SSYs are Londonelva, Svalbard (82 Mg km^{-2} yr^{-1}) and Nicolay Lake, Canada (110 Mg km^{-2} yr^{-1}), both in high Arctic locations (79°N and 77 °N, respectively) with erodible lithologies and sparse vegetation cover. Londonelva catchment comprises loose carbonate and highly frost-weathered bedrock (Bogen and Bønses, 2003), and Nicolay Lake Catchment comprises fine-grained marine and lacustrine surficial deposits emerged by post-glacial isostatic rebound, atop poorly consolidated sandstone and mudstone bedrock (Lamoureux, 2000). In addition to high SSYs, two anomalously low SSYs are observed (**Figure 3.5**). A-Fjord, Marmorilik, Greenland recorded an anomalously low average SSY (11.5 Mg km^{-2} yr^{-1} for 1978-1989), despite the high glacial coverage (59%), which is attributed to the trapping efficiency of lakes in the catchment (Hasholt, 2016). Tape et al. (2011) report an anomalously low SSY (0.25 Mg km^{-2} yr^{-1}) for the non-glacial 'Lake 4', Chandler River Corridor, Brooks Range, Alaska. Situated on an elevated river terrace, the water body lacks any identifiable inlet or drainage channels, and is surrounded by stabilizing shrubs.

SSYs for arctic catchments with similar glacial coverage (7-10%) to Lake Peters' catchment and the Carnivore Creek sub-catchment vary by an order of magnitude, ranging from 12 Mg km^{-2} yr^{-1} to 675 Mg km^{-2} yr^{-1}. Both Lake C2, northern Ellesmere Island, Canada (12 Mg km^{-2} yr^{-1}; 9% glacier coverage; Hardy, 1996) and the glacial-fed Beirelv River at Klipa, Norway (35 Mg km^{-2} yr^{-1}; 10% glacier coverage; Bogen, 1996) produce SSYs of the same order of magnitude as calculated for Lake Peters' catchment (**Table 3.3**). SSY for Lake C2 is probably low because discharge in the monitored period (1990-1992) was almost exclusively snowmelt, with absence of rainfall events (Hardy, 1996). Beirelv River's SSY is similar to our 2015 fluvial-based results (**Table 3.3**), but lower than SSYs calculated for Lake Peters' catchment using the lake-based method and the fluvial-based method for 2016. Bogen (1996) describes hard igneous and metamorphic rocks in the area, limiting erosion and sediment supply. SSY reported for Lake Linnévatnet, Svalbard (675 Mg km^{-2} yr^{-1}; 7% glacier coverage; Schiefer et al., 2017) is an order of magnitude higher than all other SSYs for arctic catchments with similar glacial coverage. This is related to multiple recent extreme events elevating the average SSY, as well as subglacial processes promoting sediment production and transport (Schiefer et al., 2017).

Interestingly, the SSY for the Chamberlin Creek sub-catchment is lower than Lake Peters' catchment and the Carnivore Creek sub-catchment, despite significantly higher glacial coverage (26%, 8%, 9% glacial coverage, respectively) (**Figure 3.4).** Four arctic locations shown in **Figure 3.4** have similar glacial coverage (20-23%) to the Chamberlin Creek sub-catchment, and three of these also have higher reported SSYs (Endalselva, Svalbard—Bogen and Bønses, 2003; Blakkaga, Norway—Bogen, 1996; and the Zackenburg River in Greenland—Hasholt, 2016). Only Røde Elv, Disko Island, Greenland has a lower reported SSY (Hasholt, 2016). The relatively low SSY for Chamberlin Creek is at least partly attributed to fine sediment exhaustion (see Thurston, in prep—Chapter 2). Such exhaustion is relatable to the steep slope and stream power effectively transporting fine sediment through the relatively small catchment–potentially dwarfing wintertime glacial weathering (Østrem, 1975; Rasch et al., 2000), and/or subglacial thermal processes (Hodson and Ferguson, 1999; Bogen and Bønses, 2003; Irvine-Fynn et al., 2005).

3.7 Conclusions

Although sediment yield is inherently difficult to measure and model, we have shown that spatially modeled lacustrine sediment flux and fluvial-based multivariate models of SSC can both be applied to obtain sediment yields for a remote arctic catchment. A combined lake-based and fluvial-based approach is promoted because: it increases precision and reliability of inherently variable sediment yield calculations (Menounos et al., 2006); enables both within-lake and catchment-scale processes to be interpreted from lake- and fluvial-based modeling, respectively; and allows contemporary sediment yields to be compared with longer-term sediment yields to better interpret major drivers and system changes. Lake-based approaches can be successful in the absence of varves, and the longer-term records produced are particularly useful for assessing inter-annual variability and extreme event sedimentation (Menounos et al., 2006; Schiefer, 2006a). The lake-based approach requires intensive lake coring and sampling, a spatially distributed chronological control depth, and

reliable dating results. Fluvial-based approaches require intensive stream sampling to provide a direct measure of contemporary sediment yields, and are favored for improving our understanding of shorter-term geomorphic and hydroclimatic processes. Such knowledge can subsequently be applied to inform paleo-reconstructions and environmental system modeling of sediment transfer and sediment yields.

Our methods have assessed within-lake processes, catchment-scale processes, and regional arctic processes driving sediment transfer. At Lake Peters, within-lake processes are fairly typical of arctic and sub-arctic lakes, with sediment density and associated sediment flux decreasing down-lake, sediment bypassing away from the primary inflow, and some sediment focusing in the proximal basin (**Figure 3.4**). Catchment-scale processes are complex, but sediment yield is largely driven by intense summer rainfall events, annual SWE, and sediment exhaustion (Thurston, in prep—Chapter 2). At the regional scale, our results signify that considering catchment area, lithology, glacial coverage and thermal regime when undertaking glaciofluvial system modeling of arctic sediment yields, will be imperative for producing fruitful results.

3.8 Acknowledgements

The authors are grateful for support from the National Science Foundation, Arctic System Science Program, which provided collaborative grant funding (award # 1418000). The authors also acknowledge additional support from the Environmental Professionals of Arizona (EPAZ) Environmental Scholarship Program. Permits to undertake this research in the Arctic National Wildlife Refuge were granted by the United States Department of the Interior - Fish and Wildlife Service.

3.9 References

Arnborg L, Walker HJ, Peippo J. 1967. Suspended Load in the Colville River, Alaska. *Geografiska Annaler* **49 A** (2-4): 131-144.

Barsch, D., Gude, M., Mäusbacher, R., Schukraft, G., & Schulte, A. (1994). Recent fluvial sediment budgets in glacial and periglacial environments, NW Spitsbergen. *Zeitschrift für Geomorphologie, Supplementband* **97**: 111-122.

Bird WB, Abbot MB, Finney BP, Kutchko B. 2009. A 2000 year varve-based climate record from the central Brooks Range, Alaska. *Journal of Paleolimnology* **41**: 25-41. DOI: 10.1007/s10933-008-9262-y.

` Bogen J. 1996. Erosion and sediment yield in Norwegian rivers. *In Erosion and Sediment Yield: Global and Regional Perspectives*. International Association of Hydrological Sciences (eds), IAHS Publication **236**. IAHS Press: Wallingford; 73-84.

Bogen J, Bønsnes TE. 2003. Erosion and sediment transport in High Arctic rivers, Svalbard. *Polar Research* **22**(2): 175-189.

Church M, Ryder M. 1972. Paraglacial Sedimentation: A Consideration of Fluvial Processes Conditioned by Glaciation. *Geological Society of America Bulletin* **83**: 3059-3072.

Church M, Slaymaker O. 1989. Disequilibrium of Holocene sediment yield in glaciated British Columbia. *Nature* **337**: 452-454.

Calcagno V, de Mazancourt C. 2010. glmulti: An R Package for Easy Automated Model Selection with (Generalized) Linear Models. *Journal of Statistical Software* **34**(12): 1-28.

Cassano EN, Cassano JJ, Nolan M. 2011. Synoptic weather pattern controls on temperature in Alaska. *Journal of Geophysical Research* **116**: 1-19. DOI: 10.1029/2010JD015341.

Cogley JG. 1975. Properties of Surface Runoff in the High Arctic. Doctor of Philosophy Dissertation (Geography). McMaster University: Hamilton, Ontario.

Cowton T, Nienow P, Bartholomew I, Sole A, Mair D. 2012. Rapid erosion beneath the Greenland ice sheet. *Geology* **40**(4): 343-346. DOI:10.1130/G32687.1.

Curran JH, Barth NA, Veilleux AG, Ourso RT. 2016. Estimating Flood Magnitude and Frequency at Gaged and Ungaged Sites on Streams in Alaska an Conterminous Basins in Canada, Based on Data through Water Year 2012. Scientific Investigations Report 2016-5024. U.S. Department of the Interior and U.S. Geological Survey: Reston, Virginia.

Desloges JR, Gilbert R. 1994. The record of extreme hydrological and geomorphological events inferred from glaciolacustrine sediments. *Variability in Stream Erosion and Sediment Transport (Proceedings of the Canberra Symposium)* **224**: 133-142.

Evans M, Church M. 2000. A Method for Error Analysis of Sediment Yields Derived from Estimates of Lacustrine Sediment Accumulation. *Earth Surface Processes and Landforms* **25**: 1257-1267.

Forbes AC, Lamoureux SF. 2005. Climatic Controls on Streamflow and Suspended Sediment Transport in Three Large Middle Arctic Catchments, Boothia Peninsula, Nunavut, Canada. *Arctic, Antarctic, and Alpine Research* **37**(3): 304-315.

Gordeev VV. 2006. Fluvial sediment flux to the Arctic Ocean. *Geomorphology* **80**: 94-104. DOI: 10.1016/j.geomorph.2005.09.008.

Guymon GL, 1974. Regional Sediment Yield Analysis of Alaska Streams. *Journal of the Hydraulics Division–ASCE* **100**: 41-50.

Håkanson L, Jansson M. 2002. Principles of Lake Sedimentology. Blackburn Press: USA.

Hallet B, Hunter L, Bogen J. 1996. Rates of erosion and sediment excavation by glaciers: A review of field data and their implications. *Global and Planetary Change* **12**: 213-235.

Hambley GW, Lamoureux SF. 2006. Recent summer climate recorded in complex varved sediments, Nicolay Lake, Cornwall Island, Nunavut, Canada. *Journal of Paleolimnology* **35**: 629-640. DOI 10.1007/s10933-005-4302-3.

Hardy DR. 1996. Climatic influences on streamflow and sediment flux into Lake C2, northern Ellesmere Island, Canada. *Journal of Paleolimnology* **16**: 133-149.

Hasholt B. 2016. Sediment and solute transport from Greenland. In Source-to-Sink Fluxes in Undisturbed Cold Environments, Beylich A, Dixon J, Zwoliński Z (eds). Cambridge University Press: Cambridge; 79-95. DOI:10.1017/CBO9781107705791.010.

Hasholt B, Bobrovitskaya N, Bogen J, McNamara J, Mernild SH, Milburn D, Walling DE. 2005. *Sediment Transport to the Arctic Ocean and Adjoining Cold Oceans*. 15th International Northern Basins Symposium and Workshop, Luleå to Kvikkjokk, Sweden, 29 August–2 September, 41-68.

Hobbie JE. 1962. Limnological Cycles and Primary Productivity of Two Lakes in the Alaskan Arctic, PhD Thesis. Indiana University, IN; 131 pp.

Hodder KR, Gilbert R, Desloges JR. 2007. Glaciolacustrine varved sediment as an alpine hydroclimatic proxy. *Journal of Paleolimnology* **38**: 365-394. DOI: 10.1007/s10933-006-9083-9.

Hodgkins R, Cooper R, Wadham J, Tranter M. 2003. Suspended sediment fluxes in a high-Arctic glacierised catchment: implications for fluvial sediment storage. *Sedimentary Geology* **162**, 105-117. DOI: 10.1016/S0037-0738(03)00218-5.

Hodson AJ, Ferguson RI. 1999. Fluvial Suspended Sediment Transport from Cold and Warm-Based Glaciers in Svalbard. *Earth Surfaces Processes and Landforms* **24**: 957-974.

Hodson AJ, Tranter M, Dowdeswell JA, Gurnell AM, Hagen JO. 1997. Glacier thermal regime and suspended-sediment yield: a comparison of two high-Arctic glaciers. *Annals of Glaciology* **24**: 32-37.

Ketterer ME, Watson BR, Matisoff G, Wilson CG. 2002. Rapid Dating of Recent Aquatic Sediments Using Pu Activities and $^{240}Pu/^{239}Pu$ As Determined by Quadrupole Inductively Coupled Plasma Mass Spectometry. *Environmental Science and Technology* **36**: 1307-1311.

Lammers RB, Shiklomanov AI, Vörösmarty CJ, Fekete BM, Peterson BJ. 2001. Assessment of contemporary Arctic river runoff based on observational discharge records. *Journal of Geophysical Research* **106**(D4): 3321-3334.

Lamoureux S. 2000. Five centuries of interannual sediment yield and rainfall-induced erosion in the Canadian High Arctic recorded in lacustrine varves. *Water Resources Research* **36**(1): 309-318.

Lamoureux SF, Gilbert R. 2004. A 750-yr record of autumn snowfall and temperature variability and winter storminess recorded in the varved sediments of Bear Lake, Devon Island, Arctic Canada. *Quaternary Research* **61**: 134-147. DOI: 10.1016/j.yqres.2003.11.003.

Lewis T, Gilbert R, Lamoureux SF. 2002. Spatial and temporal changes in sedimentary processes at proglacial Bear Lake, Devon Island, Nunavut. *Arctic, Antarctic and Alpine Research* **34**: 119-129.

Lewis T, Lafrenière MJ, Lamoureux SF. 2012. Hydrochemical and sedimentary responses of paired High Arctic watersheds to unusual climate and permafrost disturbance, Cape Bounty, Melville Island, Canada. *Hydrological Processes* **26**. DOI: 10.1002/hyp.8335.

Lewis T, Lamoureux SF. 2010. Twenty-first century discharge and sediment yield predictions in a small high Arctic watershed. *Global and Planetary Change* **71**: 27-41. DOI: 10.1016/j.gloplacha.2009.12.006.

Lewkowicz AG, Wolfe PM. 1994. Sediment Transport in Hot Weather Creek, Ellesmere Island, N.W.T., Canada, 1990-1991. *Arctic and Alpine Research* **26**(3): 213-226.

Milliman JD, Syvitski JPM. 1992. Geomorphic/Tectonic Control of Sediment Discharge to the Ocean: The Importance of Small Mountainous Rivers. *The Journal of Geology* **100**: 525-544.

Menounos B, Schiefer E, Slaymaker O. 2006. Nested temporal suspended sediment yields, Green Lake Basin, British Columbia, Canada. *Geomorphology* **79**: 114-129. DOI: 10.1016/j.geomorph.2005.09.020.

Molnia BF. 2007. Late nineteenth to early twenty-first century behavior of Alaskan glaciers as indicators of changing regional climate. *Global and Planetary Change* **56**: 23-56. DOI: 10.1016/j.gloplacha.2006.07.011.

Moore JJ, Hughen KA, Miller GH, Overpeck JT. 2001. Little Ice Age recorded in summer temperature reconstruction from varved sediments of Donard Lake, Baffin Island, Canada. *Journal of Paleolimnology* **25**: 503–517.

Naito AT, Cairns DM. 2015. Patterns of shrub expansion in Alaskan arctic river corridors suggest phase transition. *Ecology and Evolution* **5**(1): 87-101. DOI: 10.1002/ece3.1341.

Ólafsdóttir KB, Geirsdóttir Á, Miller GH, Larsen DJ. 2013. Evolution of NAO and AMO strength and cyclicity derived from a 3-ka varve-thickness record from Iceland. *Quaternary Science Reviews* **69**: 142-154.

Orwin JF, Lamoureux SF, Warburton J, Beylich A. 2010. A Framework for Characterizing Fluvial Sediment Fluxes from Source to Sink in Cold Environments. *Geografiska Annaler* **92 A**(2): 155-176.

Rainwater FH, Guy HP. 1961. Some Observations on the Hydrochemistry and Sedimentation of the Chamberlin Glacier Area Alaska. In *Shorter Contributions to General Geology*, United States Geological Survey (eds), USGS Professional Paper 414-C. United States Government: Washington; C1-C14.

Reed BL. 1968. Geology of the Lake Peters Area Northeastern Brooks Range, Alaska. *Geological Survey Bulletin.* **1236**: 1-132.

Schiefer E. 2006a. Contemporary sedimentation rates and depositional structures in a montane lake basin, southern Coast Mountains, British Columbia, Canada. *Earth Surface Processes and Landforms* **31**: 1311-1324. DOI: 10.1002/esp.1332.

Schiefer E. 2006b. Depositional regimes and areal continuity of sedimentation in a montane lake basin, British Columbia, Canada. *Journal of Paleolimnology* **35**: 617-628. DOI: 10.1007/s10933-005-5265-0.

Schiefer E. 2006c. Predicting Sediment Physical Properties within a Montane Lake Basin, Southern Coast Mountains, British Columbia, Canada. *Lake and Reservoir Management* **22**(1): 69-78.

Schiefer E, Kaufman D, McKay N, Retelle M, Werner A, Roof S. 2017. Fluvial suspended sediment yields over hours to millennia in the High Arctic at proglacial lake Linnévatnet, Svalbard. *Earth Surface Processes and Landforms*. DOI: 10.1002/esp.4264.

Schiefer E, Slaymaker O, Klinkenberg B. 2001. Physiographically Controlled Allometry of Specific Sediment Yield in the Canadian Cordillera: a Lake Sediment-Based Approach. *Geografiska Annaler* **83 A**: 55-65.

Serreze MC, Barrett AP, Stroeve JC, Kindig DN, Holland MM. 2009. The emergence of surface-based Arctic amplification. *The Cryosphere* **3**: 11-19.

Smith SV, Bradley RS, Abbott MB. 2004. A 300 year record of environmental change from Lake Tuborg, Ellesmere Island, Nunavut, Canada. *Journal of Paleolimnology* **32**: 137-148.

Sollid, J. L., Etzelmüller, B., Vatne, G., & Ødegård, R. 1994. Glacial dynamics, material transfer and sedimentation of Erikbreen and Hannabreen, Liefdefjorden, northern Spitsbergen. *Zeitschrift für Geomorphologie* **97**: 123-144.

Stavros C, Hill DF. 2013. National Centers for Environmental Information: National Oceanic and Atmospheric Administration. Retrieved May 2017 from: ftp://ftp.ncdc.noaa.gov/pub/data/gridded-nw-pac/.

Striberger J, Björck S, Ingólfsson Ó, Kjær KH, Snowball I, Uvo CB. 2011. Climate variability and glacial processes in eastern Iceland during the past 700 years based on varved lake sediments. *Boreas* **40**: 28-45. DOI 10.1111/j.1502-3885.2010.00153.x.

Syvitski JPM. 2002. Sediment discharge variability in Arctic rivers: implications for a warmer future. *Polar Research* 21(2): 323-330.

Tape KD, Verbyla D, Welker JM. 2011. Twentieth century erosion in Arctic Alaska foothills: The influence of shrubs, runoff, and permafrost. *Journal of Geophysical Research* **116**: 1-11. DOI: 10.1029/2011JG001795.

Thomas EK, Briner JP. 2009. Climate of the past millennium inferred from varved proglacial lake sediments on northeast Baffin Island, Arctic Canada. *Journal of Paleolimnology* **41**: 209-224. DOI: 10.1007/s10933-008-9258-7.

Thurston (in prep). Modeling Fine-grained Fluxes for Estimating Sediment Yields and Understanding Hydroclimatic and Geomorphic Processes at Lake Peters, Brooks Range, Arctic Alaska, Unpublished MS Thesis. Northern Arizona University, Flagstaff; 89 pp.

Walling DE, Fang D. 2003. Recent trends in the suspended sediment loads of the world's rivers. *Global and Planetary Change* **39**: 111-126. DOI: 10.1016/S0921-8181(03)00020-1.

Zemp M, Holger F, Gärtner-Roer I, Nussbaumer SU, Hoelzle M, Paul F, Haeberli W, Denzinger F, Ahlstrøm AP, Anderson B, Bajracharya S, Baroni C, Braun LN, Cáceres BE, Casassa G, Cobos G, Dávila LR, Degado Grandadoes H, Demuth MN, Espizua L, Fischer A, Fujita K, Gadek B, Ghazanfar A, Hagen JO, Holmlund P, Karimim N, Zhongqin L, Pelto M, Pitte P, Popovnin VV, Portocarrero CA, Prinz R, Sangewar CV, Severskiy I, Sigurdsson O, Soruco A, Usubaliev R, Vincent C. 2015. Historically unprecedented global glacier decline in the early 21st century. *Journal of Glaciology* **61**(228): 745-760. DOI: 10.3189/2015JoG15J017.

4 CONCLUSION

4.1 Research Outcomes

Regional-scale, catchment-scale, and within-lake arctic sediment transfer processes have been investigated with regards to hydroclimatic and geomorphic change at Lake Peters, Brooks Range, Alaska. SSYs available from catchments above the Arctic Circle vary by four orders of magnitude. Catchment area, lithology, glacial coverage and thermal regime, are principal drivers of inter-catchment variability in SSYs. Whilst catchment area and lithology hold approximately constant over relatively long temporal scales, glaciers are sensitive to contemporary climate change, and are anticipated to continue to shrink and experience basal warming. In response, sediment yields in currently glaciated catchments will probably increase over the coming century, before decreasing upon sediment exhaustion associated with cessation of the paraglacial cycle (Church and Ryder, 1972; Church and Slaymaker, 1989).

At the catchment-scale, the response of sediment transfer processes to climate and geomorphic forcing is complex. Both precipitation and temperature are drivers of sediment transfer, but there is no clear trend for when or where one is more significant than the other in the Arctic. Sediment yields in small mountainous catchments might be more responsive to precipitation, whilst sediment yields of larger coastal catchments are sensitive to surface temperatures. Sediment transfer in Lake Peters' catchment respond to both precipitation and temperature, with precipitation being dominant as the majority of annual sediment yield is associated with heavy rainfall. Sediment yields at Lake Peters are anticipated to increase over coming decades, with forecast increases of rainfall and warmer temperatures in northern Alaska. Following deglaciation, sediment yields will likely decline as proglacial sediment sources are exhausted.

Although there are clear catchment-scale trends, sub-catchments can show markedly different responses to climatic and geomorphic forcing. Between Carnivore and Chamberlin creeks, sub-catchment size appears to be important, with seasonal sediment exhaustion apparent in the smaller, steep Chamberlin Creek sub-catchment. The two sub-catchments will, therefore, likely respond differently to climate change. In Carnivore Creek sub-catchment, sediment yields are expected to increase over coming decades. In Chamberlin Creek sub-catchment, sediment exhaustion will probably limit such increases, and may lead to declining sediment yields, even though energy to drive transfer will be greater. As the one large glacier (Chamberlin Glacier) continues to decrease in size, glacial sediment production will diminish. The big picture response of Lake Peters' catchment will likely follow that of Carnivore Creek sub-catchment, which provides over 95% of the total sediment yield to Lake Peters.

Lake Peters acts as an effective sediment trap, and within-lake processes cause the influx of sediment to be deposited in a manner negatively related to distance down-lake, except near the primary inflow where sediment bypassing occurs, and positively related to water depth. High magnitude sedimentation events, estimated to be carried by hundreds of cumecs of discharge per

day, deposit thick, coarse marker beds within Lake Peters. The most recent high magnitude event that is recorded in spatially distributed sediment cores dates to the early 1970s. The greatest sediment focusing occurs in the proximal basin, although marker beds correlate through both the proximal and distal lake basins, providing a means to estimate average annual sediment yields over decades, or longer, in the absence of varves.

4.2 Implications for Environmental Policy

Glaciers of the Brooks Range are climate sensitive (Ellis and Calkin, 1984; Sikorski et al., 2009). Although detailed glacial studies are sparse, the Brooks Range glaciers are thought to be predominantly polythermal, with climate sensitivity heightened by the relatively arid environment, low mass flux, and mass balance responsiveness to summer ablation (Sikorski et al., 2009). The cirque shapes, relatively high altitudes, and northerly orientation of moraines deposited by glacial expansion during the Little Ice Age (LIA) (*ca.* 1200-1850 CE) in the central Brooks Range are indicative of Neoglacial climate sensitivity. Much of the glaciers' surface areas are concentrated around the equilibrium-line altitude of Neoglacial maxima (1300 – 1800 m) (Ellis and Calkin, 1984). As Alaska's climate continues to warm (Loso, 2009; Cassano et al., 2011) and rainfall increases (Bintanja and Andry, 2017), glaciers of the Brooks Range are likely to continue receding. Winter runoff over pan-Arctic Alaska will likely continue to increase (Lammers et al., 2001), as will sediment yields (Syvitski, 2002; Lewis and Lamoureux, 2010). Although the magnitude at which sediment yields will increase has not been modeled for Arctic Alaska, the estimate of a 100% to 600% increase this Century made by Lewis et al. (2010) for West River catchment, Melville Island, Arctic Canada provides a ball-park estimate of what could be expected in some other arctic regions.

Moore et al. (2009) suggests that glacial retreat in western North America since the LIA has enhanced geomorphic hazards, including outburst floods from moraine-dammed lakes, mass failures of over-steepened valley walls, and debris flows originating from moraines. Mass failures of valley walls are likely in the steep Carnivore and Chamberlin Creek sub-catchments at Lake Peters, but the lake is not moraine-dammed, and evidence of debris flow was not observed in traversed valleys. Such mass failure events would only be deemed a hazard, and of policy consequence, if there is tangible risk to people or infrastructure.

Historically, indigenous peoples occupied high altitude lakes within the Brooks Range. Archaeological evidence indicates repeated long-term Northern Archaic settlement at Lake Agiak, central Brooks Range (350 km southwest of Lake Peters) in the mid-Holocene, associated with caribou hunting (Wilson and Rasic, 2008). Camps and artifacts of mid-Holocene age have also been found at Lake Schrader, and hunting and fishing by indigenous people occurred in the area of Lakes Peters and Schrader until the 1930s (Hobbie, 1962). Today, human activity at Lake Peters is limited to occasional use by pack-rafting groups, hikers, recreational and subsistence fisher-people, as well as by scientific researchers.

From a policy standpoint, anthropogenic implications of hydrological change at Lake Peters is relatively low for the pan-Arctic, because of effective high-altitude sediment trapping, and because protection from development is provided from the mountains to the coast. Lake Peters acts as an effective sediment trap, but is one of the largest lakes in the northeastern Brooks Range; therefore, other catchments are unlikely to experience the same degree of effective sediment trapping. Discharge from Lake Peters ultimately reaches the Arctic Ocean via the Sadlerochit River on the Coastal Plain, and in the Sadlerochit River catchment, *wilderness* status under the Wilderness Act (1964), has provided protection from development. Approximately 99% of the Coastal Plain has been classified as wetland, with dense vegetation and permafrost at shallow depths (Lyons and Trawicki, 1994). This contrasts Canada, where increasing sediment loads, especially episodic event loads, may impact hydroelectric projects, water supply utilities, as well as natural hazard warning processes (Moore et al., 2009). At Lake Peters and within the hydrologically connected Sadlerochit River drainage, potential damage to sites of archaeological significance, and ecological implications of increasing and episodic sediment loads, are more pertinent than hazards to people and property.

The Sadlerochit River has been described by Craig and McCart (1975) as a thermal-spring-fed biological oases. Glacially-fed streams, with cold temperatures and high SSCs, are generally associated with lower invertebrate biomass and biodiversity compared with nival streams (Moore et al., 2009). Glacial-fed streams that reemerge from springs in the foothills, or on the Coastal Plain, are buffered from these effects, resulting in greater biomass and biodiversity compared to tundra and mountain streams (Craig and McCart, 1975). Streams of the Coastal Plain were sampled to have 22 to 184,000 organisms per square meter, and 18 to 22 taxonomic groups in 1971-73, with the lowest numbers in turbid mountain streams, and the highest numbers in spring-fed streams. A significant inverse relation between benthic invertebrates and stream discharge was found, with less invertebrates in streams with larger discharges (Craig and McCart, 1975). Consequently, increasing runoff and sediment yields, would be expected to decrease density and diversity of aquatic invertebrates (Moore et al., 2009). This could be of consequence in all coastal stream types, including spring-fed streams if groundwater inflow to the springs increases, along with rainfall on the Coastal Plain.

The common anadromous fish species of the Coastal Plain include: Arctic char (*Salvelinus alpinus*), Dolly Varden (*Salvelinus malma*), Arctic cisco (*Coregonus autumnalis*), Broad whitefish (*Coregonus nasus*), Chum salmon (*Oncorhynchus keta*), Least cisco (*Coregonus sardinella*), Ninespine stickleback (*Pungitius pungiti*), Pink salmon (*Onchorhynchus gorbuscha*), and Rainbow smelt (*Osmerus mordax*). Freshwater fish species include: Arctic grayling (*Thymallus arcticus*), Burbot (*Lota lota*), Lake trout (*Salvelinus namaycush*), and Round whitefish (*Prosopium cylindraceum*), Slimy Sculpin (*Cottus cognatus*) (lists compiled from Craig and McCart, 1975; Lyons and Trawicki, 1994; and Brown et al., 2014). High sediment loads, increasing stream temperatures, and changes in water temperature associated with glacier retreat can all impact fish (Moore et al., 2009). Grayling is widely distributed on the Coastal Plain, but spawning is restricted to tundra streams, whereas Arctic Char is found in mountain and spring streams (Craig and McCart, 1975). In the Hulaula River catchment (20 km east

of Lake Peters), perennial springs provide important overwintering habitat for Dolly Varden (Brown et al., 2014).

Increasing suspended sediment yields may also impact ecology by driving changes to the structure and area of deltaic habitat in the pan-Arctic. Suspended sediment load has been positively correlated with bedload (Turkowski et al., 2010), and increasing bedload may cause structural modification of deltaic habitat. Delta habitat is especially important for migratory birds and shorebirds (Lyons and Trawicki, 1994). With regards to the area of deltaic habitat, erosion of the Alaska Beaufort Sea coast increased from 6.8 m yr^{1} (1955 to 1979), to 8.7 m yr^{-1} (1979 to 2002), to 13.6 m yr^{-1} (2002 to 2007) (Jones et al., 2009). Jones et al. (2009) attributed the increasing erosion rates to increasing summertime sea surface temperature, declining sea ice extent, rising sea level, and increasing storm power and wave action. This contrasts Greenland, where deltas prograded from the 1980s to 2010s, following a stable period from the 1940s to 1980s (Bendixen et al., 2017). The progradation is positively correlated with increasing freshwater runoff during open-water periods, and indirectly with air temperature (Bendixen et al., 2017). Therefore, the implications of increasing sediment yields for Arctic coasts is driven by multiple physical processes, and is location-specific, which makes future coastal responses to increasing temperature, rainfall, runoff, and sediment transfer uncertain. It is feasible that the open-coasts of Alaska will continue to erode, but sheltered bay areas may experience progradation. Coastal policies should be precautionary, and consider effects of increasing coastal erosion.

Sediment transfer effects carbon budgets, which should also be taken into account in Arctic policy-making. Rivers draining pan-Arctic Alaska transfer mineral-bound organic carbon to the Arctic Ocean, where the ocean acts as a carbon reservoir. Vonk et al. (2015) found a general decrease in organic carbon content per surface area ratio from river-to-sea on the Mackenzie River Delta, Canada. About 45% of terrestrial bound organic carbon was calculated to be lost on the Delta, and 55% buried on the continental shelf. Some of the organic carbon was found to reside in soils for millennia before being released to the river (Vonk et al., 2015). Increasing sediment yields across pan-Arctic Alaska may increase mineral-bound terrestrial carbon transfer to the ocean, although the degree to which this will impact carbon budgets is uncertain.

4.3 Recommendations for Future Research

Considering both research outcomes at Lake Peters, and the broader scientific and policy context associated with increasing sediment transfer, the following recommendations are made for future research:

- Glaciers are important weathering agents, and sources of sediment entrainment. Characteristics of glaciers in Lake Peters' catchment, and generally in the Brooks Range, are poorly understood, and should be subject of further investigation to determine thermal processes and how they are responding, and will continue to respond, to climate forcing.

- Arctic sediment yields in small, mountainous catchments might be dominantly responsive to precipitation, whilst sediment yields of larger coastal catchments might be sensitive to surface temperatures. The significance of climate forcing for Arctic hydrological regimes, along with consideration of the spatial scale, should continue to be a priority for research. Understanding climate forcing of hydrological processes is fundamental for assessing current system processes, and modeling future environmental change.
- A sediment budget approach will improve our understanding of both hillslope processes, and sediment storage and exhaustion. The significance of hillslope processes for arctic sediment yields, especially episodic sedimentation, requires further investigation, along with climate forcing of hillslope processes. Although geomorphic evidence is often used as an indicator of hillslope processes, little quantification of the volume of sediment sourced from arctic hillslopes, temporal occurrence, or spatial distribution of hillslope processes is available. Further work to understand arctic sediment storage and exhaustion effects is also needed in both small mountain catchments, on a larger spatial scale between the mountains and the coast, and on both seasonal to paraglacial time-scales. The usefulness of the concept of paraglacial sediment exhaustion should be considered.
- Erosion of the Coastal Plain, draining the Brooks Range in Alaska, has been measured, but not modeled. Modeling future response of the Alaska Beaufort Sea coast with-predicted warming and increasing rainfall scenarios, considering terrestrial sediment yields, as well as coastal dynamics, would help inform policy response.

4.4 References

Bendixen M, Iversen LL, Bjørk AA, Elberling B, Westergaard-Nielsen A, Overeem I, Barnhart KR, Khan SA, Box JE, Abermann J, Langley K, and Kroon A. 2017. Delta progradation in Greenland driven by increasing glacial mass loss. *Nature* **550**: 101-104. DOI:10.1038/nature23873.

Bintanja R, Andry O. 2017. Towards a rain-dominated Arctic. *Nature Climate Change* **7**: 263-268. DOI: 10.1038/NCLIMATE3240**.**

Brown RJ, Loewen MB, Tanner TL. 2014. Overwintering Locations, Migrations, and Fidelity of Radio-Tagged Dolly Varden in the Hulahula River, Arctic National Wildlife Refuge, 2007-09. *Arctic* **67**(2): 149-158. DOI: 10.14430/arctic4379.

Cassano EN, Cassano JJ, Nolan M. 2011. Synoptic weather pattern controls on temperature in Alaska. *Journal of Geophysical Research* **116**: 1-19. DOI: 10.1029/2010JD015341.

Craig PC, McCart PJ. 1975. Classification of Stream Types in Beaufort Sea Drainages between Prudhoe Bay, Alaska, and the MacKenzie Delta, N. W. T., Canada. *Arctic and Alpine Research* **7**(2): 183-198.

Ellis JM, Calkin PE. 1984. Chronology of Holocence glaciation, central Brooks Range, Alaska. *Geological Society of America Bulletin* **95**: 897-912.

Hobbie JE. 1962. Limnological Cycles and Primary Productivity of Two Lakes in the Alaskan Arctic, PhD Thesis. Indiana University, IN; 131 pp.

Jones BM, Arp CD, Jorgenson MT, Hinken KM, Schmutz JA, and Flint PL. 2009. Increase in the rate and uniformity of coastline erosion in Arctic Alaska. *Geophysical Research Letters* **36**(L03503): 1-5. DOI: 10.1029/2008GL036205.

Lewis T, Lamoureux SF. 2010. Twenty-first century discharge and sediment yield predictions in a small high Arctic watershed. *Global and Planetary Change* **71**: 27-41. DOI: 10.1016/j.gloplacha.2009.12.006.

Loso MG. 2009. Summer temperatures during the Medieval Warm Period and Little Ice Age inferred from varved proglacial lake sediments in southern Alaska. *Journal of Paleolimnology* **41**: 117-128. DOI 10.1007/s10933-008-9264-9.

Lyons SM, Trawicki JM. 1994. Water resource inventory and assessment, Coastal Plain, Arctic National Wildlife Refuge, 1987-1992 final report, WRB 94-3. U.S. Department of the Interior, Fish and Wildlife Service: Anchorage, Alaska.

Moore RD, Fleming SW, Menounos B, Wheate R, Fountain A, Stahl K, Holm K, and Jakob M. 2009. Glacier change in western North America: influences on hydrology, geomorphic hazards and water quality. *Hydrological Processes* **23**: 42-61. DOI: 10.1002/hyp.7162.

Sikorski JJ, Kaufman DS, Manley WF, Nolan M. 2009. Glacial-Geologic Evidence for Decreased Precipitation during the Little Ice Age in the Brooks Range, Alaska. *Arctic, Antarctic, and Alpine Research* **41**: 138-150. DOI: 10.1657/1938-4246(07-078)[SIKORSKI]2.0.CO;2.

Syvitski JPM. 2002. Sediment discharge variability in Arctic rivers: implications for a warmer future. *Polar Research* 21(2): 323-330.

Turkowski JM, Rickenmann D, Dadson SJ. 2010. The partitioning of the total sediment load of a river into suspended load and bedload: a review of empirical data. *Sedimentology* **57**: 1126-1146.

Vonk JE, Giosan L, Blusztajn J, Montlucon D, Pannatier EG, McIntyre C, Wacker L, Macdonald RW, Yunker MB, Eglinton TI. 2015. Spatial variations in geochemical characteristics of the modern Mackenzie Delta sedimentary system. *Geochimica et Cosmochimica Acta* **171**: 100-120. DOI: 10.1016/j.gca.2015.08.005.

Wilderness Act. 1964. Retrieved December 2016 from: http://www.wilderness.net/NWPS/documents //publiclaws/PDF/16_USC_1131-1136.pdf.

Wilson AK, Rasic JT. 2008. Northern Archaic Settlement and Subsistence Patterns at Agiak Lake, Brooks Range, Alaska. *Arctic Anthropology* **45(**2): 128-145.

5 APPENDICES

5.2 Appendix I – Methods

5.2.1 Instruments and Software List (additional to in-text only)

- A Hach FH950 Portable Velocity Meter fitted with a computer and 20' Cable ("velocity meter") was used to measure velocity, width and depth at the hydrological stations, automatically computing discharge.
- Photography of hydrological stations was undertaken using Wingscapes time-lapse cameras.
- The laboratory research balance used for weighing sediment samples was a Sartorius research balance.
- Surfaces of cores were photographed while wet, and again after air-drying to near maximum visual contrast of laminae, using a Nikon 3200 digital camera on a fixed stand.
- Spatial mapping was undertaken with ArcGIS version 10.3.
- Sediment modeling and non-spatial graphics was undertaken with R version 3.2.4.

5.2.2 Raw Data

Please refer to the attached Microsoft Excel file for raw fluvial and lake data, and to the attached folder for photographic records. Additional data used to select the models will be made available via the National Science Foundation (NSF) Arctic Data Center.

The Microsoft Excel file includes the following sheets:

- Meta_data: information in this sheet explains abbreviations, units, and provides additional notes regarding the data.
- CAR_Fluvial: information in this sheet is specific to Carnivore Creek (CAR) fluvial-based modeling (Chapter 2). Data includes: the hydrological and climatological data used for building models; the hydrological and climatological data used for producing continuous records of suspended sediment concentration (SSC); and the continuous SSC data output from both the turbidity (NTU)-based and discharge (Q)-based models.
- CHB_Fluvial: information in this sheet is specific to Chamberlin Creek (CHB) fluvial-based modeling (Chapter 2). Data includes: the hydrological and climatological data used for building models; the hydrological and climatological data used for building continuous suspended sediment concentration (SSC) models; and the continuous SSC data output from both the turbidity (NTU)-based and discharge (Q)-based models.
- Surface_Cores: information in this sheet is specific to lake-based modeling (Chapter 3). Data includes: water depth, distance from the Carnivore Creek inflow, dry bulk density (DBD) for each surface core sampled, and the sediment flux to the reference depth in Marker Bed A calculated from these parameters. Information also includes the water depth and distance from the Carnivore Creek inflow for X, Y coordinates on a 100 m by 100 m grid across Lake Peters, used

for spatially modeling sediment flux. Finally, to compare the measured and spatially modeled sediment flux, information includes a selection of modeled points from the 100 m by 100 m grid of Lake Peters that match the locations of the surface cores, and the residuals that represent the difference between the measured and modeled sediment flux.

5.2.3 Boolean Loops and Functions (additional to in-text)

#Correlation function to test correlations between explanatory variables

```
CorFunction = function(x,y){ #create a function with x and y as the inputs
  cor = cor(x,y) #use the built-in "cor" function to test the correlation between x and y
  autocor1 = cor(x[-1], x[-length(x)]) #estimate the first-order autoregressive model for X
  autocor2 = cor(y[-1], y[-length(y)]) #estimate the first-order autoregressive model for y
  EffN = (length(x)) * ((1-autocor1*autocor2)/(1+autocor1*autocor2)) #estimate the effective sample size
  EffDF = EffN-2 #the effective degrees for freedom (approximation of the actual degrees of freedom) are equal to the effective sample size minus 2
  DF = X-2 #calculate the degrees of freedom (number of values free to vary) by subtracting the number of relations from the number of observations (*note that X needs to be set)
  if(EffDF > 0){
    EffDF = EffDF #if the effective degrees of freedom are greater than 0, use the effective degrees of freedom
  } else{
    EffDf = DF #otherwise, if the effective degrees of freedom are greater than 0, use the degrees of freedom
  }
  test = autocor1*autocor2 #multiply the autoregressive model of x by the autoregressive model of y
  t = cor*sqrt(EffDF)/(1-(cor^2)) #calculate the t-value for the correlation of x and y, using either the effective degrees of freedom or the degrees of freedom (depending on results from above)
  p = pt(-abs(t), EffDF) #calculate the p-value – probability of randomly exceeding the t-stat on either tail of the distribution
  out = list(cor = cor, autocor1 = autocor1, autocor2 = autocor2, EffN = EffN, EffDF = EffDF, test = test, t = t, p = p) #print the results as a list
  return(out)
}

Cor1 = CorFunction(na.omit(Variable_1), na.omit(Variable_2)); print(Cor1) #apply the correlation function built above to test the correlation between two variables, first omitting rows with NA (no data)
```

#Array, Boolean for-loop, and which-loop to find the best variables from each correlated group for the sediment model

```
A1 = array(data = NA, dim = c(ncol(M1), ncol(M2), ncol(M3), ncol(M4)))

for(a in 1:ncol(M1)){
  for(b in 1:ncol(M2)){
    for(c in 1:ncol(M3)){
      for(d in 1:ncol(M4)){
        R = glmulti(M_logSSC ~ M1[,a] + M2[,b] + M3[,c] + M4[,d] + M5 + M6, level = 1)
        R2 = summary(R)
        A1[a,b,c,d] = R2$bestic
      }
    }
  }
}

best.ind1 = which(A1==min(A1),arr.ind = TRUE); print(best.ind1)
```

#Function to find models in order of best AICs (e.g. not just the best model, but top 10 models)

```
min.n <- function(x,n,value=TRUE){
```

```
  s <- sort(x, index.return=TRUE)
  if(value==TRUE){s$x[n]} else{s$ix[n]}}

x = A1

min.n(x,2)

which(A1==min.n(x,2),arr.ind = TRUE)
```

#Use of glmulti – input of best variables returned by the for-loop and which-loop above to eliminate variables and find the best sediment models (the dependent variable used was log SSC)

```
Model = glmulti(Dependent_Variable ~ Explanatory_Variable_1 + Explanatory_Variable_2 + Explanatory_Variable_3 + Explanatory_Variable_4 + Explanatory_Variable_5 + Explanatory_Variable_6, level = 1)

#Linear model of glmulti output

Best_Model = lm(Dependent_Variable ~ Explanatory_Variable_1 + Explanatory_Variable_2 , data = X)

summary(Best_Model)

print(Best_Model)

AIC(Best_Model)
```

#Prediction bands for models

```
Data = read.csv("Data.csv"); head(CAR_Q_Mod)

Data_DF = as.data.frame(Data)

Prediction_Interval = predict.lm(Best_Model, Data_DF, interval = "prediction")

Prediction_Interval_DF = as.data.frame(Prediction_Interval)

write.csv(Prediction_Interval_DF, file = "Prediction_1 ")
```

5.3 Appendix II – Results

5.3.1 Supporting information for Figure 2.2

A) Discharge (Q) – stage power relation for Carnivore Creek, using discrete data from 5/21/15 to 8/5/15.

B) Q – stage power relation for Chamberlin Creek, using discrete data from 5/22/15 to 8/11/15.

C) Water-pressure (from TROLL) – y difference (y-diff; shown on photographs) linear relation for Carnivore Creek, using discrete data from 6/28/15 to 8/1/15.

D) Linear relations of stage calculated from Hobo U20 water-pressure against stage calculated from Troll 9500 water-pressure for Chamberlin Creek: Relation 1: using continuous data from 05/25/15 to 05/27/15; Relation 2: using continuous data from 06/14/15 to 06/18/15.

E) Stage – cross-sectional area linear relation for Carnivore Creek, using discrete data from 05/19/15 to 08/10/15; and from 05/23/16 to 08/17/16.

F) Q – cross-sectional area linear relation for Chamberlin Creek, using discrete data from 5/16/15 to 8/11/15.

G) Q – stage (from Hobo) power relation for Chamberlin Creek, using discrete data from 5/23/16 to 6/2/16.

H) Q – stage exponential relation for Chamberlin Creek, using discrete data from 8/9/16 to 8/16/16.

I) Stage – y difference (y-diff; shown on photographs) linear relation for Chamberlin Creek: Relation 1: using discrete data from 6/4/16 to 6/20/16; Relation 2: using discrete data from 6/4/16 to 6/20/16.

J) Linear relation of discharge in Chamberlin Creek against discharge in Carnivore Creek, using continuous hourly data with a 2-hour lag from 5/22/15 to 8/6/15 and 5/23/16 to 6/20/16.

5.3.2 Supporting Climate Data Regressions

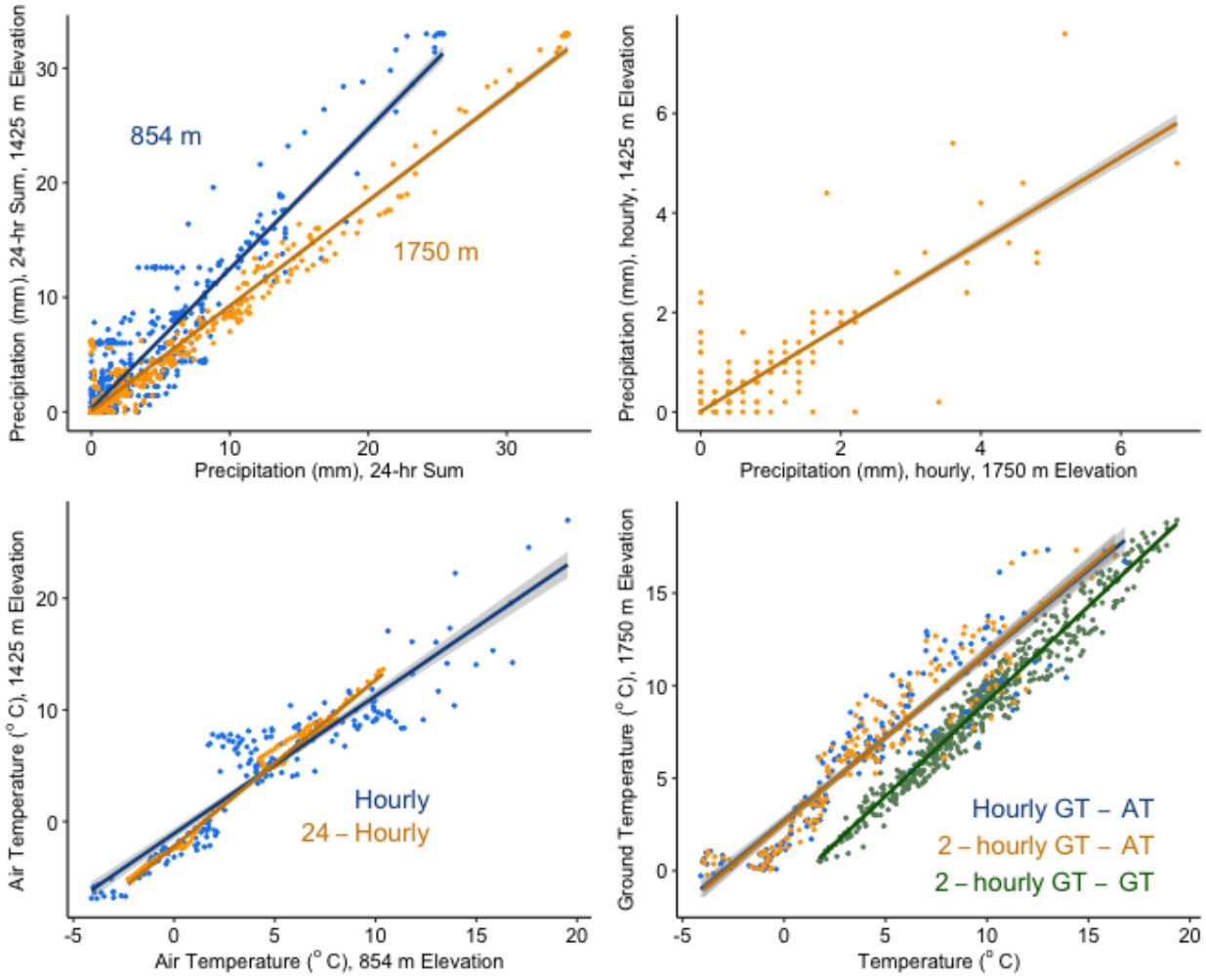

Figure 5.1: Regression relations used to achieve continuous meteorological timeseries (for input into sediment models). Raw data is provided in **Appendix I**, and these regressions were used to fill data gaps.

A) Relation 1 (blue): precipitation (Precip.) at 1425 m elevation summed over the previous 24-hours – precipitation at 854 m elevation summed over the previous 24-hours, using continuous data from 6/1/16 at 11:00 to 7/16/16 at 23:00; Precip_24. 1425 m = 1.22 x Precip_24. 854 m + 0.267; Res. SE = 2.01 on 1091 DF; Adj. R^2 = 0.868; F-stat = 7150; p-value = 2.2 x 10^{-16}. Regression was used to fill a gap in Precip_24. 1425 m from 5/22/16 at 19:00 to 5/31/16 at 12:00, which was used for sediment modeling.

Relation 2 (orange): precipitation (Precip.) at 1425 m elevation summed over the previous 24-hours – precipitation at 1750 m elevation summed over the previous 24-hours, using continuous data from 6/1/16 at 11:00 to 7/16/16 at 23:00; Precip_24. 1425 m = 0.919 x Precip_24. 1750 m + 0.055; Res.SE = 1.18 on 1091 DF; Adj. R^2 = 0.954; F-stat = 22800; p-value = 2.2 x 10^{-16}. Regression was used to fill a gap in Precip_24. 1425 m from 7/17/16 at 0:00 to 8/14/16 at 10:00, which was used for sediment modeling.

B) Hourly precipitation (Precip.) at 1425 m elevation – hourly precipitation at 1750 m elevation, using continuous data from 6/1/16 at 11:00 to 7/16/16 at 23:00; Precip. 1425 m = 0.852 x Precip. 1750 m + 0.11; Res SE. = 0.259 on 1091 DF; Adj. R^2 = 0.771; F-stat = 3684; p-value = 2.2 x 10^{-16}. Regression was used to fill a gap in Precip. 1425 m from 7/17/16 at 0:00 to 8/14/16 at 10:00, which was used for the time-series (**Figure 2.3**) and statistics (**Table 2.2**).

C) Relation 1 (blue): hourly air temperature (AT) at 1425 m elevation – hourly air temperature at 854 m elevation, using continuous data from 5/24/15 at 10:00 to 5/31/15 at 23:00; AT 1425 m = 1.23 x AT 854 m -1.08; Res. SE = 2.52 on 180 DF; Adj. R^2 = 0.853; F-stat = 1052; p-value = 2.2 x 10^{-16}. Regression was used to fill a gap in hourly AT 1425 m from 5/20/15 at 16:00 to 5/25/15 at 10:00, which was used for the time-series (**Figure 2.3**) and statistics (**Table 2.2**).

Relation 2 (orange): air temperature (AT) at 1425 m elevation averaged over the previous 24-hours – air temperature at 854 m elevation summed over the previous 24-hours; AT_24 1425 m = 1.49 x AT_24 854 m -2.22; Res. SE = 0.570 on 157 DF; Adj. R^2 = 0.987; F-stat = 15700; p-value = 2.2 x 10^{-16}. This regression was used to fill a gap in AT_24 1425 m from 5/22/15 at 16:00 to 5/25/15 at 10:00, which was used for sediment modeling.

D) Relation 1 (blue): hourly ground temperature (GT) at 1750 m elevation– hourly air temperature (AT) at 854 m elevation, using continuous data from 5/24/15 at 16:00 to 5/31/15 at 23:00; GT = 0.902 x AT + 2.71; Res. SE = 1.61 on 174 DF; Adj. R^2 = 0.863; F-stat = 1106; p-value = 2.2 x 10^{-16}. Regression was used to fill a gap in GT from 5/20/15 at 16:00 to 5/24/15 at 15:00, which was used for the time-series (**Figure 2.3**) and statistics (**Table 2.2**).

Relation 2 (orange): ground temperature (GT) at 1750 m elevation averaged over the previous 2-hours – air temperature (AT) at 854 m elevation summed over the 2-hours, using continuous data from 5/24/15 at 16:00 to 5/31/15 at 23:00; GT_2 = 0.918 x AT_2 + 2.62; Res. SE = 1.48 on 173 DF; Adj. R^2 = 0.883; F-stat = 1308; p-value = 2.2 x 10^{-16}. Regression was used to fill a gap in GT_2 1750 m from 5/20/15 at 16:00 to 5/24/15 at 15:00, which was used for sediment modeling.

Relation 3 (green): ground temperature (GT) at 1750 m elevation averaged over the previous 2-hours – GT at 1425 m elevation summed over the previous 2-hours, using continuous data from 6/7/15 at 15:00 to 8/4/15 at 10:00; GT_2 1750 m = 1.025 x GT_2 1425 m – 1.09; Res. SE = 0.82 on 559 DF; Adj. R^2 = 0.960; F-stat = 13410; p-value = 2.2 x 10^{-16}. Regression was used to fill a gap in GT_2 1750 m from 5/24/15 at 16:00 to 6/7/15 at 14:00, which was used for sediment modeling.

5.3.3 Arctic Specific Sediment Yields (SSY)

Table 5.1: Arctic Specific Sediment Yields (SSYs) sourced from literature, corresponding to Figure 3.4.

Reference	Stream/ River	Location	Years of Yield	Area (km^2)	Glacier Coverage (%)	SSY (Mg km^{-2} yr^{-1})
Church and Ryder, 1972	Lewis River, Baffin Island	Canada	1963-1965	205	89	735
Cogley, 1975	Mecham River, Cornwallis Island	Canada	1970-1971	95	0	17.4
Barsch et al., 1994	Beinbekken	Svalbard	1990-1991	5	0	38
Lewkowicz and Wolfe, 1994	Hot Weather Creek, Ellesmere Island	Canada	1990-1991	155	0	18.2
Sollid et al., 1994	Erikbreen Glacier, Liefdefjorden	Svalbard	3 years	9	100	514
Bogen, 1996	Juleelva	Norway	3 years	1.1	0	23
Bogen, 1996	Langfjordbreelva	Norway	5 years	4.6	100	475
Bogen, 1996	Elvegårdselv	Norway	2 years	119.4	0	18
Bogen, 1996	Beiarelv at Klipa	Norway	6 years	350	10	35
Bogen, 1996	Ovre Beiarelv	Norway	6 years	2.4	100	482
Bogen, 1996	Engabreen	Norway	7 years	36.2	100	430
Bogen, 1996	Blakkåga	Norway	5 years	303	20	270
Hardy et al., 1996	Lake C2, Ellesmere Island	Canada	1990-1992	21	9	12.4
Hodson et al., 1997	Austre Brøggerbreen	Svalbard	1991-1992	32	54.000	98
Hodson et al., 1997	Finsterwalderbreen	Svalbard	1994-1995	68	65.000	1805
Lamoureux, 2000	Nicolay Lake	Canada	1798-1995	91.2	0	109.8
Rasch et al. 2000	Zackenbergelven River, near Zackenberg Station	Greenland	1994-2005	514	19.72	112

Bogen and Bønsnes, 2003	Londonelva	Svalbard	1992-1996	0.7	0	82.5
Bogen and Bønsnes, 2003	Bayelva	Svalbard	1989-2000	30.9	55	359
Bogen and Bønsnes, 2003	Endalselva	Svalbard	1994-1998	28.8	22.5	281
Hodgkins et al., 2003	Finsterwalderbreen	Svalbard	1999-2000	68	64.706	2027.5
Forbes and Lamoureux, 2005	Lord Lindsay River, above Sanagak Lake, central Boothia Peninsula	Canada	2001-2002	1485	0	1.15
Forbes and Lamoureux, 2005	East Tributary of Lord Lindsay River	Canada	2001-2002	465	0	1.2
Gordeev, 2006	Pyasina River	Russia	1970-1995	182	0	18.8
Gordeev, 2006	Khatanga River	Russia	1970-1995	364	0	4.6
Gordeev, 2006	Olenjok River	Russia	1970-1995	219	0	5.1
Gordeev, 2006	Omoloy River	Russia	1970-1995	39	0	1
Gordeev, 2006	Yana River	Russia	1970-1995	225	0	17.8
Gordeev, 2006	Alazeya River	Russia	1970-1995	68	0	3.4
Tape et al., 2011	Lake 1, Chandler River corridor	Alaska	1951-2009	2	0	11.1
Tape et al., 2011	Lake 2, Chandler River corridor	Alaska	1951-2009	1.5	0	51.6
Tape et al., 2011	Lake 3, Chandler River corridor	Alaska	1951-2009	0.3	0	11.8
Tape et al., 2011	Lake 4, Chandler River corridor	Alaska	1951-2009	2.7	0	0.25

Lewis et al., 2012	West, Cape Bounty, Melville Island	Canada	2006-2009	8	0	49.675
Lewis et al., 2012	East, Cape Bounty, Melville Island	Canada	2006-2009	11.6	0	25.35
Hasholt, 2016	A-Fjord, Marmorilik (Location 1)	Greenland	1978-1989	177	59	11.5
Hasholt, 2016	Q-Fjord, below Wegener Glacier, Marmorilik (Location 2)	Greenland	1983-1989	31	65	417
Hasholt, 2016	Røde Elv, Disko Island (Location 13)	Greenland	1976, 1983, 2013	96	23	15
Hasholt, 2016	Watson River, near Sønder Strom Airport (Location 17)	Greenland	2007-2013	10200	94	943
Hasholt, 2016	Leverett Glacier, Watson River (Lorcation 18)	Greenland	2009-2010	600	100	6040
Hasholt, 2016	Zackenbergelven River, below Linderman River (Location 31)	Greenland	1997-2001	512	20	89
Schiefer et al., 2017	Lake Linnévatnet	Svalbard	2004-2010	26	7	675